

OPTUM COMPUTATIONAL ENGINEERING

Optum<sup>G2</sup>

MATERIALS



Version 2016



## Contents

<b>1</b>	<b>STRESS, STRAIN AND SIGN CONVENTIONS</b>	<b>7</b>
1.1	Effective stress . . . . .	8
<b>2</b>	<b>ELASTICITY</b>	<b>9</b>
2.1	Isotropic elasticity . . . . .	9
2.1.1	Undrained conditions . . . . .	10
2.2	Anisotropic elasticity . . . . .	11
<b>3</b>	<b>ELASTOPLASTICITY</b>	<b>12</b>
3.1	Additive decomposition . . . . .	12
3.2	Elasticity . . . . .	12
3.3	Flow rule . . . . .	13
3.4	Yield function . . . . .	13
3.5	Hardening rule . . . . .	13
3.6	Complementarity conditions . . . . .	13
3.7	Initial stresses . . . . .	13
<b>4</b>	<b>HYDRAULIC MODELS</b>	<b>14</b>
4.1	Linear model . . . . .	15
4.2	Tanh relative hydraulic conductivity model . . . . .	15
4.3	van Genutchen model . . . . .	16
<b>5</b>	<b>COMMON PROPERTIES</b>	<b>19</b>
<b>6</b>	<b>DRAINAGE</b>	<b>21</b>
6.1	Cavitation Cut-Off . . . . .	21
6.2	Relation to “Method A, B, C” . . . . .	22
<b>7</b>	<b>SPATIAL VARIATION OF PARAMETERS</b>	<b>25</b>
7.1	Gradient . . . . .	25
7.2	Profile . . . . .	26
7.3	Map . . . . .	26
7.4	Multiple data sets . . . . .	27
<b>8</b>	<b>MOHR-COULOMB</b>	<b>28</b>
	Material . . . . .	28
	Drainage . . . . .	28
	Stiffness . . . . .	28
	Strength . . . . .	29
	Flow Rule . . . . .	29
	Tension cut-off (optional) . . . . .	32
	Compression Cap (optional) . . . . .	32
	Fissures (optional) . . . . .	35
	Unit weights . . . . .	36
	Initial Conditions . . . . .	36
	Hydraulic Model . . . . .	36
8.1	Notes . . . . .	36

8.2	Influence of dilation angle on limit load . . . . .	37
8.3	Strength reduction . . . . .	38
8.4	Capabilities and limitations of Mohr-Coulomb . . . . .	38
8.4.1	Initial stiffness versus unloading/reloading stiffness . . . . .	39
8.4.2	Undrained conditions . . . . .	39
<b>9</b>	<b>DRUCKER-PRAGER</b>	<b>42</b>
	Material, Drainage, Stiffness . . . . .	42
	Strength . . . . .	42
	Flow Rule . . . . .	42
	Tension cut-off (optional) . . . . .	42
	Compression Cap (optional) . . . . .	43
	Unit weights, Initial Stresses, Permeability . . . . .	43
9.1	Notes . . . . .	43
9.2	Influence of dilation on limit load . . . . .	43
9.3	Drucker-Prager vs Mohr-Coulomb . . . . .	44
9.4	Strength reduction . . . . .	46
9.5	Undrained conditions . . . . .	46
<b>10</b>	<b>TRESCA</b>	<b>47</b>
	Material . . . . .	47
	Stiffness . . . . .	47
	Strength . . . . .	47
	Tension cut-off, Unit Weights, Initial Conditions, Hydraulic Model . . . . .	47
10.1	Standard Tresca . . . . .	47
10.2	Generalized Tresca . . . . .	48
10.3	Theoretical and empirical relations for undrained shear strength . . . . .	49
10.4	Strength Reduction . . . . .	52
<b>11</b>	<b>ANISOTROPIC UNDRAINED SHEAR (AUS)</b>	<b>53</b>
	Material . . . . .	53
	Stiffness . . . . .	53
	Strength . . . . .	53
	Tension cut-off, Unit Weights, Initial Conditions, Hydraulic Model . . . . .	53
11.1	Background . . . . .	54
11.2	Undrained shear strengths . . . . .	54
11.2.1	Isotropic strength . . . . .	55
11.2.2	Anisotropic strength . . . . .	57
11.3	Hardening . . . . .	58
11.4	Plastic potential . . . . .	59
11.5	Parameter estimation . . . . .	59
11.5.1	Strengths . . . . .	59
11.5.2	Strains halfway to failure . . . . .	60
11.5.3	Example . . . . .	60
11.6	Governing equations . . . . .	61
11.7	Notes . . . . .	64
11.7.1	Limit analysis . . . . .	64

11.7.2 Strains halfway to failure . . . . .	64
<b>12 HOEK-BROWN</b>	<b>65</b>
Material, Drainage, Stiffness . . . . .	65
Strength . . . . .	65
Flow Rule . . . . .	65
Compression cap, Unit Weights, Initial Stresses, Permeability . . . . .	66
12.1 Strength . . . . .	67
12.2 Elastic parameters . . . . .	72
12.3 Relation to Mohr-Coulomb parameters . . . . .	73
12.4 Strength reduction . . . . .	74
<b>13 GSK</b>	<b>76</b>
Material, Drainage, Stiffness . . . . .	76
Strength . . . . .	76
Flow Rule . . . . .	78
Compression Cap, Unit Weights, Initial Stresses, Permeability . . . . .	78
13.1 Examples of application . . . . .	79
13.2 Strength reduction . . . . .	81
13.3 Notes . . . . .	82
<b>14 BOLTON</b>	<b>83</b>
Material, Drainage, Stiffness . . . . .	83
Strength . . . . .	83
Flow Rule . . . . .	84
Compression Cap, Unit Weights, Initial Conditions, Hydraulic Model . . . . .	84
14.1 Strength reduction . . . . .	84
<b>15 MODIFIED CAM CLAY</b>	<b>86</b>
Stiffness . . . . .	86
Strength . . . . .	88
Initial Conditions . . . . .	90
Unit Weights, Hydraulic Model . . . . .	91
15.1 Limit Analysis and Strength Reduction . . . . .	91
15.1.1 Drained conditions . . . . .	91
15.1.2 Undrained conditions . . . . .	91
15.2 Creep . . . . .	92
<b>16 HARDENING MOHR-COULOMB (HMC)</b>	<b>94</b>
16.1 Typical soil behavior . . . . .	94
Stiffness . . . . .	96
Strength . . . . .	97
Flow rule . . . . .	97
Pressure dependence . . . . .	97
Unit Weights, Initial Conditions, Hydraulic Model . . . . .	97
16.2 Model overview . . . . .	98
16.2.1 Initial state and small-strain stiffness . . . . .	98
16.3 Calibration to Erksak sand . . . . .	100

16.4 Calibration to Lund sand . . . . .	101
16.5 Calibrating $E_{ur}$ and $E_{50}$ . . . . .	102
16.6 Undrained behavior . . . . .	103
16.7 Governing equations . . . . .	103
16.7.1 Pressure dependence . . . . .	104
16.8 Incremental stress-strain relations . . . . .	105
16.9 Limit Analysis and Strength Reduction . . . . .	105
<b>17 LINEAR ELASTIC</b>	<b>106</b>
<b>18 RIGID</b>	<b>107</b>
<b>19 FLUIDS</b>	<b>108</b>
<b>20 PLATES</b>	<b>109</b>
20.1 Plate . . . . .	109
20.2 Rigid Plate . . . . .	110
20.3 Additional features . . . . .	111
<b>21 GEOGRIDS</b>	<b>113</b>
<b>22 CONNECTORS</b>	<b>114</b>
<b>23 HINGES</b>	<b>115</b>
<b>24 PILE ROWS</b>	<b>116</b>
24.1 Piles . . . . .	117
24.2 Soil-Pile Stiffness . . . . .	118
24.3 Soil-Pile Strength . . . . .	118
24.4 Additional properties . . . . .	118
24.5 Base . . . . .	118
24.6 Elastic Zone . . . . .	119
<b>25 NAIL ROWS</b>	<b>121</b>

## 1 STRESS, STRAIN AND SIGN CONVENTIONS

OptumG2 makes use of a global Cartesian coordinate system with  $x$  and  $y$  being the horizontal and vertical axes respectively (see Figure 1). Rotations,  $\theta$ , are counted positive counter-clockwise.

The sign conventions used in OptumG2 are consistent with those used in most of the solid mechanics literature. Stresses are negative in compression and positive in tension (see Figure 1.1). Similarly, negative normal strains correspond to compaction and positive normal strains correspond to dilation.

OptumG2 assumes plane strain conditions. As such, there are four potentially non-zero stress components:

$$(\sigma_x, \sigma_y, \sigma_z, \tau_{xy}, 0, 0) \quad (1.1)$$

and three potentially non-zero strain components:

$$(\varepsilon_x, \varepsilon_y, 0, \gamma_{xy}, 0, 0) \quad (1.2)$$

However, the theory summarized in the following sections is valid in the general three-dimensional setting.

The principal stresses are ordered as:

$$\sigma_1 \leq \sigma_2 \leq \sigma_3 \quad (1.3)$$

That is,  $\sigma_1$  is the most compressive principal stress while  $\sigma_3$  is the least compressive. In many cases, the intermediate principle stress,  $\sigma_2$ , will coincide with the out-of-plane stress  $\sigma_z$ .

Similarly, the principal strains are ordered according to:

$$\varepsilon_1 \leq \varepsilon_2 \leq \varepsilon_3 \quad (1.4)$$

such that  $\varepsilon_1$  and  $\varepsilon_3$  are, respectively, the most and least compressive principal strains. Under plane strain conditions, the intermediate principal strain often coincides with the out-of plane strain,  $\varepsilon_2 = \varepsilon_z = 0$ .

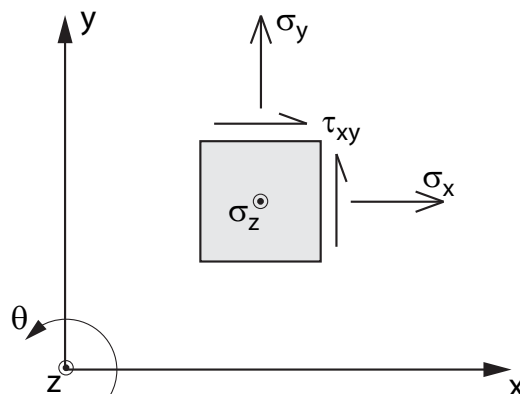


Figure 1.1: Global coordinate system and sign conventions.

## 1.1 Effective stress

For fluid saturated media, stress-strain relationships are usually formulated with respect to *effective stresses*. These are related to the total stresses by

$$\boldsymbol{\sigma}' = \boldsymbol{\sigma} - \mathbf{m}p_f \quad (1.5)$$

where  $\boldsymbol{\sigma}'$  are the effective stresses,  $\boldsymbol{\sigma}$  are the total stresses,  $p_f$  is the fluid pressure (negative in compression) and  $\mathbf{m} = (1, 1, 1, 0, 0, 0)^T$ . The fluid pressures may be given a priori (for example in terms of the hydrostatic pressure distribution underneath the water table) or they may be generated in response to mechanical loading (for example in connection with rapid loading of fine grained materials). The role of pore pressures in soil mechanics is covered in detail in Section 4 of the Theory Manual.



## 2 ELASTICITY

For elastic materials the strains and effective stresses are related to each other in a one-to-one manner, i.e. the strains generated through loading along one stress path will be recovered when unloading along the same stress path. Assuming linear elasticity, the relation between the strains and the effective stresses can be expressed as:

$$\boldsymbol{\varepsilon}^e = \mathbb{C}\boldsymbol{\sigma}' \iff \boldsymbol{\sigma}' = \mathbb{D}\boldsymbol{\varepsilon}^e \quad (2.1)$$

where  $\mathbb{C}$  is the compliance modulus and  $\mathbb{D}$  is the stiffness modulus.

### 2.1 Isotropic elasticity

The most common assumption regarding the stiffness of geomaterials is that of isotropy, i.e. that the properties are the same in all directions, e.g. vertically and horizontally. In this case, the compliance and stiffness moduli, may be expressed either in terms of Young's modulus  $E$  and Poisson's ratio  $\nu$  or in terms of bulk modulus  $K$  and shear modulus  $G$ . The compliance modulus is given by

$$\mathbb{C} = \frac{1}{E} \begin{bmatrix} 1 & -\nu & -\nu & & & \\ -\nu & 1 & -\nu & & & \\ -\nu & -\nu & 1 & & & \\ & & & 2(1+\nu) & & \\ & & & & 2(1+\nu) & \\ & & & & & 2(1+\nu) \end{bmatrix} \quad (2.2)$$

or equivalently by:

$$\mathbb{C} = \begin{bmatrix} \frac{1}{9}K^{-1} + \frac{1}{3}G^{-1} & \frac{1}{9}K^{-1} - \frac{1}{6}G^{-1} & \frac{1}{9}K^{-1} - \frac{1}{6}G^{-1} & & & \\ \frac{1}{9}K^{-1} - \frac{1}{6}G^{-1} & \frac{1}{9}K^{-1} + \frac{1}{3}G^{-1} & \frac{1}{9}K^{-1} - \frac{1}{6}G^{-1} & & & \\ \frac{1}{9}K^{-1} - \frac{1}{6}G^{-1} & \frac{1}{9}K^{-1} - \frac{1}{6}G^{-1} & \frac{1}{9}K^{-1} + \frac{1}{3}G^{-1} & & & \\ & & & G^{-1} & & \\ & & & & G^{-1} & \\ & & & & & G^{-1} \end{bmatrix} \quad (2.3)$$

where

$$K = \frac{E}{3(1-2\nu)}, \quad G = \frac{E}{2(1+\nu)} \quad (2.4)$$

The stiffness modulus is given by:

$$\mathbb{D} = \frac{E}{(1+\nu)(1-2\nu)} \begin{bmatrix} 1-\nu & \nu & \nu & & & \\ \nu & 1-\nu & \nu & & & \\ \nu & \nu & 1-\nu & & & \\ & & & \frac{1}{2}(1-2\nu) & & \\ & & & & \frac{1}{2}(1-2\nu) & \\ & & & & & \frac{1}{2}(1-2\nu) \end{bmatrix} \quad (2.5)$$

or equivalently by:

$$\mathbb{D} = \begin{bmatrix} K + \frac{4}{3}G & K - \frac{2}{3}G & K - \frac{2}{3}G & & & \\ K - \frac{2}{3}G & K + \frac{4}{3}G & K - \frac{2}{3}G & & & \\ K - \frac{2}{3}G & K - \frac{2}{3}G & K + \frac{4}{3}G & & & \\ & & & G & & \\ & & & & G & \\ & & & & & G \end{bmatrix} \quad (2.6)$$

The relations between  $E$ ,  $\nu$ ,  $K$ , and  $G$  are summarized in the table below.

	$E =$	$\nu =$	$K =$	$G =$
$(E, \nu)$	$E$	$\nu$	$\frac{E}{3(1 - 2\nu)}$	$\frac{E}{2(1 + \nu)}$
$(K, G)$	$\frac{9KG}{3K + G}$	$K - \frac{2G}{3}$	$K$	$G$

Table 2.1: Relation between elastic parameters.

### 2.1.1 Undrained conditions

Under undrained conditions, the relation between the elastic strains and the total pressures can be shown to be given by (see the Theory Manual)

$$\epsilon^e = \mathbb{C}_u \sigma \quad (2.7)$$

where

$$\mathbb{C}_u = \frac{1}{E_u} \begin{bmatrix} 1 & -\frac{1}{2} & -\frac{1}{2} & & & \\ -\frac{1}{2} & 1 & -\frac{1}{2} & & & \\ -\frac{1}{2} & -\frac{1}{2} & 1 & & & \\ & & & 3 & & \\ & & & & 3 & \\ & & & & & 3 \end{bmatrix} = \frac{1}{3G} \begin{bmatrix} 1 & -\frac{1}{2} & -\frac{1}{2} & & & \\ -\frac{1}{2} & 1 & -\frac{1}{2} & & & \\ -\frac{1}{2} & -\frac{1}{2} & 1 & & & \\ & & & 3 & & \\ & & & & 3 & \\ & & & & & 3 \end{bmatrix}$$

where

$$E_u = \frac{3E}{2(1 + \nu)} \quad (2.8)$$

is the undrained Young's modulus.

This is the elastic law used for the Tresca material (Set A requiring input of  $E_u$  and Set B requiring input of  $G$ ).

## 2.2 Anisotropic elasticity

As a result of their deposition, natural soils often display cross-anisotropy with the elastic parameters differing between the vertical and horizontal directions. It may be shown that the most general cross-anisotropic elasticity model will involve a total of five parameters. Alternatively, a simplified model that accounts for the basic features of the anisotropy may be used. One such model has been proposed by Graham and Houlsby (1983). In addition to two elasticity parameters this model involves one additional parameter that acts as a measure of the anisotropy. The stress-strain relation of the Graham-Houlsby may be expressed as:

$$\begin{pmatrix} \varepsilon_{xx} \\ \varepsilon_{yy} \\ \varepsilon_{zz} \\ \gamma_{xy} \\ \gamma_{yz} \\ \gamma_{zx} \end{pmatrix} = \frac{1}{E_{yy}} \begin{bmatrix} 1/\alpha^2 & -\nu_{xy} & -\nu_{xy}/\alpha \\ -\nu_{xy} & 1 & -\nu_{xy} \\ -\nu_{xy}/\alpha & -\nu_{xy} & 1/\alpha^2 \\ & & & 2(1 + \alpha\nu_{xy})/\alpha \\ & & & & 2(1 + \alpha\nu_{xy})/\alpha \\ & & & & & 2(1 + \alpha\nu_{xy})/\alpha^2 \end{bmatrix} \begin{pmatrix} \sigma'_{xx} \\ \sigma'_{yy} \\ \sigma'_{zz} \\ \tau_{xy} \\ \tau_{yz} \\ \tau_{zx} \end{pmatrix}$$

where  $E_{yy}$  is the Young's modulus measured in the  $y$ -direction,  $\nu_{xy}$  is the Poisson's ratio in the  $x$ -direction to strain applied in the  $y$ -direction, and  $\alpha$  is an anisotropy parameter. For thermodynamic consistency, it may be shown that the Poisson's ratio should be limited to

$$-1 \leq \alpha\nu_{xy} \leq \frac{1}{2} \quad (2.9)$$

Alternatively, the above relation may be written as:

$$\begin{pmatrix} \varepsilon_{xx} \\ \varepsilon_{yy} \\ \varepsilon_{zz} \\ \gamma_{xy} \\ \gamma_{yz} \\ \gamma_{zx} \end{pmatrix} = \frac{1}{E_{yy}} \begin{bmatrix} 1/\alpha^2 & -\nu_{xy} & -\nu_{xy}/\alpha \\ -\nu_{xy} & 1 & -\nu_{xy} \\ -\nu_{xy}/\alpha & -\nu_{xy} & 1/\alpha^2 \\ & & & E_{yy}/G_{xy} \\ & & & & E_{yy}/G_{xy} \\ & & & & & E_{yy}/G_{xx} \end{bmatrix} \begin{pmatrix} \sigma'_{xx} \\ \sigma'_{yy} \\ \sigma'_{zz} \\ \tau_{xy} \\ \tau_{yz} \\ \tau_{zx} \end{pmatrix}$$

where

$$G_{xy} = \frac{2(1 + \alpha\nu_{xy})E_{yy}}{\alpha}, \quad G_{xx} = \frac{2(1 + \alpha\nu_{xy})E_{yy}}{\alpha^2} \quad (2.10)$$

The anisotropy parameter,  $\alpha$ , can be related to the Young's moduli as well as the shear moduli in the different directions:

$$\alpha = \sqrt{\frac{E_{xx}}{E_{yy}}} = \frac{G_{xx}}{G_{xy}} \quad (2.11)$$

where  $E_{xx}$  and  $E_{yy}$  are the Young's moduli measured in the two directions,  $G_{xx}$  is the shear modulus in any plane perpendicular to the  $y$ -direction and  $G_{xy}$  is the shear modulus in any plane parallel to the  $y$ -direction.

### 3 ELASTOPLASTICITY

OptumG2 makes extensive use of the theory of elastoplasticity in the formulation of constitutive models. In standard laboratory tests such as triaxial compression tests, these models imply an initially elastic response at low levels of loading. This is followed by the accumulation of plastic, or irreversible strains, up to a point where the stress level either asymptotes towards a steady state or - in some cases - drops to a lower level. The typical stress-strain response for an elastoplastic material is shown in Figure 3.1.

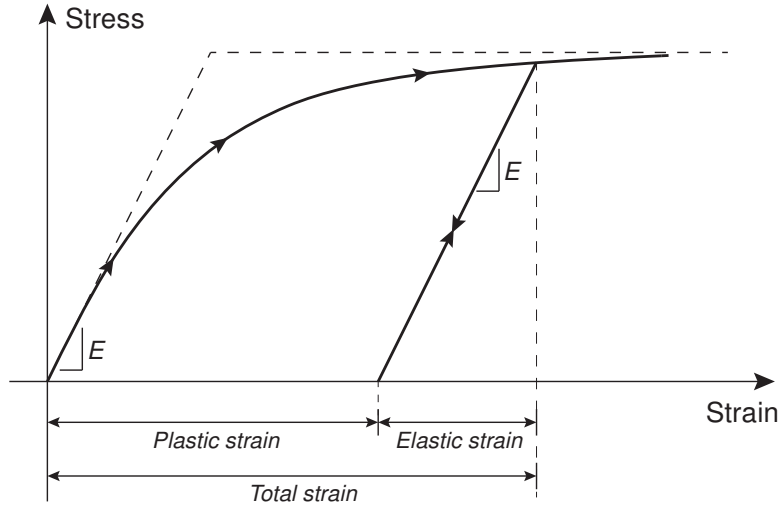


Figure 3.1: Stress-strain behaviour of an elastoplastic material.

In the following, the theory of elastoplasticity will briefly be reviewed before the various material types available in OptumG2 will be documented in detail.

#### 3.1 Additive decomposition

The fundamental assumption in elastoplasticity theory is the additive decomposition of elastic and plastic strains (see Figure 3.1):

$$\boldsymbol{\varepsilon} = \boldsymbol{\varepsilon}^e + \boldsymbol{\varepsilon}^p \quad (3.1)$$

where  $\boldsymbol{\varepsilon}$  are the total strains,  $\boldsymbol{\varepsilon}^e$  are the elastic strains and  $\boldsymbol{\varepsilon}^p$  are the plastic strains.

#### 3.2 Elasticity

Assuming linear elasticity, the elastic strains are related to the effective stresses via Hooke's law:

$$\boldsymbol{\varepsilon}^e = \mathbb{C}\boldsymbol{\sigma}' \iff \boldsymbol{\sigma}' = \mathbb{D}\boldsymbol{\varepsilon}^e \quad (3.2)$$

where  $\mathbb{C}$  is the compliance modulus and  $\mathbb{D}$  is the stiffness modulus (see Section 2). This law is often stated in incremental form, but holds also in terms of total quantities of effective stress and elastic strain.

### 3.3 Flow rule

The plastic strains are related to the stresses via a flow rule that usually is expressed as

$$\dot{\epsilon}^p = \dot{\lambda} \frac{\partial G}{\partial \sigma'} \quad (3.3)$$

where  $G$  is the flow potential,  $\dot{\lambda} \geq 0$  is a scalar (the so-called plastic multiplier), and a superposed dot indicates incremental quantities.

### 3.4 Yield function

The stresses are limited by the yield function. This is always a function of the stresses but may also involve various additional variables to account for hardening. The yield function can thus be written as

$$F(\sigma', \kappa) \quad (3.4)$$

where  $\sigma'$  are the effective stresses and  $\kappa$  is a set of stress-like hardening variables. The yield function is specified such that  $F < 0$  corresponds to purely elastic states while  $F = 0$  indicates yielding. States leading to  $F > 0$  are not permissible under any circumstances. Although many models make use of only one yield function, it is in principle possible to incorporate an arbitrary number into a single model.

### 3.5 Hardening rule

The evolution of the hardening variable  $\kappa$  is specified via a hardening rule which in general can be written as

$$\dot{\kappa} = \dot{\lambda} \mathbf{h}(\sigma', \kappa) \quad (3.5)$$

where  $\mathbf{h}$  is the hardening function.

### 3.6 Complementarity conditions

The plastic multiplier,  $\dot{\lambda}$ , must be such that it is non-zero only for stress states corresponding to yielding. This requirement can be expressed via the complementarity conditions:

$$F(\sigma', \kappa) \leq 0, \quad \dot{\lambda} \geq 0, \quad \dot{\lambda} F(\sigma', \kappa) = 0 \quad (3.6)$$

### 3.7 Initial stresses

Nonlinear boundary value problems generally require knowledge of the initial state. In geotechnics, the initial stress state is often characterized by the earth pressure coefficient  $K_0$  which relates the vertical and horizontal stress components by:

$$K_0 = \frac{\sigma'_h}{\sigma'_v} \quad (3.7)$$

where  $\sigma'_h = \sigma'_x = \sigma'_z$  and  $\sigma'_v = \sigma'_y$  are the horizontal and vertical effective stresses respectively. In OptumG2,  $K_0$  is a material parameter which can be used to specify the initial stresses according to the relation above. Furthermore, an additional parameter  $\sigma_0$  can be specified such that the horizontal and vertical stresses can be related by

$$\sigma'_h = K_0 \sigma'_v + \sigma_0 \quad (3.8)$$

## 4 HYDRAULIC MODELS

Variably saturated flow through porous media can be described by the mass balance equation

$$n \frac{\partial S}{\partial t} + \nabla^T \mathbf{q} = 0 \quad (4.1)$$

supplemented with the generalized Darcy's law

$$\mathbf{q} = -K_r \mathbf{K} \nabla h_s = -K_r \mathbf{K} \nabla \left( y - \frac{p_w}{\gamma_w} \right) \quad (4.2)$$

where:

$n$  = Porosity

$S$  = Degree of saturation

$\mathbf{q} = (q_x, q_y)^T$  = Fluid velocity [m/day]

$\mathbf{K}$  = Saturated hydraulic conductivity modulus [m/day]

$K_r$  = Relative hydraulic conductivity which is a function of degree of saturation

$y$  = Vertical coordinate

$\gamma_w$  = Unit weight of water (= 9.8 kN/m<sup>3</sup>)

$p_s$  = Pressure

$h_s$  = Head (=  $y - p_s/\gamma_w$ )

Combining (4.1) and (4.2) leads to what is sometimes (especially in 1D) called Richards equation:

$$n \frac{\partial S}{\partial t} = \nabla^T \left[ K_r \mathbf{K} \nabla \left( y - \frac{p_s}{\gamma_w} \right) \right] \quad (4.3)$$

Typical values of hydraulic conductivity for different materials are shown in Figure 4.1.

$K$ (cm/s)	10 <sup>2</sup>	10 <sup>1</sup>	1	10 <sup>-1</sup>	10 <sup>-2</sup>	10 <sup>-3</sup>	10 <sup>-4</sup>	10 <sup>-5</sup>	10 <sup>-6</sup>	10 <sup>-7</sup>	10 <sup>-8</sup>	10 <sup>-9</sup>	10 <sup>-10</sup>
$K$ (m/day)	10 <sup>5</sup>	10 <sup>4</sup>	1,000	100	10	1	0.1	0.01	10 <sup>-3</sup>	10 <sup>-4</sup>	10 <sup>-5</sup>	10 <sup>-6</sup>	10 <sup>-7</sup>
	Permeable			Semi-Permeable				Impermeable					
Unconsolidated Sand & Gravel	Gravel		Well Sorted Sand or Sand & Gravel		Fine Sand, Silt, Loess, Loam								
Unconsolidated Clay & Organic					Peat		Layered Clay		Fat/Unweathered Clay				
Consolidated Rocks	Highly Fractured Rocks				Oil Reservoir Rocks		Sandstone		Limestone, Dolomite		Granite		

Figure 4.1: Typical values of hydraulic conductivity  $K = K_x = K_y$ .

Besides the constants  $n$  and  $\mathbf{K}$ , the solution of this equation requires the relative hydraulic conductivity relation and the saturation-pressure relation (also known as the water retention curve or the soil water characteristic curve).

In OptumG2, the saturated hydraulic conductivity modulus is always given by

$$\mathbf{K} = \begin{bmatrix} K_x & \\ & K_y \end{bmatrix} \quad (4.4)$$

where  $K_x$  and  $K_y$  are the saturated hydraulic conductivities in the  $x$  and  $y$  directions respectively.

The relative hydraulic conductivity relation and the retention curve are given by one of three available models described below.

#### 4.1 Linear model

The Linear model is a single-parameter model which approximates the degree of saturation,  $S$ , by (see Figure 4.2):

$$S = \begin{cases} 0 & \text{for } \hat{h} \leq -h^* \\ 1 + \hat{h}/h^* & \text{for } -h^* < \hat{h} < 0 \\ 1 & \text{for } \hat{h} \geq 0 \end{cases} \quad (4.5)$$

where  $\hat{h} = -p/\gamma_w$  is the pressure head at zero elevation (note that the pore pressure  $p$  is negative in the fully saturated range) and  $h^*$  is a material parameter, the default value of which is  $h^* = 0.5$  m.

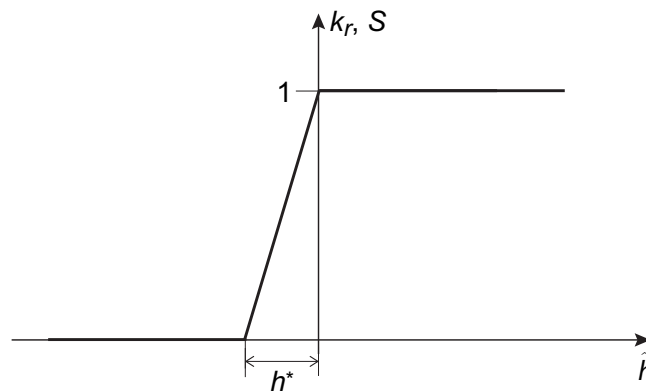


Figure 4.2: Hydraulic model Linear.

The relative hydraulic conductivity is taken simply as the degree of saturation:

$$K_r = S \quad (4.6)$$

#### 4.2 Tanh relative hydraulic conductivity model

The Tanh model is a single-parameter model which approximates the degree of saturation as:

$$S = \frac{1}{2} \left[ 1 + \tanh \left( \frac{2\hat{h}}{h^*} \right) \right] \quad (4.7)$$

where the parameter  $h^*$  specifies the approximate range over which  $S$  increases from zero to 1 (see Figure 4.3). The default value of the model parameter is  $h^* = 0.5$  m.

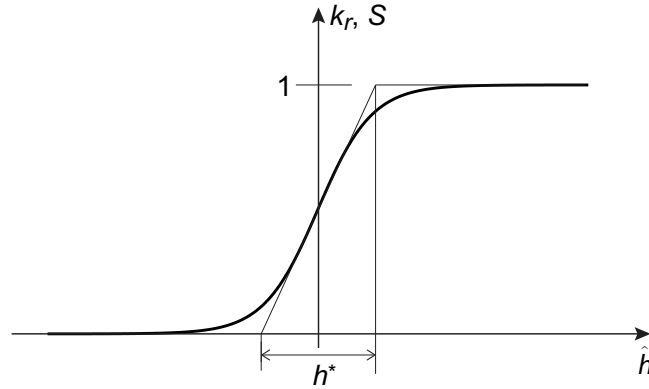


Figure 4.3: Hydraulic model Tanh.

As with the Linear model, the Tanh model takes the degree of saturation as the relative hydraulic conductivity:

$$K_r = S \quad (4.8)$$

### 4.3 van Genuchten model

The van Genuchten model is the most widely used hydraulic model in the soil sciences. It relates degree of saturation to pressure head by:

$$S = \begin{cases} S_r + (S_s - S_r) \left(1 + |\alpha \hat{h}|^n\right)^{-m} & \text{for } \hat{h} \leq 0 \\ S_s & \text{for } \hat{h} > 0 \end{cases} \quad (4.9)$$

where  $\hat{h} = -p/\gamma_w$ ,  $m = 1 - 1/n$  and:

$S_r$  = Residual degree of saturation (may be slightly greater than 0).

$S_s$  = Fraction of water filled pores at full saturation (may be slightly less than 1).

$\alpha$  [ $\text{m}^{-1}$ ] = Model parameter related to the air entry pressure.

$n$  = Model parameter related to the rate at which water is extracted from the soil once the air entry pressure has been exceeded.

The relative hydraulic conductivity is related to the effective saturation,  $S_e$ , as:

$$K_r = \begin{cases} S_e^{1/2} \left[1 - \left(1 - S_e^{1/m}\right)^m\right]^2 & \text{for } S_e < 1 \\ 1 & \text{for } S_e = 1 \end{cases} \quad (4.10)$$

where

$$S_e = \frac{S - S_r}{S_s - S_r}. \quad (4.11)$$



Alternatively,  $K_r$  can be expressed in terms of  $\hat{h}$  as:

$$K_r = \begin{cases} \frac{\left[1 - |\alpha \hat{h}|^{n-1} (1 + |\alpha \hat{h}|^n)^{-m}\right]^2}{(1 + |\alpha \hat{h}|^n)^{m/2}} & \text{for } \hat{h} \leq 0 \\ 1 & \text{for } \hat{h} > 0 \end{cases} \quad (4.12)$$

Typical values of the parameters  $n$  and  $\alpha$  are given in Table 4.1 and typical retention and relative hydraulic conductivity curves are shown in Figure 4.4.

Material	No. of Samples	Clay Content		$n$		$\alpha$ ( $\text{m}^{-1}$ )	
		Min	Max	Min	Max	Min	Max
Sand	2	14	18	2.22	2.56	2.74	2.65
Loamy sand	10	23	108	1.33	2.56	4.41	2.35
Sandy loam	11	70	178	1.12	2.38	4.90	1.27
Sandy clay loam	15	208	349	1.06	1.85	3.92	1.47
Loam	7	122	260	1.23	1.96	4.90	1.76
Silt loam	5	120	270	1.14	1.25	9.60	1.47
Silty clay loam	8	280	390	1.14	1.43	8.82	0.98
Clay loam	6	304	348	1.05	1.64	4.90	0.78
Sandy clay	5	352	421	1.10	1.49	4.90	1.76
Silty clay	2	420	460	1.09	1.10	6.37	5.39
Clay	1	452	452	1.51	1.51	0.88	0.88

Table 4.1: Soil properties of 72 samples collected from the literature and the fitted van Genuchten model  $n$  and  $\alpha$  (after Ghanbarian-Alavijeh et al. 2010).

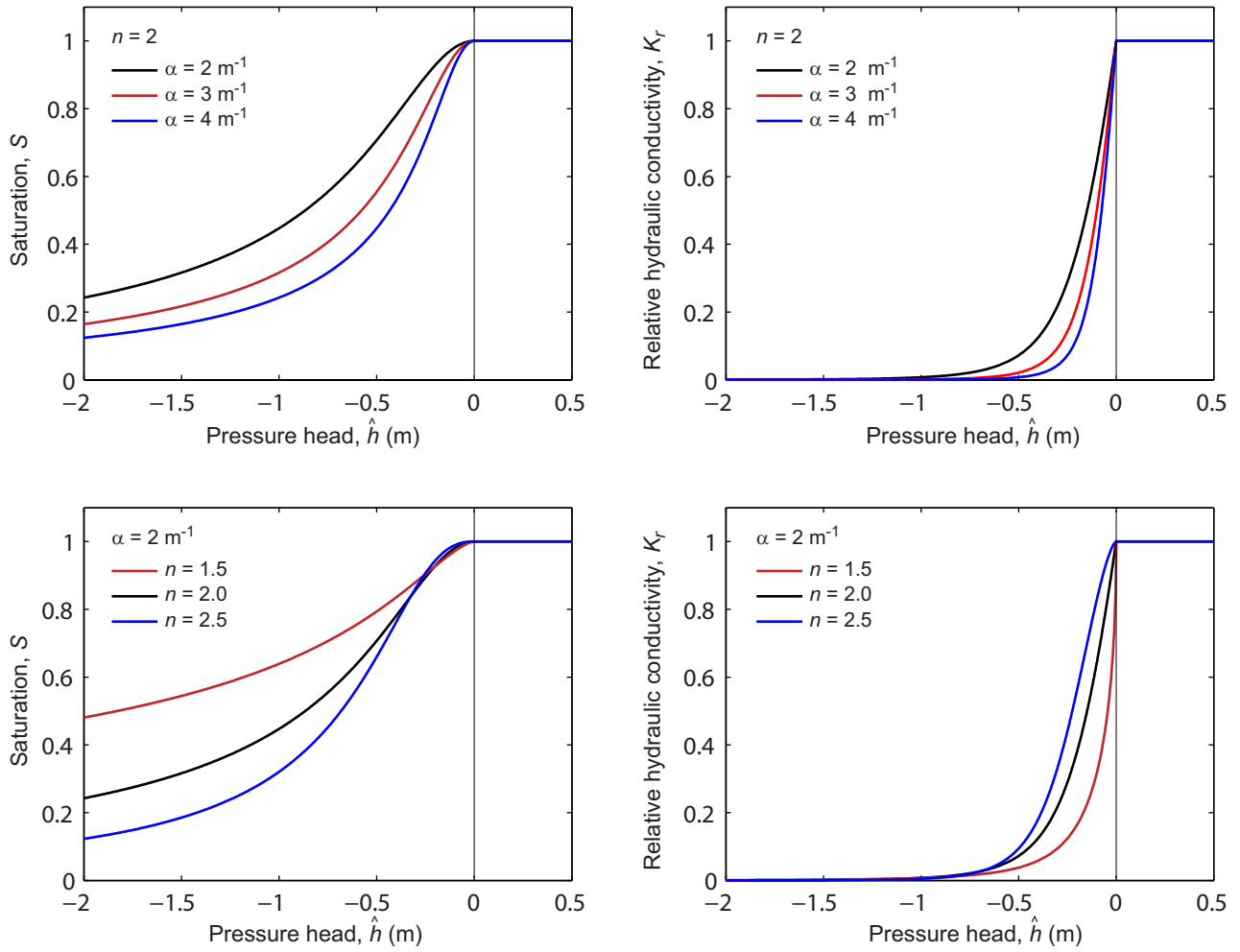


Figure 4.4: Dependence of  $S(\hat{h})$  and  $K_r(\hat{h})$  on  $\alpha$  (top) and  $n$  (bottom).

## 5 COMMON PROPERTIES

The materials available in OptumG2 are grouped into six different material categories:

1. *Solids* for the modeling of solid materials (soil, rock, concrete, etc) and interfaces between such materials.
2. *Fluids* for the modeling of bodies of water and other fluids.
3. *Plates* for the modeling of foundation plates, sheet pile walls and other structures that can be idealized as one-dimensional elements in the  $x$ - $y$  plane.
4. *Geogrids* for the modeling of geogrids or similar elements that cannot sustain tension.
5. *Connectors* for the modeling of fixed-end anchors and plate-to-plate connections.
6. *Hinges* for the modeling of hinges in Plates.

Each material category contains a one or more material types. For example, the material types within the Solids category include the *Mohr-Coulomb*, *Drucker-Prager*, and *Hoek-Brown* material types. These represent general models and can be further specialized to represent particular materials, for example the *Loose Sand-MC*, *Firm Clay-MC* and *Loose Sand-HMC* materials that are available as predefined materials.

In OptumG2, the properties of any material can be gauged either by selecting the geometric object (surface, line, point) to which it has been assigned or by selecting the material in the Materials ribbon. This will bring up a property window located on the right hand side of the canvas. The properties of the material are here organized into a number of different categories, of which *Material* is common to all materials. Some examples are shown in Figure (5.1).



Figure 5.1: Properties of three materials belonging to the Solids (left), Beams (center) and Geogrids (right) categories respectively.

### Material

The Material category contains the following properties:

- **Name:** the name of the material. This field is editable and any changes will be reflected in the ribbon and throughout the project.
- **Category:** material category (non-editable).
- **Color:** Material color. This field is editable and any changes will be reflected in the ribbon and throughout the project.
- **Material Type.** Examples for Solids include Mohr-Coulomb, Drucker-Prager, and Hoek-Brown.

- Reducible Strength (Yes/No). Determines whether or not the strength parameters of a given material will be reduced in the course of Strength Reduction analysis (see the Analysis Manual).

Besides the common properties, each material type involves a certain number of more specific properties that describe the strength, stiffness, hydraulic conductivity, etc. These will be described in detail for each material type in what follows.

## 6 DRAINAGE

OptumG2 requires that a Drainage condition is specified for each Solid material. There are three possible settings: Drained/Undrained, Always Drained, and Non-Porous. Moreover, for each analysis (each stage), a Time Scope must be chosen. There are two possibilities: Short Term or Long Term. These two settings, Drainage Condition and Time Scope, determine whether the material behaves in a drained or an undrained manner. The basic idea is that some materials behave in an undrained manner in the short term (e.g. clay) while others always behave as drained both in the short term and in the long term (e.g. sand).

The rules for whether a given point in the domain behaves in a drained or an undrained manner are summarized in the table below.

	Drained/Undrained	Always Drained	Non-Porous
Short Term	Undrained	Drained	Drained
Long Term	Drained	Drained	Drained

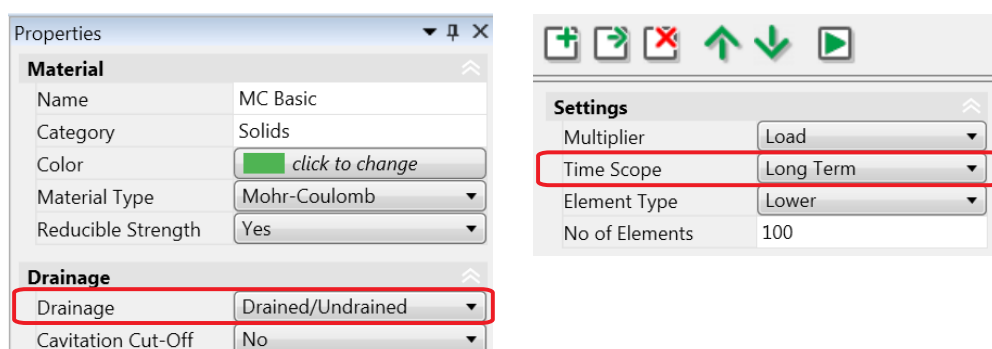


Figure 6.1: Material behavior as function of Drainage and Time Scope.

### 6.1 Cavitation Cut-Off

Under undrained conditions, materials that tend to dilate will produce positive (tensile) excess pore pressures. Under standard conditions, the magnitude of the total pore pressure cannot exceed the atmospheric pressure. This constraint can be imposed via the Cavitation Cut-Off option, see Figure 6.2. Setting Cavitation Cut-Off = Yes, gives the possibility to specify a cavitation pressure,  $p_{cav}$ , such that the total pore pressure is limited by

$$p_s + p_e \leq p_{cav} \quad (6.1)$$

where  $p_s$  and  $p_e$  are the seepage and excess pore pressures respectively. Once  $p_s + p_e = p_{cav}$ , the behaviour becomes effectively drained and volume is no longer preserved. Note that tensile pore pressure are positive consistent with the sign convention adopted for stress and strain.

Cavitation cut-offs are only relevant for Elastoplastic and Multiplier Elastoplastic analysis and are ignored for all other analysis types.

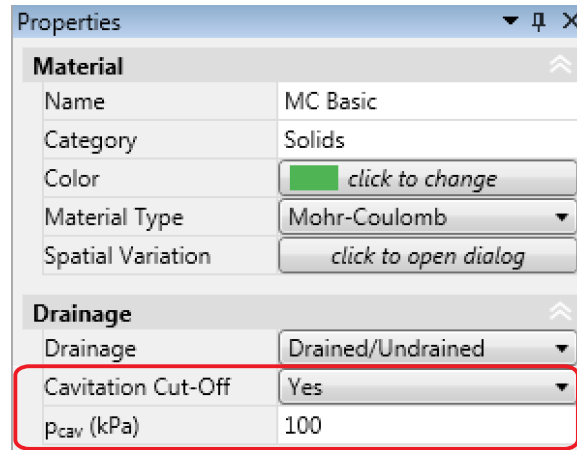


Figure 6.2: Material with Cavitation Cut-Off.

## 6.2 Relation to “Method A, B, C”

Undrained analysis can be carried out in a number of ways of which the three most common are (see Theory Manual, Section 4):

- Use the original drained parameters – for Mohr-Coulomb  $E$ ,  $\nu$ ,  $c$ , and  $\phi$  – in a coupled deformation-excess pore pressure calculation. This is the most general and in many ways the theoretically most satisfactory approach.
- Use drained stiffness parameters and undrained strength parameters – for Mohr-Coulomb  $E$ ,  $\nu$ , and  $s_u$  – in a coupled deformation-excess pore pressure calculation. This is a rather awkward hybrid approach that generally is not recommended. Note also that even though excess pore pressures are calculated, these are not in general representative of the actual excess pore pressures.
- Use undrained parameters for both stiffness and strength – for Mohr-Coulomb  $E_u$  and  $s_u$  – in which case only a standard deformation analysis without excess pore pressures is necessary.

These three approaches are often referred to as Method A, B and C respectively.

In OptumG2, the three different approaches can easily be accommodated. The table below summarizes the relevant settings for a Mohr-Coulomb material with Drainage = Drained/Undrained. It is noted that while undrained analysis according to ‘Method C can be carried out with the Mohr-Coulomb model, the Tresca model caters specifically for this approach. In particular, the use of Tresca allows for the specification of the shear stiffness  $G$  while the use of Mohr-Coulomb requires that the undrained Young’s modulus be specified (along with a Poisson’s ratio equal to 0.5). Moreover, the use of Tresca allows for a separate partial factor to be applied to the undrained shear strength,  $s_u$ , when using Design Approaches. In conclusion, the recommendations for undrained analysis are:

- Use either the original model, e.g. Mohr-Coulomb, with drained parameters and Time Scope = Short Term (corresponding to Method A), or
- Use the Tresca model with undrained parameters (corresponding to Method C).

	<b>Stiffness</b>	<b>Strength</b>	<b>Time Scope</b>
<b>Method A</b>	$E, \nu$	$c, \phi$	Short Term
<b>Method B</b>	$E, \nu$	$c = s_u, \phi = 0$	Short Term
<b>Method C</b>	$E = E_u, \nu = 0.5$	$c = s_u, \phi = 0$	Any
	$E_u$ or $G$ (Tresca)	$s_u$ (Tresca)	

Table 6.1: Settings for undrained analysis of Drained/Undrained Mohr-Coulomb material.

Note that while the former approach implies a distribution of undrained shear strength that may or may not be in accordance with what is observed in the field (see Section 8.4.2), the latter approach specifies the distribution of undrained shear strength directly.





## 7 SPATIAL VARIATION OF PARAMETERS

OptumG2 contains a number of options for varying the material parameters spatially. When selecting a material input field in the property grid, two buttons appear on the left: a calculator and a table. Selecting the table opens a window in which the variation of the material parameters can be specified. The following options are available:

- Constant: the trivial option of a constant value of the parameter throughout.
- Gradient: for specifying a linear variation.
- Profile: for specifying the an arbitrary variation with depth via a sequence of points.
- Map: for specifying an arbitrary variation throughout x-y space via a sequence of points.

The three last options are described in below.

### 7.1 Gradient

The gradient option requires a reference value of the parameter ( $V_{ref}$ ), two reference points ( $x_{ref}$  and  $y_{ref}$ ), two gradients (x-grad and y-grad).

$$V(x, y) = V_{ref} + xgrad(x - x_{ref}) + ygrad(y - y_{ref}) \tag{7.1}$$

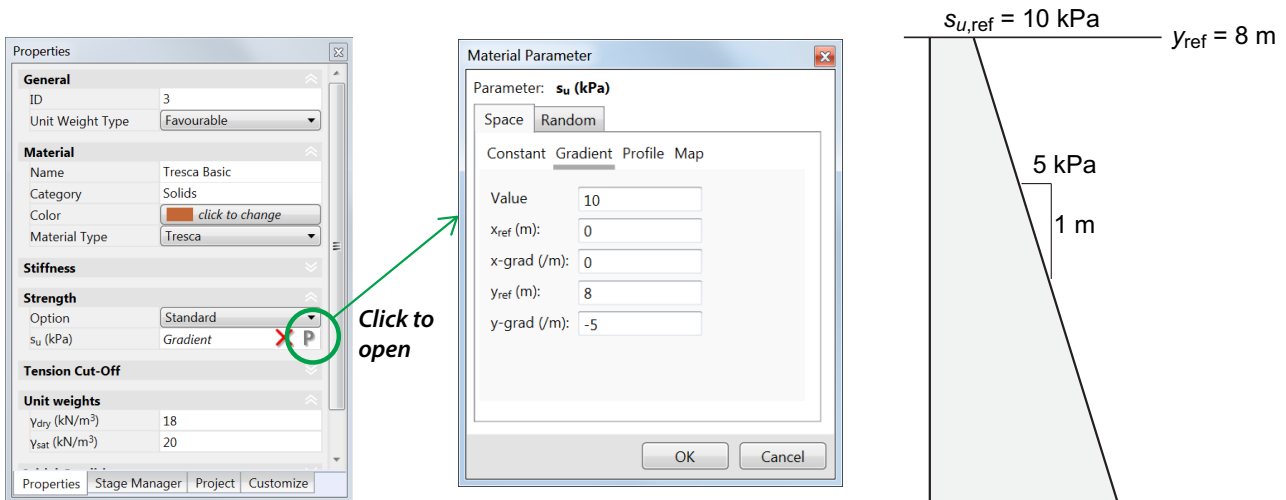


Figure 7.1: Specification of linear distribution of material parameter using Gradient.

An example is shown above. The resulting distribution of the parameter  $s_u$  is here given by

$$s_u(x, y) = s_u(y) = 10 - 5(y - 8) \tag{7.2}$$

In other words,  $s_u$  varies linearly with depth while there is no variation horizontally.

Note that the right-handed coordinate system used in OptumG2 implies a negative gradient for parameters that increase with depth. It is strongly advised that spatially varying material parameters be verified by the Material Parameters tool under the Results ribbon.

### 7.2 Profile

The Profile option offers a flexible way of specifying arbitrary variations of material parameters with depth. This done by specifying points (y, value) in the table under Profile. An example is shown below.

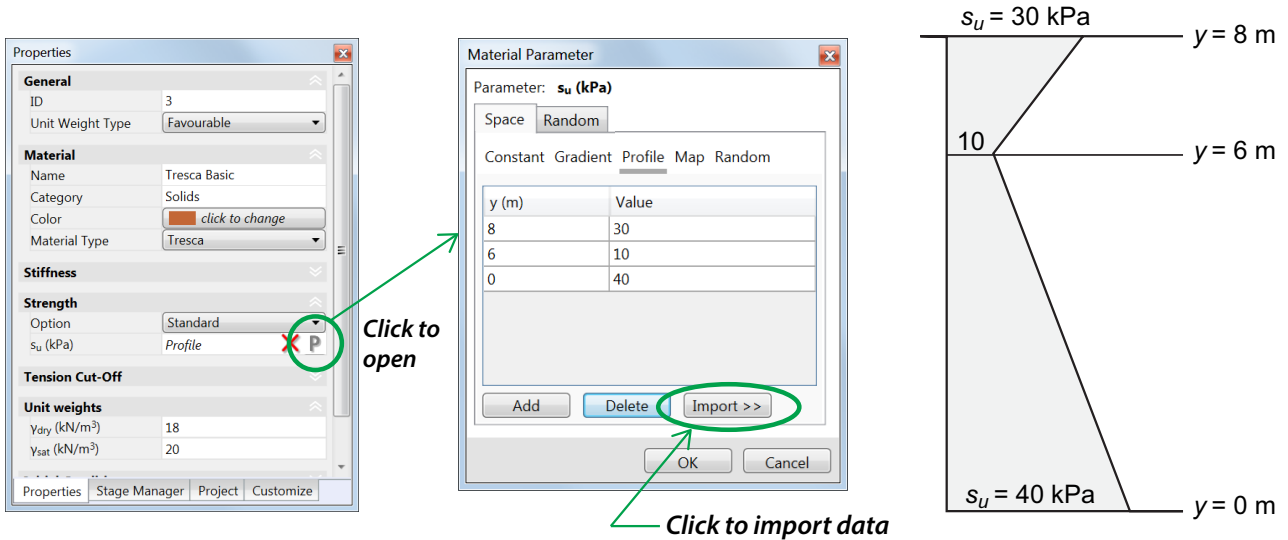


Figure 7.2: Specification of material parameter variation with depth using Profile.

The data may be entered manually or imported from an MS Excel or similar file.

### 7.3 Map

This is the most general option for defining material data. Data in the form (x, y, value) are specified as shown below.

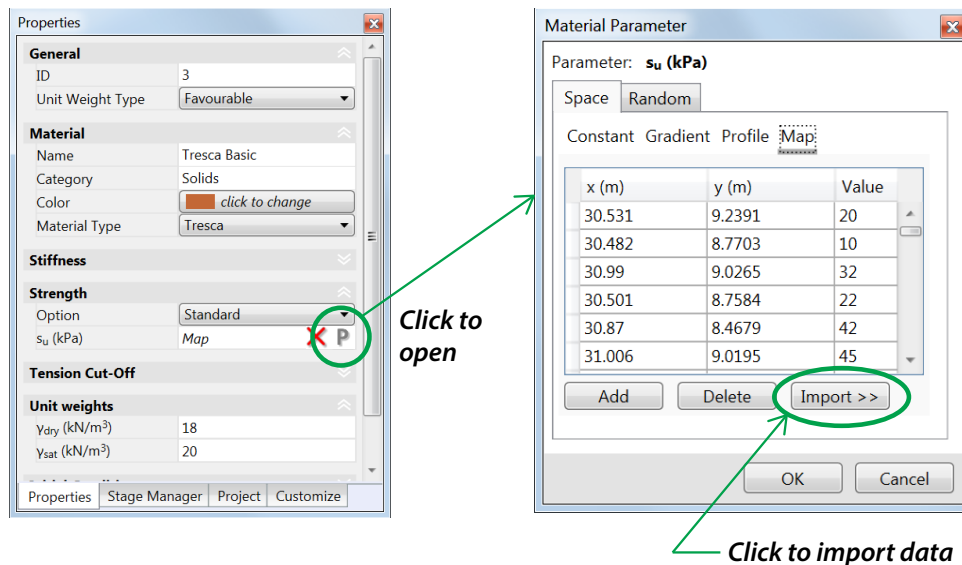


Figure 7.3: Specification of general material parameter distribution using Map.

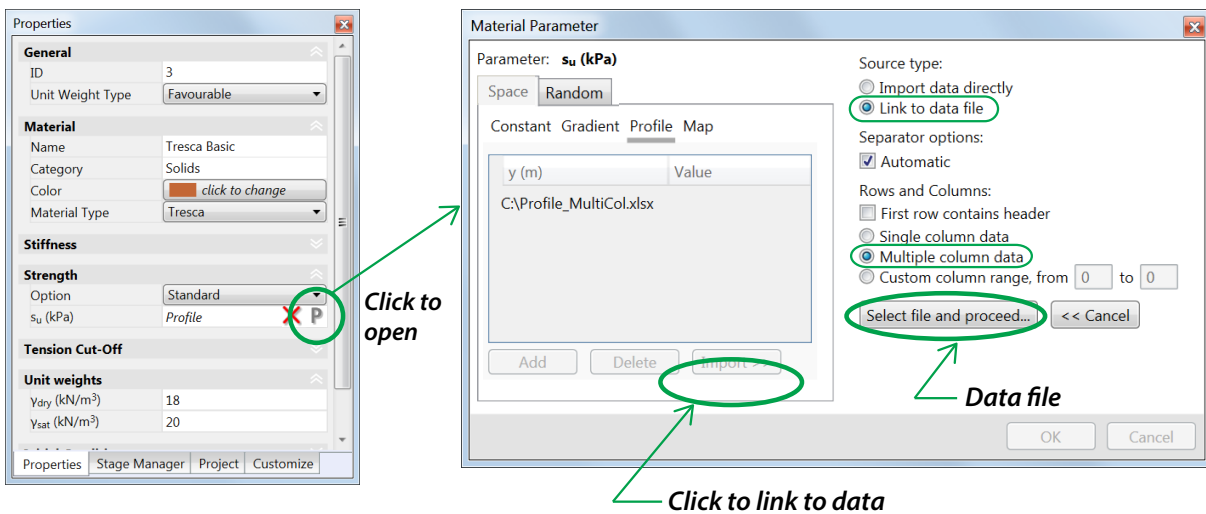
As for Profile, data may be added manually or imported from an MS Excel file.

### 7.4 Multiple data sets

For Profile and Map, it is possible to specify multiple data sets for the same material parameter, for example two different profiles which will be processed in the course of two separate analyses.

The specification of multiple data sets is sketched in Figure 7.4. When opening the Material Parameter dialog, Import is clicked and the option *Link to data file* is selected under Source type. Next, the option *Multiple column data* is selected under Rows and Columns. Finally, the data file is selected.

The data file is of the same format as standard Profile or Map data files but may contain more than one column of material data (see Figure 7.4).



The image shows a Microsoft Excel spreadsheet with two columns of data labeled 'Set 1' and 'Set 2'. The first column is labeled 'y-coord' and contains values from 1 to 7. The second column is labeled 'Set 1' and contains values 10, 9, 8, 7, 6, 5, 4. The third column is labeled 'Set 2' and contains values 0, 1, 2, 3, 4, 5, 6. The spreadsheet is titled 'Book1 - Microsoft Excel'.

	A	B	C	D	E	F	G	H	I	J
1	10	0	0							
2	9	1	2							
3	8	2	4							
4	7	3	6							
5	6	4	8							
6	5	5	10							
7	4	6	12							

Figure 7.4: Specification of material parameters via linked data file (top) and example of multi-column Profile data file (bottom).

The linked data option is well suited for parameter studies where the sensitivity of various quantities (bearing capacity, settlement, etc) to the material parameters is sought quantified.

## 8 MOHR-COULOMB

The Mohr-Coulomb material is a solid material that may be applied both to surfaces and to lines. In the latter case the line will act as a *Shear Joint*. The Mohr-Coulomb material assumes linear elasticity and a yield function defined by two parameters, cohesion and friction angle. The flow rule is generally nonassociated and defined by a dilation angle and, optionally, a dilation cut-off. In addition, it is possible to specify a tension cut-off and a compression cap. The various parameters can be accessed via the property window. They have been grouped into a number of categories that in the following will be documented in turn.

### Material

See Section 5.

### Drainage

See Section 6.

### Stiffness

The Mohr-Coulomb model offers three different kinds of elasticity: linear isotropic elasticity, nonlinear isotropic elasticity and linear anisotropic elasticity. In the first case, the material parameters can be defined in two ways:

either (Set A):

- Young's modulus,  $E$  [MPa]
- Poisson's ratio,  $\nu$

or (Set B):

- Bulk modulus,  $K$  [MPa]
- Shear Modulus,  $G$  [MPa]

The two sets of parameters,  $(E, \nu)$  and  $(K, G)$ , are related by

$$K = \frac{E}{3(1 - 2\nu)}, \quad G = \frac{E}{2(1 + \nu)} \quad (8.1)$$

or

$$E = \frac{9KG}{3K + G}, \quad \nu = \frac{3K - 2G}{2(3K + G)} \quad (8.2)$$

It should be noted that the two parameter sets are not linked automatically. For example, if Set A is chosen and  $E$  and  $\nu$  entered, changing the parameter set to Set B, does *not* lead to an automatic computation of  $K$  and  $G$  on the basis of  $E$  and  $\nu$ .

Secondly, for the Nonlinear option, the Young's modulus is pressure dependent following

$$E = E_{ur,ref} \Pi(\sigma'_3) \quad (8.3)$$

where

$$\Pi(\sigma'_3) = \left( \frac{-\sigma'_3 + c/\tan \phi}{p_{\text{ref}} + c/\tan \phi} \right)^m \quad (8.4)$$

with  $\sigma'_3$  being the minor principal stress. The associated parameters are:

- $p_{\text{ref}}$  [kPa] : Reference pressure (confining pressure in triaxial compression test).
- $m$  : Fitting parameter.

The parameter  $m$  depends on the soil type. For soft clays,  $m$  should be chosen as  $m \approx 1$  (giving rise to relations similar to those used in the Modified Cam Clay model) while for sands and other coarse grained materials  $m \approx 0.5$  is appropriate.

The final option, Graham-Houlsby, implements the anisotropic elasticity of (Graham and Houlsby 1983, see also Section 2.2). The input parameters are:

- Young's modulus in the  $y$ -direction,  $E_{yy}$  [MPa]
- Poisson's ratio in the  $x$ -direction to strain applied in the  $y$ -direction,  $\nu_{xy}$
- Ratio of the Young's moduli in the  $x$ - and  $y$ -directions,  $E_{xx}/E_{yy}$

## Strength

The basic Mohr-Coulomb yield function is given by

$$F = |\sigma_1 - \sigma_3| + (\sigma_1 + \sigma_3) \sin \phi - 2c \cos \phi \quad (8.5)$$

where  $\sigma_1$  and  $\sigma_3$  are the major and minor principal stresses respectively and the material parameters are:

- Cohesion,  $c$  [kPa]
- Friction angle,  $\phi$  [°]

Some possible depictions of the Mohr-Coulomb yield surface are shown in Figure 8.1.

## Flow Rule

The Mohr-Coulomb flow potential is given by

$$G = |\sigma_1 - \sigma_3| + (\sigma_1 + \sigma_3) \sin \psi \quad (8.6)$$

To start with, the Flow Rule category distinguishes between two settings: Associated and Nonassociated. In the former case,  $G = F$  is assumed while in the latter case, input of a dilation angle  $\psi_0$  is required. In addition, for a Nonassociated flow rule, it is possible to specify a Dilation Cap such that the dilation angle is set to zero once the value of a particular strain quantities reaches a critical values. Two different dilation caps, Volumetric and Shear are available. These differ by the strain quantity used to cap the dilation. For Dilation Cap = Volumetric, the dilation angle varies according to [see Figure 8.2(a)]:

$$\psi = \begin{cases} \psi_0 & \text{for } \varepsilon_v \leq \varepsilon_{v,\text{cr}} \\ 0 & \text{for } \varepsilon_v > \varepsilon_{v,\text{cr}} \end{cases} \quad (8.7)$$

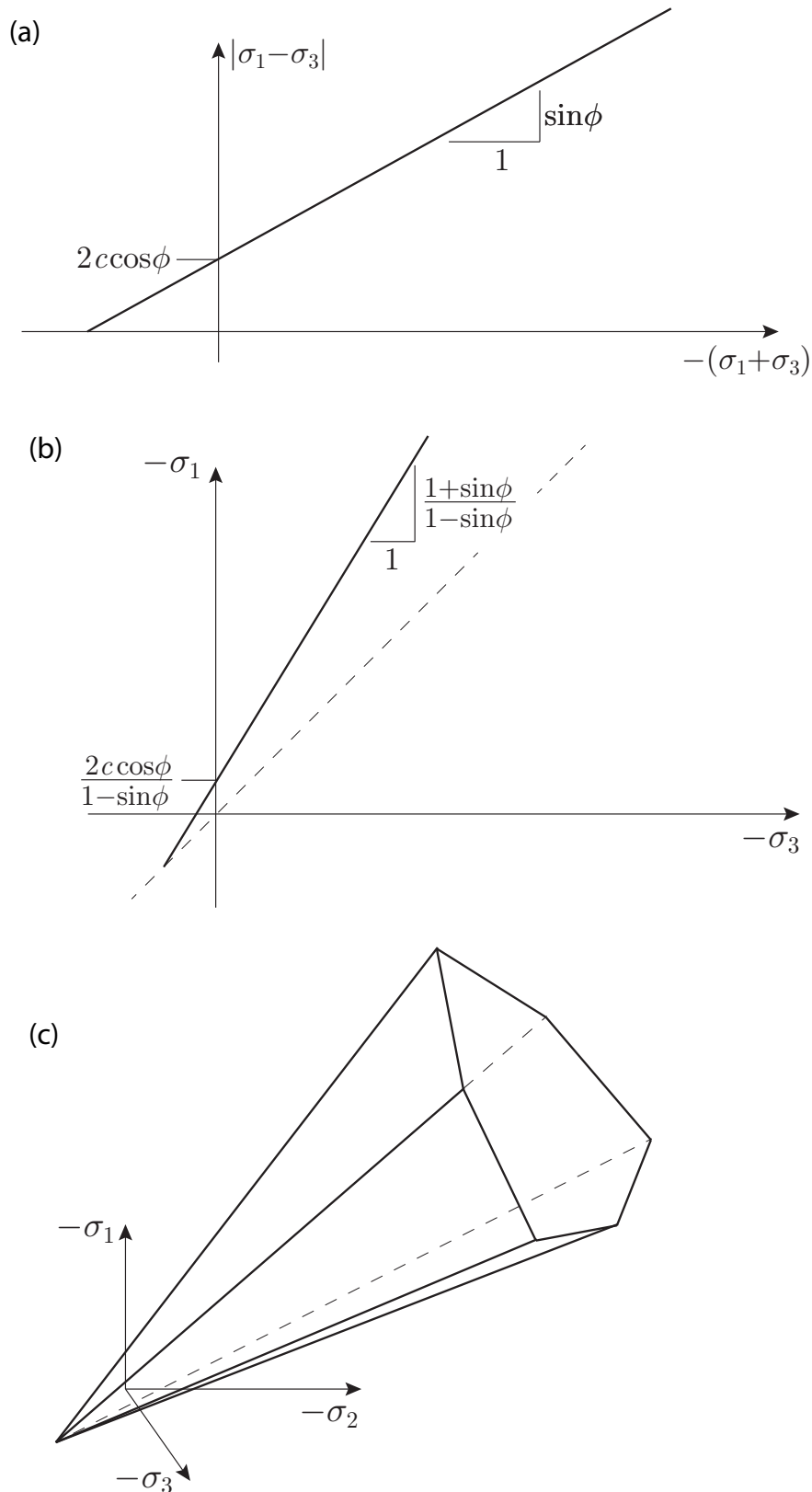


Figure 8.1: Possible depictions of Mohr-Coulomb yield surface in principal stress space. In (a) and (b), the principal stress ordering is  $\sigma_1 \leq \sigma_2 \leq \sigma_3$  while no particular ordering is assumed in (c).

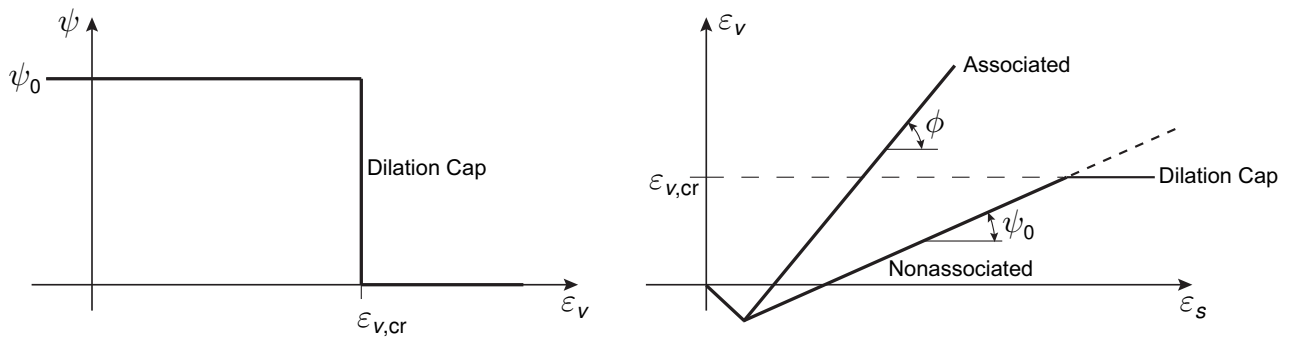
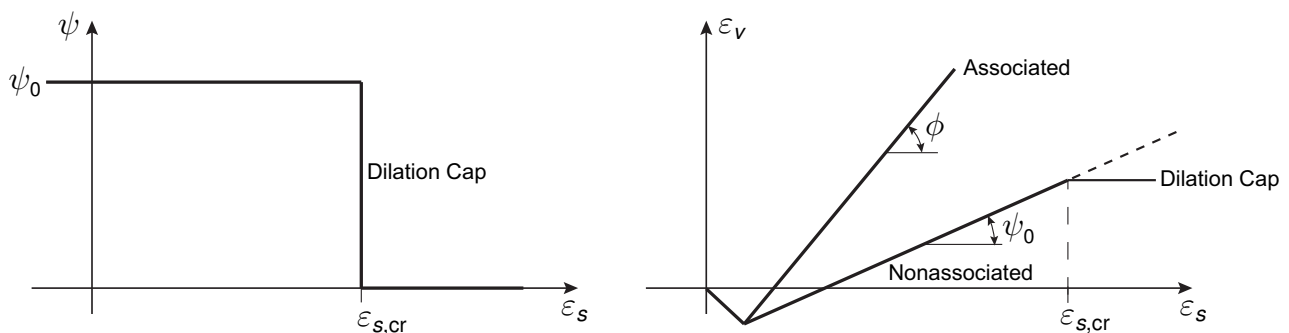
**(a) Dilation Cap = Volumetric:****(b) Dilation Cap = Shear:**

Figure 8.2: Variation of dilation angle and volumetric strain versus shear strain response.

where  $\varepsilon_v = \varepsilon_1 + \varepsilon_2 + \varepsilon_3$  is the volumetric strain. Using a Dilation Cap, a shear strain-volumetric strain behaviour such as that shown schematically in Figure 8.2(b) can be accounted for.

For Dilation Cap = Shear, the dilation angle varies according to [see Figure 8.2(b)]:

$$\psi = \begin{cases} \psi_0 & \text{for } \varepsilon_s \leq \varepsilon_{s,cr} \\ 0 & \text{for } \varepsilon_s > \varepsilon_{s,cr} \end{cases} \quad (8.8)$$

where  $\varepsilon_s = \sqrt{(\varepsilon_1 - \frac{1}{3}\varepsilon_v)^2 + (\varepsilon_2 - \frac{1}{3}\varepsilon_v)^2 + (\varepsilon_3 - \frac{1}{3}\varepsilon_v)^2}$  is a measure of the shear (or deviatoric) strain.

In summary, the Flow Rule category involves the following settings and parameters:

- Flow Rule (Associated/Nonassociated)
  - Flow Rule = Nonassociated: Dilation angle  $\psi_0$  [°]
  - Flow Rule = Nonassociated: Dilation Cap (No/Volumetric/Shear)
    - Dilation Cap = Volumetric:  $\varepsilon_{v,cr}$  [%]
    - Dilation Cap = Shear:  $\varepsilon_{s,cr}$  [%]

### Tension cut-off (optional)

It is possible to introduce a tension cut-off. This is given by

$$F_t = |\sigma_1 - \sigma_3| + (\sigma_1 + \sigma_3) \sin \phi_t - 2k_t \sin \phi_t \quad (8.9)$$

where the parameters are:

- Tensile strength,  $k_t$  [kPa].
- Inclination of the tension cut-off cone,  $\phi_t$  [°].

The default values correspond to a regular tension cut-off ( $k_t = 0$ ,  $\phi_c = 90^\circ$ ).

Note: the flow rule used for the tension cut-off is associated. As such, the use of a tension cut-off under undrained conditions may lead to counterintuitive results, including an apparent increase in strength. Hence, the use of tension cut-offs under undrained conditions is not recommended.

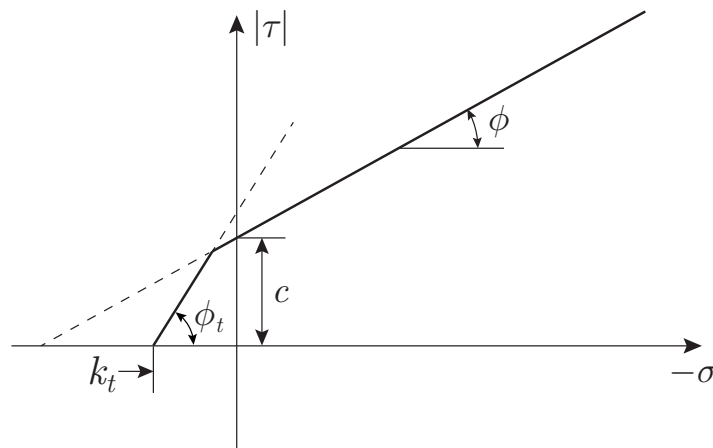


Figure 8.3: Mohr-Coulomb yield envelope with tension cut-off in  $\sigma$ - $\tau$  space.

### Compression Cap (optional)

It is further possible to introduce a compression cap. This is given by

$$F_c = |\sigma_1 - \sigma_3| - (\sigma_1 + \sigma_3) \sin \phi_c - 2\kappa_c \sin \phi_c \quad (8.10)$$

where the cap hardens according to:

$$\dot{\kappa}_c = -H \dot{\varepsilon}_{v,c}^p \quad (8.11)$$

where  $\varepsilon_{v,c}^p$  is the part of the plastic volumetric strain associated with the compression cap.

The parameters that define the hardening compression cap are given by:

- Initial compressive strength,  $\kappa_{c,0}$  [kPa].
- Inclination of the compression cone,  $\phi_c$  [°].
- Hardening (Yes/No)
  - Hardening = Yes: Hardening parameter,  $H_c$  [kPa].



The flow potential of the compression cap is the cap yield function, i.e. flow on the cap is associated.

The Mohr-Coulomb yield functions are shown in Figure 8.4. Alternatively, in terms of the normal and shear stresses on the critical plane, the yield functions take on the appearance shown in Figure 8.5.

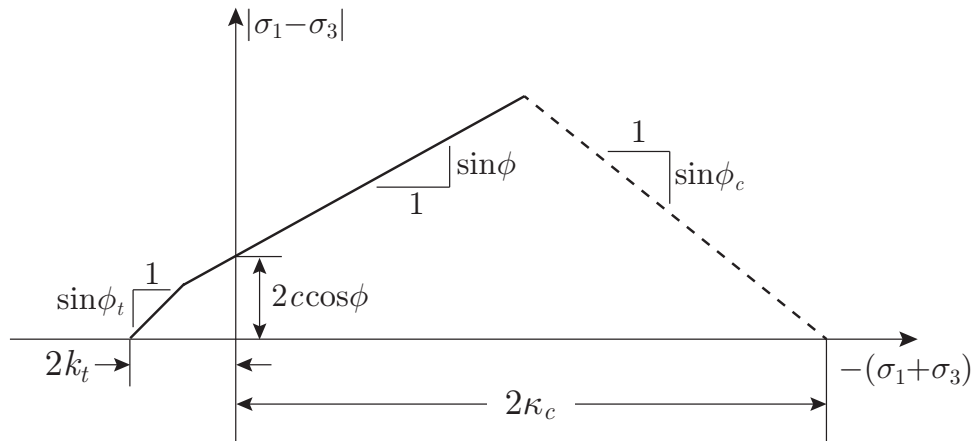


Figure 8.4: Mohr-Coulomb yield functions in  $(\sigma_1 + \sigma_3) - |\sigma_1 - \sigma_3|$  space.

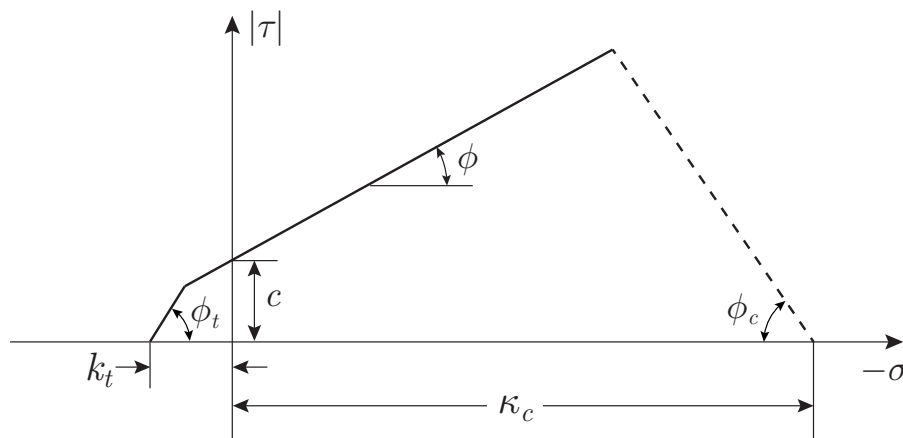


Figure 8.5: Mohr-Coulomb yield functions in  $\sigma - \tau$  space.

For confined compression under drained conditions, the compression cap implies a bilinear stress-strain response as shown in Figure 8.6.

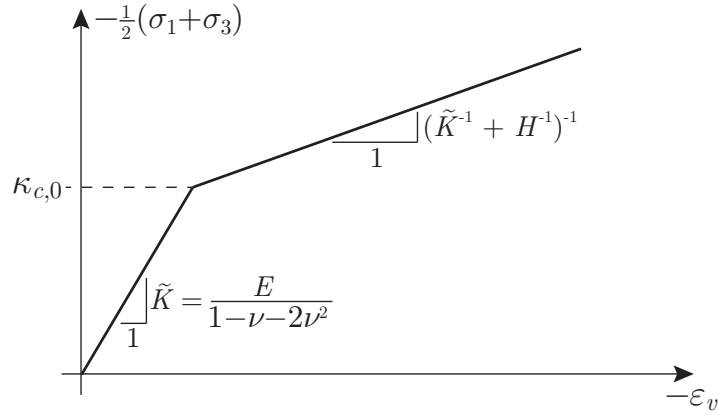


Figure 8.6: Stress-strain response under drained confined compression.

Under undrained conditions, the stress path (for  $\psi = 0$ ) is as shown in Figure 8.7. The undrained shear strength,  $s_u$ , depends on both the elastic and plastic parameters and is given by

$$s_u = c \cos \phi - \frac{\left[ \left( \frac{1}{2}(\sigma'_{1,0} + \sigma'_{3,0}) \frac{H}{\tilde{K}} - \kappa_{c,0} \right) \sin \phi_c + c \cos \phi \right] \sin \phi}{\left( 1 + \frac{H}{\tilde{K}} \right) \sin \phi_c + \sin \phi} \quad (8.12)$$

where

$$\tilde{K} = \frac{E}{1 - \nu - 2\nu^2} \quad (8.13)$$

and  $\sigma'_{1,0}$ ,  $\sigma'_{3,0}$ , and  $\kappa_{c,0}$  are the initial effective stresses and hardening variable respectively. From (8.12) the following limits of  $s_u$  are obtained:

$$s_u = c \cos \phi + \frac{(\kappa_{c,0} \sin \phi_c - c \cos \phi) \sin \phi}{\sin \phi + \sin \phi_c} \quad \text{for } H = 0 \text{ (stationary cap)} \quad (8.14)$$

$$s_u = c \cos \phi - \frac{1}{2}(\sigma'_{1,0} + \sigma'_{3,0}) \sin \phi \quad \text{for } H = \infty \text{ (no effect of cap)}$$

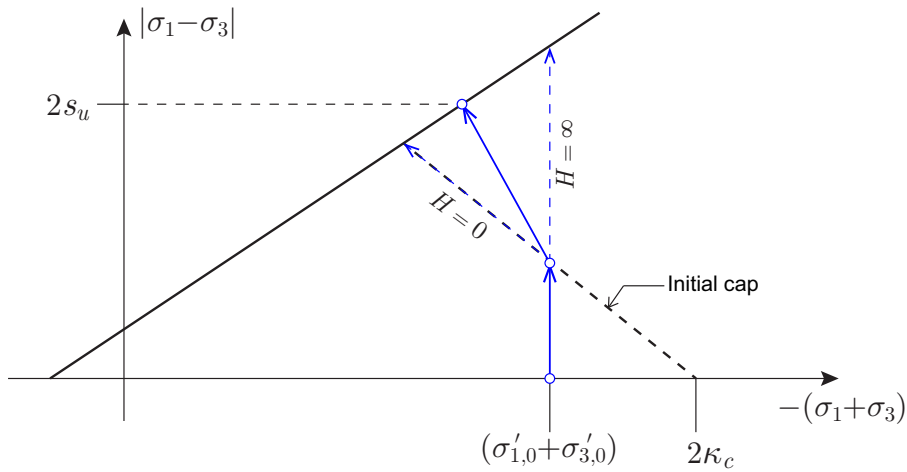


Figure 8.7: Stress path under undrained conditions.

An example of the influence of the  $H/\tilde{K}$  ratio is shown in Figure 8.8.

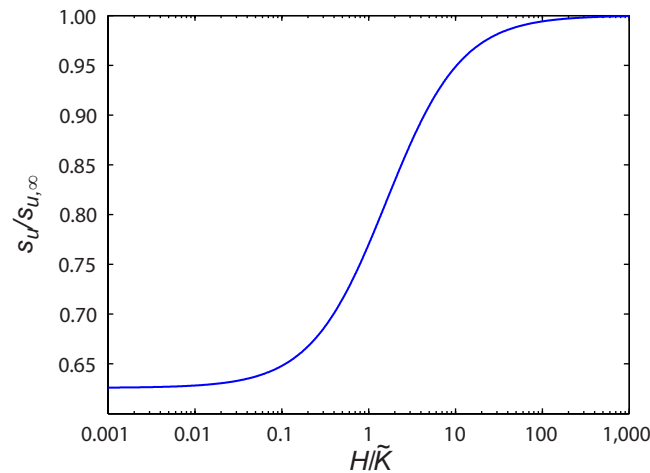


Figure 8.8: Undrained shear strength (normalized by the strength for  $H/\tilde{K} = \infty$ ) as function of  $H/\tilde{K}$ . Parameters:  $c = 0$ ,  $\phi = 25^\circ$ ,  $\phi_c = 45^\circ$ ,  $\sigma'_{1,0} = \sigma'_{3,0} = -100$  kPa,  $\kappa_{c,0} = 100$  kPa.

### Fissures (optional)

The strength of materials with regular fissure patterns may be accounted for by using a combination of the usual Mohr-Coulomb failure criterion supplemented with additional constraints on the normal and shear stresses on the fissure planes (Davis 1980; Zheng et al. 1997). In OptumG2, it is possible to define two fissure planes such that the strength is limited by:

$$\begin{aligned}
 F(\boldsymbol{\sigma}) &\leq 0 \\
 |\tau_1| + \sigma_1 \tan \phi_1 - c_1 &\leq 0, \quad \sigma_1 \leq k_{t1} \\
 |\tau_2| + \sigma_2 \tan \phi_2 - c_2 &\leq 0, \quad \sigma_2 \leq k_{t2}
 \end{aligned} \tag{8.15}$$

where  $F$  is the usual Mohr-Coulomb yield function (8.5) and  $(\sigma_1, \tau_1)$  and  $(\sigma_2, \tau_2)$  are the normal and shear stresses on the two fissure planes. In OptumG2, up to two fissure planes (not necessarily mutually orthogonal) can be defined via the following parameters:

- Orientation of Plane  $i$ ,  $\alpha_i$  [°].
- Cohesion on Plane  $i$ ,  $c_i$  [kPa].
- Friction angle on Plane  $i$ ,  $\phi_i$  [°].
- Tensile strength of Plane  $i$ ,  $k_{ti}$  [kPa].

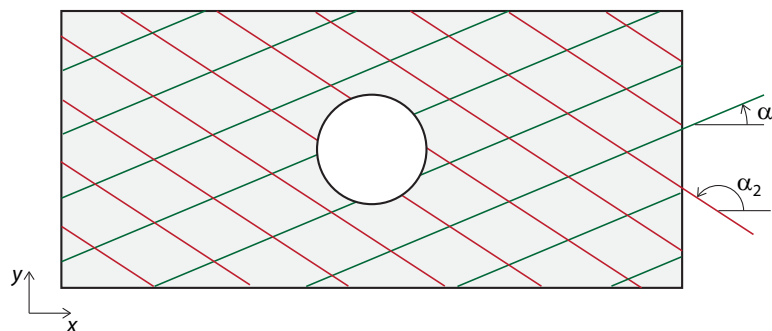


Figure 8.9: Example of circular tunnel in fissured material and definition of angles  $\alpha_1$  and  $\alpha_2$ .

where  $i = 1, 2$  and the angles  $\alpha_i$  are as shown in Figure 8.9. Note: setting  $k_{ti} = \text{Infinity}$  implies that the constraint  $\sigma_i \leq k_{ti}$  is ignored.

## Unit weights

The weight of the materials is specified via:

- Dry unit weight,  $\gamma_{\text{dry}}$  [kN/m<sup>3</sup>].
- Saturated unit weight,  $\gamma_s$  [kN/m<sup>3</sup>].

For calculations involving seepage or stationary water tables, the unit weight at any given point is calculated as:

$$\gamma = (1 - S)\gamma_{\text{dry}} + S\gamma_{\text{sat}} \quad (8.16)$$

where  $S$  is the degree of saturation.

## Initial Conditions

The initial stresses are specified via two parameters:

- The earth pressure coefficient  $K_0$ .
- The parameter  $\sigma_0$  (kPa).

The Initial Stress analysis aims to determine an admissible stress field that satisfies:

$$\sigma'_x = K_0\sigma'_y + \sigma_0 = K_0\sigma'_z + \sigma_0 \quad (8.17)$$

For  $\sigma_0 = 0$ , we have the classic relations

$$\frac{\sigma'_x}{\sigma'_y} = \frac{\sigma'_x}{\sigma'_z} = K_0 \quad (8.18)$$

## Hydraulic Model

The hydraulic properties of the materials are specified via:

- Hydraulic model (Linear, van Genuchten, Tanh).
- Hydraulic conductivity in the  $x$  direction,  $k_x$  [m/day].
- Hydraulic conductivity in the  $y$  direction,  $k_y$  [m/day].
- Parameters related to the particular hydraulic model (see Section 4 for details).

## 8.1 Notes

**Dilation Cap:** The dilation angle is updated at the beginning of each load step or each new stage. As such, for Dilation Cap = Volumetric, the total volumetric strain at the end of the load or stage may in calculations be observed to be somewhat higher than  $\varepsilon_{v,cr}$ , especially locally around footing edges and other singularities.

**Dilation in Short Term analysis** the dilation angle may affect the results significantly and an inadequate choice of dilation angle may lead to unexpected and counterintuitive results. In particular, for Drained/Undrained materials under Short Term analysis, any other value than  $\psi = 0$  will lead to an infinite limit load (see the Theory manual). Consequently,  $\psi$  is automatically set to zero for such analyses.

	$\phi = 0^\circ$	$5^\circ$	$10^\circ$	$15^\circ$	$20^\circ$	$25^\circ$	$30^\circ$	$35^\circ$	$40^\circ$	$45^\circ$
$\psi = 0^\circ$	1.0000	1.0038	1.0154	1.0353	1.0642	1.1034	1.1547	1.2208	1.3054	1.4142
$5^\circ$	–	1.0000	1.0039	1.0158	1.0364	1.0668	1.1086	1.1642	1.2370	1.3321
$10^\circ$	–	–	1.0000	1.0040	1.0164	1.0382	1.0707	1.1161	1.1776	1.2597
$15^\circ$	–	–	–	1.0000	1.0042	1.0174	1.0407	1.0762	1.1266	1.1962
$20^\circ$	–	–	–	–	1.0000	1.0045	1.0187	1.0443	1.0838	1.1410
$25^\circ$	–	–	–	–	–	1.0000	1.0048	1.0205	1.0491	1.0941
$30^\circ$	–	–	–	–	–	–	1.0000	1.0054	1.0229	1.0556
$35^\circ$	–	–	–	–	–	–	–	1.0000	1.0061	1.0262
$40^\circ$	–	–	–	–	–	–	–	–	1.0000	1.0070
$45^\circ$	–	–	–	–	–	–	–	–	–	1.0000

Table 8.1: Strength reduction factor  $\omega_D$  for computing Davis parameters.

	$\phi = 0^\circ$	$5^\circ$	$10^\circ$	$15^\circ$	$20^\circ$	$25^\circ$	$30^\circ$	$35^\circ$	$40^\circ$	$45^\circ$
$\psi = 0^\circ$	0.00	4.98	9.85	14.51	18.88	22.91	26.57	29.84	32.73	35.26
$5^\circ$	–	5.00	9.96	14.78	19.35	23.61	27.51	31.03	34.15	36.89
$10^\circ$	–	–	10.00	14.94	19.70	24.19	28.33	32.10	35.47	38.44
$15^\circ$	–	–	–	15.00	19.92	24.62	29.02	33.05	36.68	39.90
$20^\circ$	–	–	–	–	20.00	24.90	29.54	33.84	37.75	41.23
$25^\circ$	–	–	–	–	–	25.00	29.88	34.46	38.65	42.43
$30^\circ$	–	–	–	–	–	–	30.00	34.86	39.36	43.45
$35^\circ$	–	–	–	–	–	–	–	35.00	39.83	44.26
$40^\circ$	–	–	–	–	–	–	–	–	40.00	44.80
$45^\circ$	–	–	–	–	–	–	–	–	–	45.00

Table 8.2: Davis friction angle  $\phi_D$  as function of Mohr-Coulomb friction and dilation angle.

## 8.2 Influence of dilation angle on limit load

In the analysis types Limit Analysis and Strength Reduction under Long Term conditions, the dilation angle is always assumed associated, i.e. a user defined dilation angle that differs from the friction angle will be overridden for these analysis types. On the other hand, for Elastoplastic and Multiplier Elastoplastic analysis the user specified dilation angle will be used. The question then arises as to what extent the dilation angle affects the limit load. While the full answer to this question is rather involved and multifaceted, it is indisputable that the limit load for a material with  $\psi = \phi$  will be greater than or equal to that a material with  $\psi < \phi$ . The extent to which the assumption of nonassociated flow reduces the bearing capacity is quite problem dependent. A reasonable estimate of the reduction can be obtained by conducting the limit analysis using a set of reduced parameters that depend on the original  $c$ ,  $\phi$ , and  $\psi$  as:

$$c_D = \frac{c}{\omega_D}, \quad \phi_D = \psi_D = \arctan\left(\frac{\tan \phi}{\omega_D}\right), \quad \omega_D = \frac{1 - \sin \phi \sin \psi}{\cos \phi \cos \psi} \quad (8.19)$$

where  $(c, \phi, \psi)$  are the original parameters and  $(c_D, \phi_D, \psi_D)$  are the reduced parameters (often referred to as Davis parameters after Davis 1968, who first proposed them). The strength reduction factor  $\omega_D$  and the corresponding friction angle  $\phi_D$  are tabulated below for different  $\phi$  and  $\psi$ .

It should be noted that while the Davis parameters usually lead to a bearing capacity less than that obtained in an elastoplastic analysis with the actual  $c$ ,  $\phi$  and  $\psi$ , there are also cases where the opposite is true (see the Example Manual).

### 8.3 Strength reduction

In Strength Reduction analysis, the Mohr-Coulomb criterion is treated by reducing the parameters  $c$  and  $\tan \phi$  equally (see Figure 8.10) to induce a state of collapse. The resulting factor is the strength based factor of safety:

$$FS_s = \frac{c}{c_{red}} = \frac{\tan \phi}{(\tan \phi)_{red}} \quad (8.20)$$

While the decision as to which parameters are reduced is quite subjective, the approach used in OptumG2 is very common and may further be viewed as being consistent with Eurocode 7. It does, however, suffer from the drawback that the tensile strength,  $c / \tan \phi$ , is unaffected by the reduction, i.e.  $c / \tan \phi = c_{ref} / (\tan \phi)_{ref}$ .

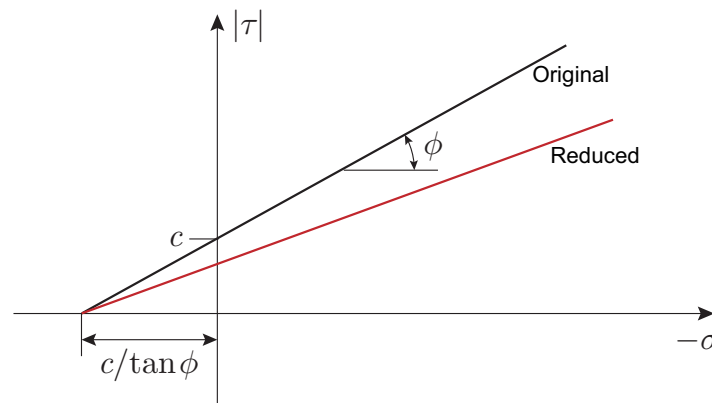


Figure 8.10: Original and reduced Mohr-Coulomb envelopes.

### 8.4 Capabilities and limitations of Mohr-Coulomb

The Mohr-Coulomb model has a number of inherent limitations and cannot be expected to capture the entire spectrum of soil behaviour. On the other hand, as with any model, the predictions of the Mohr-Coulomb model depend crucially on the choice material parameters. Generally speaking, if the material parameters are reasonable, so are the predictions of the model.

Moreover, it should be recognized that while more complex models may lead to better predictions for some particular stress paths or types of laboratory experiments, there is no guarantee that the predictions under different conditions represent reality any better than a simpler model. Indeed, while the limitations of the Mohr-Coulomb model are well known, the same is often not the case for more complex models where the predictions under conditions for which the model has not be calibrated may be quite erroneous.

As such, while the relative simplicity of the Mohr-Coulomb model imposes certain limitations, it is the same simplicity and transparency that makes it an attractive tool for practical geotechnical analysis.

In the following, two well known limitations of the Mohr-Coulomb model are briefly discussed.

### 8.4.1 Initial stiffness versus unloading/reloading stiffness

For real soils, one often observes that the stiffness in unloading/reloading is significantly higher than in initial (virgin) loading. The Mohr-Coulomb model, however, operates with a single elastic stiffness in both regimes. This means that the real soil stiffness is either underestimated in unloading/reloading (if the elastic parameters are set to match the soil response in first loading), or overestimated in first loading (if the elastic parameters are set to match the soil response in unloading/reloading). This point is illustrated in Figure 8.11.

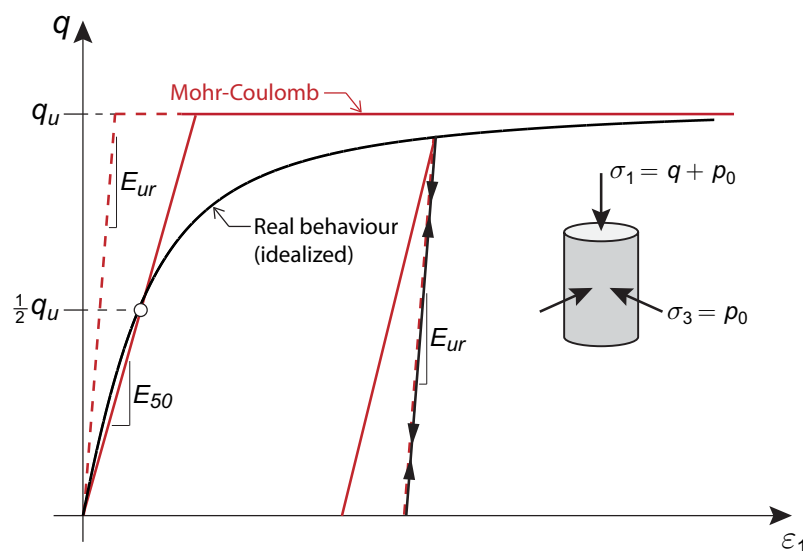


Figure 8.11: Soil behaviour in first loading and unloading/reloading compared to the Mohr-Coulomb model.

Consequently, some care must be exercised in the choice of Young's modulus. For example, for a footing loaded for the first time, the initial secant modulus,  $E_{50}$ , would be appropriate while for excavation problems, the unloading/reloading modulus,  $E_{ur}$ , may be more representative of the actual soil stiffness. As a general rule of thumb, the two moduli are related by  $E_{ur}/E_{50} \simeq 2-5$ . It should be noted, however, that many problems will be dominated by effects other than those related to the elastic moduli of the soil. For example, the deformation of retaining structures in excavation problems may be much more dependent on the soil strength and the properties of the retaining system (walls, anchors, etc) than the soil stiffness moduli. Also, the ultimate limit state is independent of the elastic properties of the soil.

The shortcomings of the Mohr-Coulomb model in capturing the different moduli in initial loading and unloading/reloading are addressed by the Extended Mohr-Coulomb (HMC) model described in Section 16.

### 8.4.2 Undrained conditions

Under undrained conditions (in OptumG2, for materials with Drainage Conditions = Drained/Undrained in analyses with Time Scope = Short Term), the Mohr-Coulomb model, with  $\psi = 0$ , implies a zero change of effective mean stress. Assuming plane strain conditions, it may be shown that the sum of

the in-plane effective stresses remains constant. This sum can further be identified as the sum of the major and minor effective stresses. The Mohr-Coulomb yield function may therefore be written as:

$$\begin{aligned}
 |\sigma_1 - \sigma_3| &= 2c \cos \phi - (\sigma'_1 + \sigma'_3)_0 \sin \phi \\
 &= 2c \cos \phi - (\sigma'_x + \sigma'_y)_0 \sin \phi \\
 &= 2c \cos \phi + (1 + K_0)\sigma'_{v,0} \sin \phi \\
 &= 2s_u
 \end{aligned}
 \tag{8.21}$$

where  $\sigma'_{v,0} = -\sigma_{y,0}$  is the initial effective vertical stress (positive in compression) and  $K_0 = \sigma_{x,0}/\sigma_{y,0}$  is the initial earth pressure coefficient. Under undrained conditions, the Mohr-Coulomb failure criterion thus reduces to that of Tresca (see Section 10) with a cohesion equal to the undrained shear strength  $s_u$ .

The stress path under undrained plane strain conditions is illustrated in Figure 8.12. The shear stress  $|\sigma_1 - \sigma_3|$  is here increased under an initial effective pressure  $-(\sigma'_x + \sigma'_y)_0$ .

$$s_u = c \cos \phi + \frac{1}{2}(1 + K_0)\sigma'_{v,0} \sin \phi \tag{8.22}$$

In other words, the undrained shear stress is a function of the initial vertical effective stress, the earth pressure coefficient, and the Mohr-Coulomb parameters  $c$  and  $\phi$ .

The conditions under general stress states, including those encountered in axisymmetry, are considerably more complex than those in plane strain. They are covered in detail in Section 10.

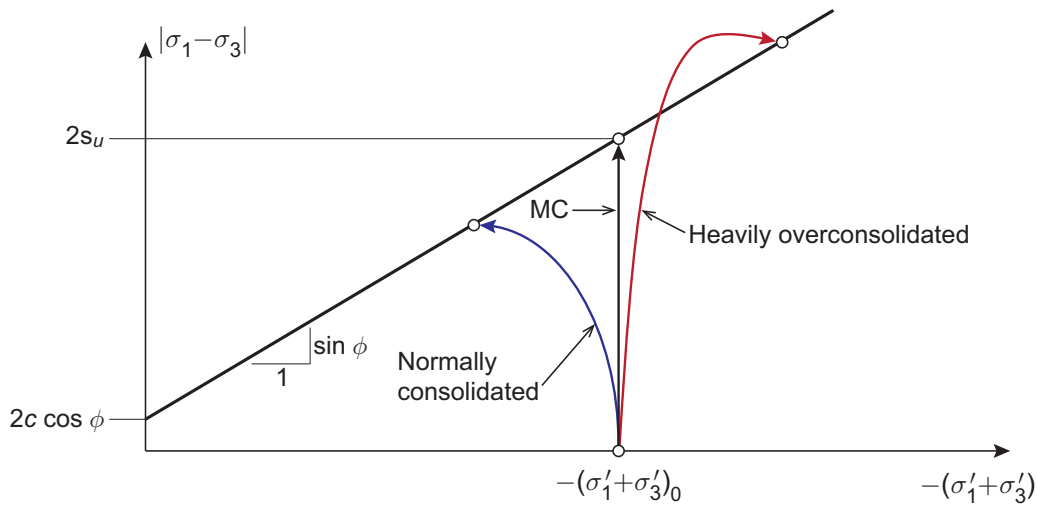


Figure 8.12: Behavior of clay under undrained conditions.

The predicted behaviour of the Mohr-Coulomb model and its implications in terms of strength are an approximation to real soil behaviour. Generally speaking, some changes to the mean effective stress will occur when soils are sheared under undrained conditions. Normally consolidated soils will tend to contract, leading to an increase in excess pore pressure and thereby a decrease in effective mean stress with the result that the maximum shear stress is lower than predicted by the Mohr-Coulomb model. On the other and, heavily overconsolidated soils will tend to dilate, leading to a decrease in excess pore pressure and thereby an increase in effective mean stress and hence a higher maximum shear stress than predicted by the Mohr-Coulomb model. The former type of



behaviour may to some extent be accounted for by a hardening cap. Otherwise, if sufficient material data is available, the Modified Cam Clay model is well suited to capture the behaviour of soft soils under undrained conditions.

## 9 DRUCKER-PRAGER

The Drucker-Prager material is very similar to the Mohr-Coulomb material but uses slightly different expressions for the yield and plastic potential function.

### Material, Drainage, Stiffness

See Section 8

### Strength

The Drucker-Prager yield function is given by

$$F = Mp + q - k \quad (9.1)$$

where

$$p = \frac{1}{3}(\sigma_x + \sigma_y + \sigma_z) \quad (9.2)$$

$$q = \sqrt{\frac{1}{2}(\sigma_x - \sigma_y)^2 + \frac{1}{2}(\sigma_y - \sigma_z)^2 + \frac{1}{2}(\sigma_z - \sigma_x)^2 + 3\tau_{xy}^2 + 3\tau_{yz}^2 + 3\tau_{zx}^2}$$

The strength parameters of the Drucker-Prager model are:

- Friction coefficient  $M$ .
- Cohesion  $k$  [kPa].

### Flow Rule

The Drucker-Prager flow potential is given by

$$G = Np + q - k \quad (9.3)$$

The settings in the flow rule category are analogous to those of the Mohr-Coulomb material with  $N$  and  $N_0$  replacing  $\psi$  and  $\psi_0$  respectively.

### Tension cut-off (optional)

It is possible to introduce a tension cut-off of the type:

$$F_t = M_t p + q - M_t k_t \quad (9.4)$$

where the parameters are:

- Slope of tension cut-off  $M_t$ .
- Tensile strength  $k_t$  [kPa].

Note that the default value  $M_t = 1.5$  corresponds to a plane strain Mohr-Coulomb friction angle of  $\phi = 90^\circ$  (see Section 9.3)

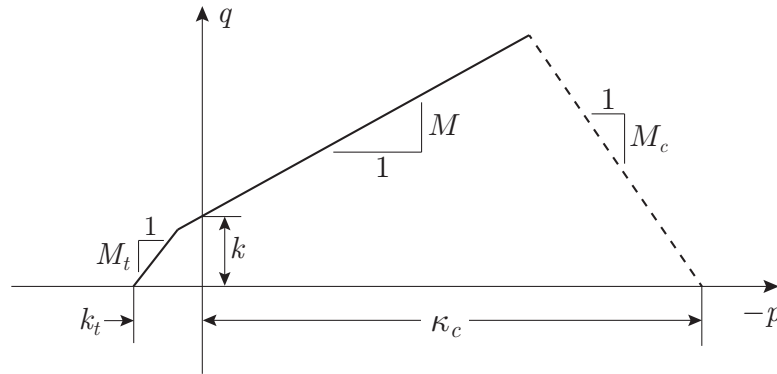


Figure 9.1: Drucker-Prager yield functions in  $p$ - $q$  space.

### Compression Cap (optional)

It is further possible to introduce a compression cap. This is given by

$$F_c = -M_c p + q - M_c \kappa_c \quad (9.5)$$

where the cap hardens according to:

$$\dot{\kappa}_c = -H \dot{\varepsilon}_{v,c}^p \quad (9.6)$$

with  $\varepsilon_{v,c}^p$  being the part of the plastic volumetric strain associated with the compression cap.

The parameters that define the hardening compression cap are given by:

- Initial compressive strength,  $\kappa_{c,0}$  [kPa].
- Slope of the compression cone,  $M_c$ .
- Hardening (Yes/No).
  - Hardening = Yes: Hardening parameter,  $H_c$  [kPa].

The flow potential of the compression cap is the cap yield function, i.e. flow on the cap is associated. The Drucker-Prager yield function and compression cap are shown in Figure 9.1.

### Unit weights, Initial Stresses, Permeability

See Section 8.

#### 9.1 Notes

**Dilation Cap:** See Section (8.1).

#### 9.2 Influence of dilation on limit load

The effects of nonassociated flow on the limit load are similar to those described for the Mohr-Coulomb model (see Section 8.2). For the Drucker-Prager model the equivalent Davis parameters are given by (see Krabbenhoft et al. 2012a, for details):

$$M_D = M/\omega_D, \quad k_D/\omega_D \quad (9.7)$$

where

$$\omega_D = \sqrt{\frac{9 + 4M^2 - 8MN}{9 - 4N^2}} \quad (9.8)$$

In other words, use of  $M_D$  and  $k_D$  in place of the original parameters will in Limit Analysis and Strength Reduction lead to results similar to those of a full nonassociated elastoplastic calculation to failure using the original  $M$ ,  $N$  and  $k$ .

### 9.3 Drucker-Prager vs Mohr-Coulomb

Assuming associated flow, the Drucker-Prager and Mohr-Coulomb surfaces can be matched in plane strain (see Figure 9.2) by the following choice of parameters:

$$M = \frac{3 \sin \phi}{\sqrt{3 + \sin^2 \phi}}, \quad k = \frac{3c \cos \phi}{\sqrt{3 + \sin^2 \phi}} \quad (9.9)$$

where  $c$  and  $\phi$  are the Mohr-Coulomb parameters. The equivalent  $k$  and  $M$  are tabulated as function of  $\phi$  and  $c$  in Table 9.1). In Limit Analysis and other analyses using an associated flow rule, the Drucker-Prager model with the equivalent Mohr-Coulomb parameters will produce results identical to the Mohr-Coulomb model. However, in elastoplastic calculations, the Drucker-Prager model will lead to a slightly less stiff response than the Mohr-Coulomb model.

In the general nonassociated case, the Drucker-Prager dilation coefficient can be matched approximately to the Mohr-Coulomb dilation angle by

$$N = \frac{3 \sin \psi}{\sqrt{3 + \sin^2 \psi}} \quad (9.10)$$

In drained elastoplastic analysis using a nonassociated flow rule, it is often observed that the Drucker-Prager model with equivalent Mohr-Coulomb parameters leads to a lower bearing capacity for a given mesh. However, as the mesh is refined, the two models will eventually result in similar bearing capacities.

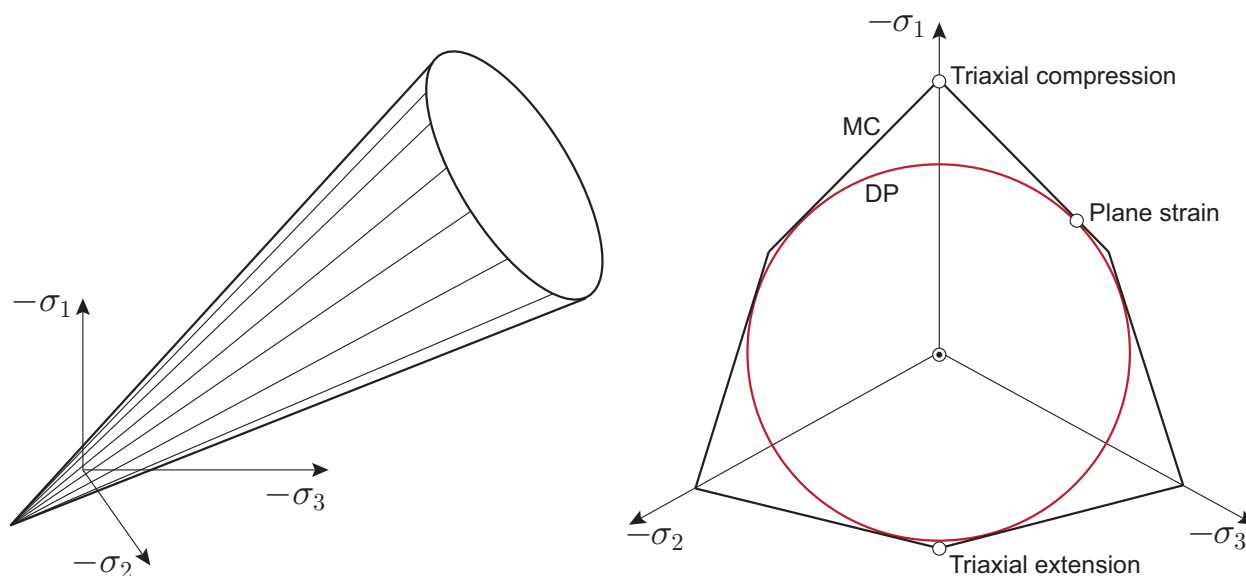


Figure 9.2: Drucker-Prager (DP) cone and matching to Mohr-Coulomb (MC) criterion in plane strain (associated flow rule).

$\phi$	$k/c$	$M$	$\phi$	$k/c$	$M$
0	1.732051	0.000000			
1	1.731699	0.030226	26	1.509171	0.736071
2	1.730644	0.060435	27	1.492839	0.760639
3	1.728888	0.090607	28	1.476049	0.784829
4	1.726432	0.120723	29	1.458816	0.808635
5	1.723279	0.150767	30	1.441153	0.832050
6	1.719434	0.180719	31	1.423074	0.855069
7	1.714900	0.210563	32	1.404594	0.877687
8	1.709684	0.240280	33	1.385726	0.899901
9	1.703791	0.269854	34	1.366484	0.921705
10	1.697228	0.299267	35	1.346881	0.943096
11	1.690004	0.328503	36	1.326932	0.964073
12	1.682125	0.357546	37	1.306650	0.984631
13	1.673602	0.386381	38	1.286046	1.004769
14	1.664444	0.414992	39	1.265135	1.024486
15	1.654661	0.443365	40	1.243929	1.043781
16	1.644263	0.471484	41	1.222440	1.062651
17	1.633262	0.499338	42	1.200681	1.081098
18	1.621671	0.526912	43	1.178662	1.099120
19	1.609499	0.554195	44	1.156396	1.116718
20	1.596762	0.581173	45	1.133893	1.133893
21	1.583470	0.607837	46	1.111165	1.150645
22	1.569637	0.634174	47	1.088221	1.166974
23	1.555277	0.660176	48	1.065073	1.182883
24	1.540404	0.685832	49	1.041730	1.198373
25	1.525030	0.711133	50	1.018201	1.213445

Table 9.1: Relation between Mohr-Coulomb and Drucker-Prager parameters according to (9.9)–(9.10).

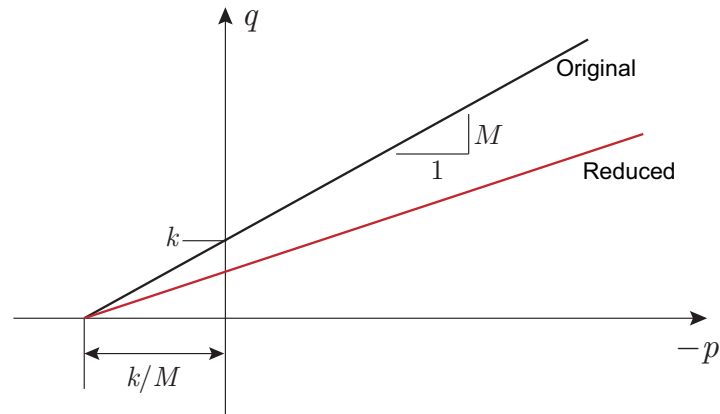


Figure 9.3: Original and reduced Drucker-Prager envelopes.

### 9.4 Strength reduction

In Strength Reduction analysis (see the Analysis Manual), the Drucker-Prager criterion is treated by reducing the parameters  $k$  and  $M$  equally (see Figure 9.3) to induce a state of collapse. The resulting factor is the strength based factor of safety:

$$FS_s = \frac{k}{k_{red}} = \frac{M}{M_{red}} \quad (9.11)$$

While the decision as to which parameters are reduced is quite subjective, the approach used for the Drucker-Prager criterion is consistent with the one used for the Mohr-Coulomb criterion. As such, the tensile strength,  $k/M$ , is unaffected by the reduction.

### 9.5 Undrained conditions

Under undrained conditions with  $N = 0$ , the effective mean stress remains constant and the Drucker-Prager yield function can be expressed as

$$F_u = q - k_u \quad (9.12)$$

where

$$k_u = k - \frac{1}{3}M(1 + 2K_0)p'_0 \quad (9.13)$$

is the undrained strength. The Drucker-Prager yield condition thus effectively reduces to that of von Mises.

## 10 TRESCA

As discussed in Section 8.4.2, the effective stress Mohr-Coulomb model is equivalent to the Tresca model under undrained conditions in plane strain. Under more general stress states than those associated with plane strain, this consistency between the effective stress Mohr-Coulomb model and total stress Tresca model is lost.

The Tresca material model addresses this issue by providing two models: the Standard Tresca model involving the yield function (8.21) and the Generalized Tresca model involving a similar total stress yield function consistent with the effective stress Mohr-Coulomb model under general stress states.

Unlike most solid materials, the Tresca material does not require input regarding drainage and no excess pore pressures are calculated regardless of the the Time Scope.

### Material

See Section 8.

### Stiffness

The Tresca model operates with undrained elastic parameters:  $E_u$  (Set A) or  $G$  (Set B).

### Strength

Two options regarding strength are available:

- Standard, requiring input of the undrained shear strength,  $s_u$  (kPa).
- Generalized, requiring input of the undrained shear strengths in triaxial compression and triaxial extension,  $s_{uc}$  and  $s_{ue}$  (kPa), respectively.

These two options are discussed in more detail below.

Spatial variation the strength parameters may be specified as for all other materials.

### Tension cut-off, Unit Weights, Initial Conditions, Hydraulic Model

See Section 8.

#### 10.1 Standard Tresca

The Standard Tresca failure criterion is given by

$$F = |\sigma_1 - \sigma_3| - 2s_u \quad (10.1)$$

with  $s_u$  being the undrained shear strength. In plane strain, there is no ambiguity about the physical meaning of  $s_u$ , it is the undrained shear strength measured in direct simple shear or similar plane strain experiments. For full consistency with the Mohr-Coulomb model, the undrained shear strength should be set to:

$$s_u = c \cos \phi + \frac{1}{2}(1 + K_0)\sigma'_{v,0} \sin \phi \quad (10.2)$$

where it is assumed that the initial effective stresses are related by  $\sigma'_x/\sigma'_y = \sigma'_z/\sigma'_y = K_0$ . However, the idea with the Tresca model, is that  $s_u$  instead is specified directly, without reference to other parameters, and possibly made to increase with depth to reflect the expected dependence on the initial vertical stress.

## 10.2 Generalized Tresca

While the Standard Tresca model in it itself is quite general, its use under any other conditions than plane strain is somewhat unsatisfactory. Firstly, the fundamental soil parameters are those which govern the response of effective stress versus strain. As such, any total stress model should, as a minimum, be equivalent to a relevant underlying effective stress model. This equivalence exists between Mohr-Coulomb and Standard Tresca in plane strain, but not under more general stress states. Secondly, it is a well established experimental fact that the undrained strength shear is a function of the stress path leading to failure. For example, undrained shear strengths measured in triaxial compression and triaxial extension may differ considerably. However, the Standard Tresca model predicts equal undrained shear strengths regardless of the stress path or type of experiment.

The Generalized Tresca model addresses these shortcomings of the standard model by using the following yield function:

$$F = |\sigma_1 - \sigma_3| + \alpha(\sigma_3 - \sigma_2) - k \quad (10.3)$$

where compressive stresses are negative and the principal stresses are ordered as  $\sigma_1 \leq \sigma_2 \leq \sigma_3$ . Consistency with the Mohr-Coulomb model in terms of the strength domain is obtained by selecting the parameters  $\alpha$  and  $k$  as:

$$\alpha = \frac{2 \sin \phi}{3 - \sin \phi}, \quad k = \frac{6}{3 - \sin \phi} \left[ \frac{1}{3}(1 + 2K_0)\sigma'_{v,0} \sin \phi + c \cos \phi \right] \quad (10.4)$$

where it is assumed that the initial effective stresses are related by  $\sigma'_{x,0}/\sigma'_{y,0} = \sigma'_{z,0}/\sigma'_{y,0} = K_0$  (in axisymmetry by  $\sigma'_{x,0}/\sigma'_{y,0} = \sigma'_{\theta,0}/\sigma'_{y,0} = K_0$ ).

Alternatively, the parameters  $\alpha$  and  $k$  can be related to the undrained shear strengths measured in triaxial compression and triaxial extension:

$$\alpha = \frac{s_{uc}}{s_{ue}} - 1, \quad k = 2s_{uc} \quad (10.5)$$

where  $s_{uc}$  is the undrained shear strength measured in triaxial compression and  $s_{ue}$  is the undrained shear strength measured in triaxial extension. These parameters,  $s_{uc}$  and  $s_{ue}$ , are those required as input in OptumG2. As with all other parameters,  $s_{uc}$  and  $s_{ue}$  can be made to increase with depth to reflect dependence on the initial effective vertical stress. The Generalized Tresca yield surface is shown in Figure 10.1. It should be noted that the allowable parameter range is

$$\frac{1}{2} \leq \frac{s_{ue}}{s_{uc}} \leq 1 \quad (10.6)$$

Outside this range the yield surface becomes non-convex and the calculation will not proceed.





$s_u/\sigma'_{v,0}$  ratio is in the range of about 0.1 to 0.5. This corresponds fairly well to what is observed experimentally for normally consolidated clays (see Figure 10.3).

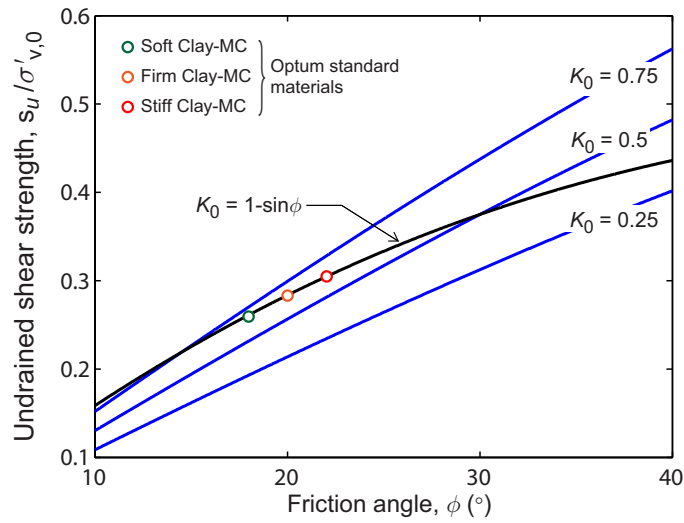


Figure 10.2: Variation of  $s_u/\sigma'_{v,0}$  implied by Mohr-Coulomb model ( $c = 0$ ).

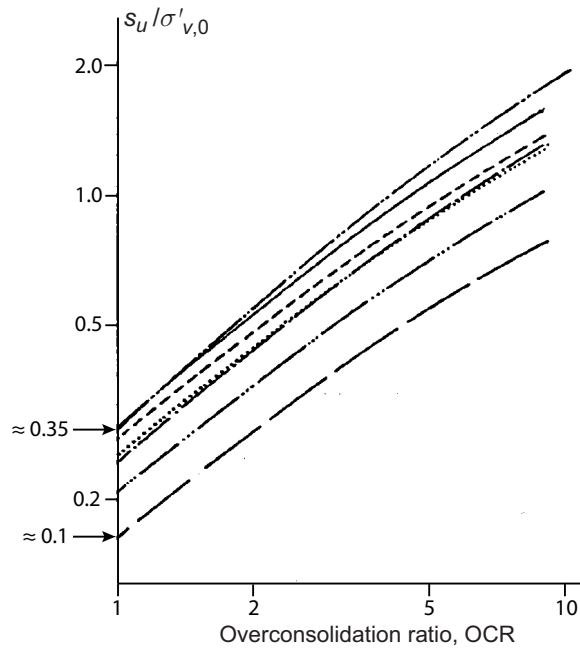


Figure 10.3: Variation of  $s_u/\sigma'_{v,0}$  with overconsolidation ratio for different clays (after Muir Wood 1990).

Moreover, a large number of empirical relations for the  $s_u/\sigma'_{v,0}$  ratio are available, some of which are summarized in Table 10.1. A detailed discussion of these and similar relations are given by Muir Wood (1990) and Ladd and DeGroot (2003).

$s_u/\sigma'_{v,0} = 0.11 + 0.0037PI$	Normally consolidated clays (Skempton 1957)
$s_u/\sigma'_{v,0} = 0.22$	Clays with OCR < 2 (Mesri 1975)
$s_u/\sigma'_{v,0} = 0.23 \pm 0.04$	Soft inorganic clays with PI < 60% (Larsson 1980)
$s_u/\sigma'_{v,0} = 0.22 OCR^{0.8}$	Inorganic clays (Ladd and DeGroot 2003)
$s_u/\sigma'_{v,0} = 0.25 OCR^{0.8}$	Silts and organic soils not including peats (Ladd and DeGroot 2003)
$s_u = 20(N_{60})^{0.72}$ (kPa)	Clays with OCR < 3 (Hara et al. 1974)
$s_u = 27N_{60}PI^{-0.22}$ (kPa)	Stiff clays (Vardenega and Bolton 2013)

Table 10.1: Empirical relations for variation of undrained shear strength with vertical stress. PI = plasticity index (%), OCR = overconsolidation ratio,  $N_{60}$  = SPT blow count.

Concerning the ratio between the triaxial compression and extension strengths, the effective stress Mohr-Coulomb model predicts:

$$\frac{s_{ue}}{s_{uc}} = \frac{3 - \sin \phi}{3 + \sin \phi} \quad (10.8)$$

where  $\phi$  is the drained friction angle. By correlating this ratio to the plasticity index, for example by (Muir Wood 1990):

$$\sin \phi = 0.81 - 0.1 \ln PI \quad (10.9)$$

we have

$$\frac{s_{ue}}{s_{uc}} = \frac{2.19 + 0.1 \ln PI}{3.81 - 0.1 \ln PI} \quad (10.10)$$

The implied variation of the  $s_{ue}/s_{uc}$  ratio with the plasticity index is shown in Figure 10.4. The available data tend to confirm a trend of this kind although the scatter in the data is significant. Further details on the modeling of arbitrary  $s_{ue}/s_{uc}$  ratios are covered under the AUS model in Section 11.

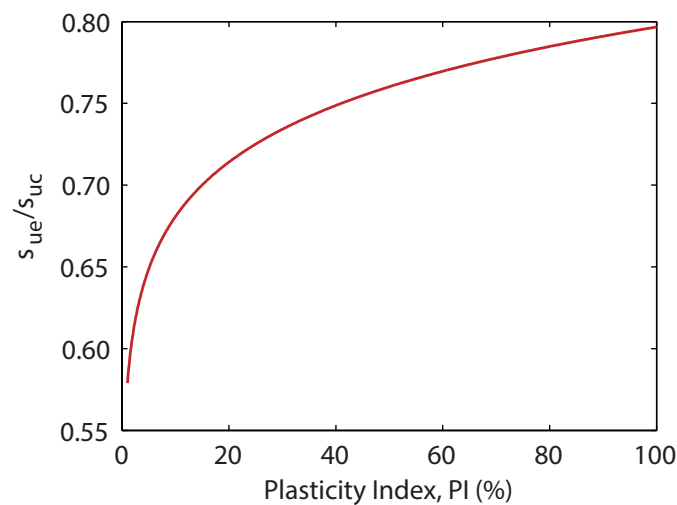


Figure 10.4: Variation of  $s_{ue}/s_{uc}$  according to (10.10).

## 10.4 Strength Reduction

In Strength Reduction analysis, the strengths are reduced to produce a state of incipient collapse. The Factor of Safety is thus defined by

$$\begin{aligned}FS_s &= \frac{S_u}{S_{u,red}} && \text{(Standard)} \\FS_s &= \frac{S_{uc}}{S_{uc,red}} = \frac{S_{uc}}{S_{ue,red}} && \text{(Generalized)}\end{aligned} \tag{10.11}$$

In practice, however, it is usually more convenient to conduct the analysis as a Limit Analysis with Multiplier = Gravity. If only Tresca materials are present, the resulting gravity multiplier, i.e. gravity based factor of safety, is equal to the strength based factor of safety:

$$\begin{aligned}FS_g &= \frac{\gamma}{\gamma_{cr}} = FS_s = \frac{S_u}{S_{u,red}} && \text{(Standard)} \\FS_g &= \frac{\gamma}{\gamma_{cr}} = FS_s = \frac{S_u}{S_{uc,red}} = \frac{S_u}{S_{ue,red}} && \text{(Generalized)}\end{aligned} \tag{10.12}$$

In contrast to Strength Reduction, Limit Analysis requires only a single iteration and is therefore usually considerably faster.

## 11 ANISOTROPIC UNDRAINED SHEAR (AUS)

The Anisotropic Undrained Shear (AUS) model may be seen as a further development of the Generalized Tresca model described in Section 10.2. It is a total stress model aimed at clays and similar materials. The input parameters comprise material data that can be easily determined in standard undrained laboratory tests. The particular features of the AUS model include:

- A hardening Generalized Tresca yield surface. This yield surface is consistent with the behaviour of frictional materials, including clays, under undrained conditions and general stress states.
- Direct specification of the undrained shear strengths in triaxial compression, triaxial extension, and simple shear.
- Distinction between elastoplastic secant stiffnesses in triaxial compression and extension.

Being a total stress model, the AUS model does not require input regarding drainage and no excess pore pressures are calculated regardless of the Time Scope.

### Material

See Section 8.

### Stiffness

The AUS model operates with standard isotropic elasticity, with input parameters being either the undrained Young's modulus,  $E_u$  (Set A), or the shear modulus,  $G$  (Set B).

In addition to the elastic stiffnesses, the axial strains halfway to failure in compression and extension are required :

- Axial strain at half the failure stress in triaxial compression,  $\varepsilon_{C,50}$  [%]
- Axial strain at half the failure stress in triaxial extension,  $\varepsilon_{E,50}$  [%]

These quantities are shown in Figure 11.1.

### Strength

The strength may be either Isotropic or Anisotropic. In both cases, the undrained shear strengths in triaxial compression and extension are the basic strength parameters (see discussion below). The full set of material parameters is:

- Undrained shear strength in triaxial compression,  $s_{uc}$  [kPa]
- Undrained shear strength in triaxial extension,  $s_{ue}$  [kPa]
- Undrained shear strength in simple shear,  $s_{us}$  (for Option = Anisotropic)

Spatial variation of the strength parameters may be specified as for all other materials.

### Tension cut-off, Unit Weights, Initial Conditions, Hydraulic Model

See Section 8.

### 11.1 Background

The typical behaviour of clays and similar materials in undrained triaxial compression and extension is roughly as sketched in Figure 11.1.

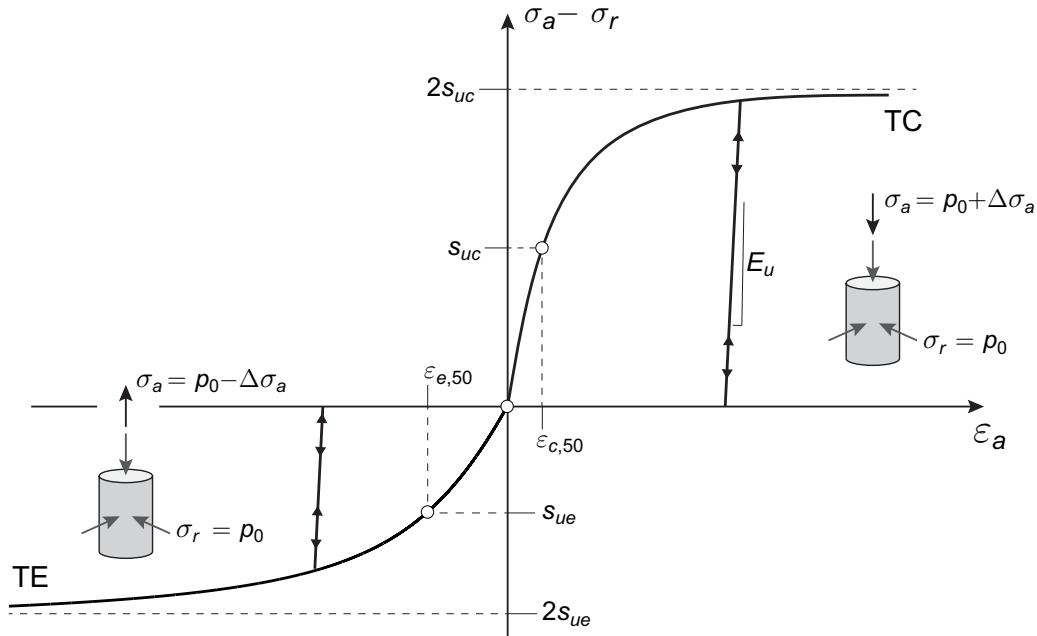


Figure 11.1: Typical stress-strain behaviour in triaxial compression (TC) and triaxial extension (TE).

In the triaxial compression test, an initial state given by  $\sigma_a = \sigma_r = p_0$  is first established. The axial stress is then increased by an amount  $\Delta\sigma_a$  until failure is reached at  $\sigma_a - \sigma_r = 2s_{uc}$ .

In the triaxial extension test, the same initial state is used, but the axial stress is now released by an amount  $\Delta\sigma_a$  until failure is reached at  $-(\sigma_a - \sigma_r) = 2s_{ue}$ .

The failure strengths in the two cases, measured by half the difference in axial and radial stress are the undrained shear strengths,  $s_{uc}$  and  $s_{ue}$ , respectively.

The following general observations hold over a wide range of conditions:

- The compression strength,  $s_{uc}$ , is usually larger than the extension strength,  $s_{ue}$ . In the field, both strengths tend to vary approximately linearly with the vertical stress and thereby approximately linearly with depth.
- The response is usually, but not always, somewhat stiffer in compression than in extension. In OptumG2, the overall elastoplastic stiffness is specified via the elastoplastic moduli in compression and extension,  $E_{uc,50}$  and  $E_{ue,50}$  respectively.

### 11.2 Undrained shear strengths

It is usually observed that the undrained shear strengths in triaxial compression ( $s_{uc}$ ), triaxial extension ( $s_{ue}$ ) and simple shear ( $s_{us}$ ) are related to each other by

$$s_{uc} < s_{us} < s_{ue} \tag{11.1}$$

The phenomenon that the undrained shear strengths resulting from different types of loading differ from one another is often referred to as anisotropy. This is somewhat unfortunate as anisotropy usually refers to the phenomenon that a material has different properties in different directions. For example, as a result of their deposition, many soils have a lower hydraulic conductivity vertically than horizontally. Similarly, some soils may have different elastic properties in the different directions, for example a higher Young's modulus vertically than horizontally.

It is also possible to contemplate that some soils would have anisotropic strengths, e.g. one strength when subjected to compression vertically and another when subjected to the same kind of compression horizontally. However, the fact that different undrained shear strengths result from different types of loading is not, in the first instance, an indication of anisotropy in the usual sense of the word. It is an entirely expected feature of any frictional material (including clays, silts and similar) whose drained strengths differ in compression and extension (see Figure 11.2).

These observations must necessarily enter into the considerations when developing a reasonable constitutive model and the AUS model is unique in this regard. In particular, it distinguishes sharply between the part of the  $s_{ue}/s_{uc}$  and  $s_{ue}/s_{us}$  ratios that would be expected from an isotropic material and the part that could reasonably be conceived as stemming from physical anisotropy, for example as a result of layering, direction of deposition, etc.

Moreover, the AUS model provides the option of including physical anisotropy or not. If physical anisotropy is not included,  $s_{ue}$  and  $s_{uc}$  are the basic strength parameters and  $s_{us}$  follows from these. If physical anisotropy is included, there is the additional possibility of specifying the  $s_{us}/s_{uc}$  ratio (within certain limits).

### 11.2.1 Isotropic strength

For the Isotropic strength option, the Generalized Tresca surface is used (see Figure 11.3) and the triaxial compression and extension strengths are the basic strength parameters. This model comes

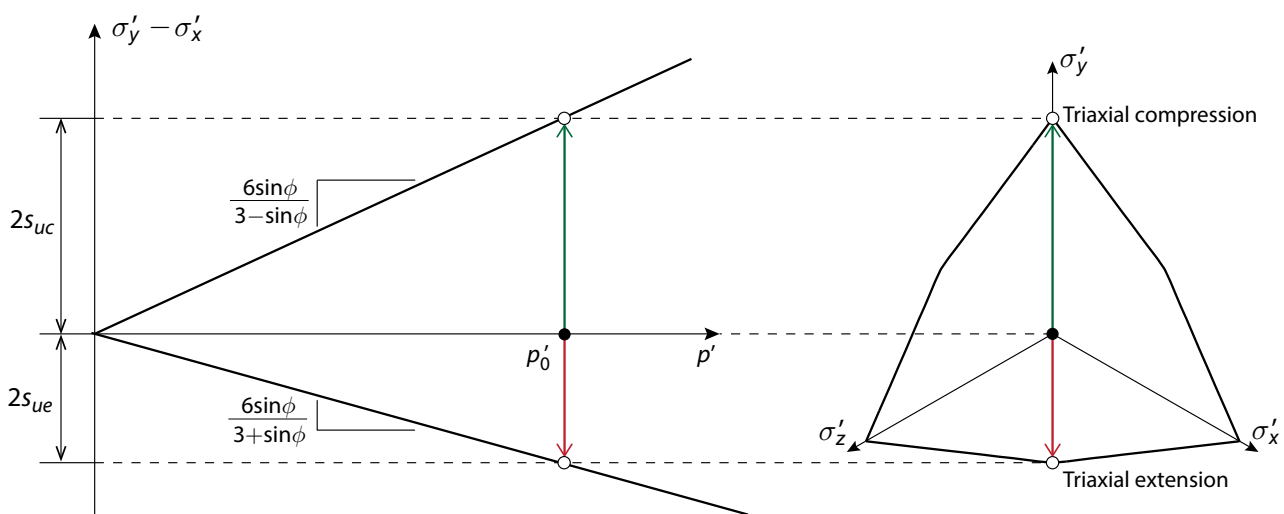


Figure 11.2: Behaviour of an isotropic linear elastic-perfectly plastic Mohr-Coulomb material in undrained triaxial compression and extension with  $y$  denoting the axial direction.

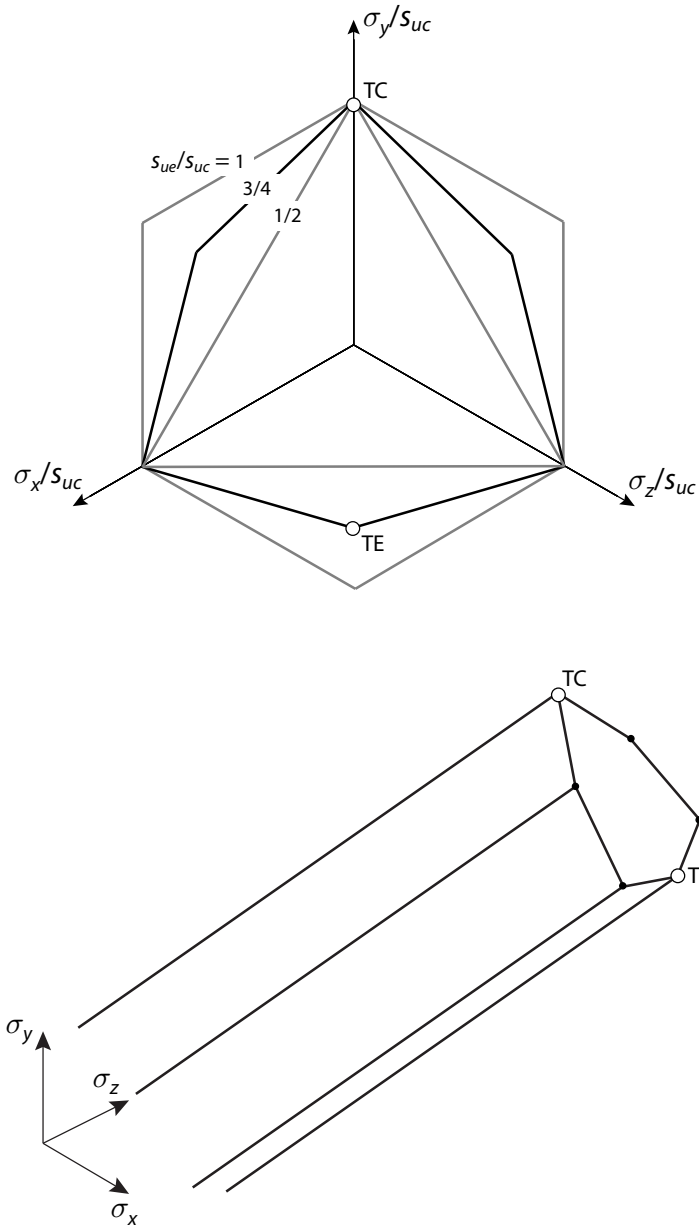


Figure 11.3: Generalized Tresca surface used in AUS with Isotropic strength option (for all shear stresses equal to zero).

with the limitation that

$$0.5 \leq \frac{s_{ue}}{s_{uc}} \leq 1 \tag{11.2}$$

For  $s_{ue}/s_{uc}$  below 0.5 the yield surface becomes non-convex and while ratios of  $s_{ue}/s_{uc}$  up to 2 in principle could be accommodated, the internal limitation in OptumG2 is that the compression strength remains greater than or equal to the extension strength.

With  $s_{ue}$  and  $s_{uc}$  specified, the strength in simple shear follows as:

$$s_{us} = \left( \frac{1}{2}s_{ue}^{-1} + \frac{1}{2}s_{uc}^{-1} \right)^{-1} = \frac{2s_{ue}s_{uc}}{s_{ue} + s_{uc}} \tag{11.3}$$



In other words,  $s_{US}$  is the harmonic mean of the triaxial extension and compression strengths. This means that  $s_{US}$  will tend to be somewhat closer to  $s_{UE}$  than to  $s_{UC}$ , something that is generally observed experimentally.

### 11.2.2 Anisotropic strength

The Anisotropic strength option allows for specification of  $s_{US}$  in addition to  $s_{UE}$  and  $s_{UC}$ . To ultimately achieve the desired strengths (if they do not comply with the Isotropic predictions outlined above) the shape of the yield surface is altered and it is shifted in the  $y$ -direction (thereby identifying this direction with the orientation of the samples in the tests from which the strengths are determined). The basic principle is illustrated in Figure 11.4.

It should be noted, however, that constraints pertaining to the convexity of the yield surface prevent a completely arbitrary  $s_{US}/s_{UC}$  ratio from being specified. In particular, for a given  $s_{UE}/s_{UC}$  ratio there is an upper and a lower limit to the  $s_{US}/s_{UC}$  ratio that can be accommodated. These limits are illustrated in Figure 11.5 and further listed in Table 11.1 for various  $s_{UE}/s_{UC}$  ratios. For  $s_{US}/s_{UC}$  ratios above the admissible range, a warning will be issued and the closest attainable  $s_{US}/s_{UC}$  ratio will be used in the subsequent analysis. For  $s_{US}/s_{UC}$  below the admissible range, an error will be issued and the calculations will not proceed.

A unique feature of the Anisotropic version of the AUS model is that anisotropy only is included to the extent that it is necessary to accommodate the specified strength ratios. If the parameters are specified according to the relations implied by the Isotropic version, no anisotropy will result. More generally, the degree of anisotropy eventually included is a function of how much the specified strength ratios differ from what would be expected from an isotropic material.

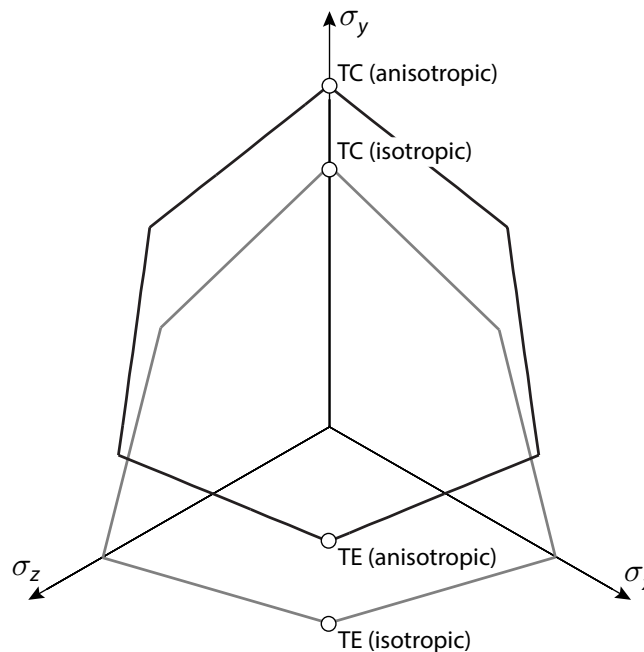


Figure 11.4: Shift of the Generalized Tresca surface to accommodate specified  $s_{UE}/s_{UC}$  and  $s_{US}/s_{UC}$  ratios with Anisotropic strength option.

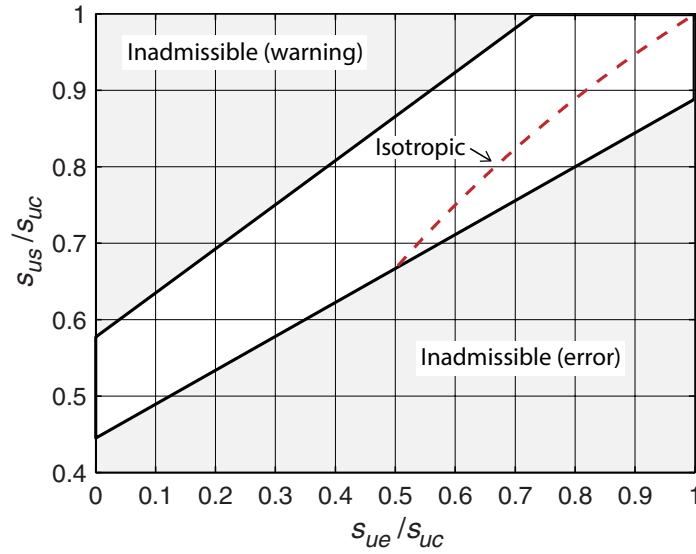


Figure 11.5: Admissible parameter space for Anisotropic strength option. The dashed line shows the  $s_{us}/s_{uc}$  implied by a user specified  $s_{ue}/s_{uc}$  for Isotropic strength option.

$s_{ue}/s_{uc}$	$(s_{us}/s_{uc})_{min}$	$(s_{us}/s_{uc})_{max}$	$(s_{us}/s_{uc})_{isotropic}$
0.00	0.45	0.57	—
0.05	0.47	0.60	—
0.10	0.49	0.63	—
0.15	0.52	0.66	—
0.20	0.54	0.69	—
0.25	0.56	0.72	—
0.30	0.58	0.75	—
0.35	0.60	0.77	—
0.40	0.63	0.80	—
0.45	0.65	0.83	—
0.50	0.67	0.86	0.67
0.55	0.69	0.89	0.71
0.60	0.72	0.92	0.75
0.65	0.74	0.95	0.79
0.70	0.76	0.98	0.82
0.75	0.78	1.00	0.86
0.80	0.80	1.00	0.89
0.85	0.82	1.00	0.92
0.90	0.84	1.00	0.95
0.95	0.86	1.00	0.97
1.00	0.88	1.00	1.00

Table 11.1: Minimum and maximum admissible  $s_{us}/s_{uc}$  as function of  $s_{ue}/s_{uc}$  together with the ratio implied by the Isotropic strength option.

### 11.3 Hardening

With the shape and shift of the yield surface in place, the model is completed by specifying an appropriate hardening law. In the AUS model the hardening is of the isotropic kind, meaning that

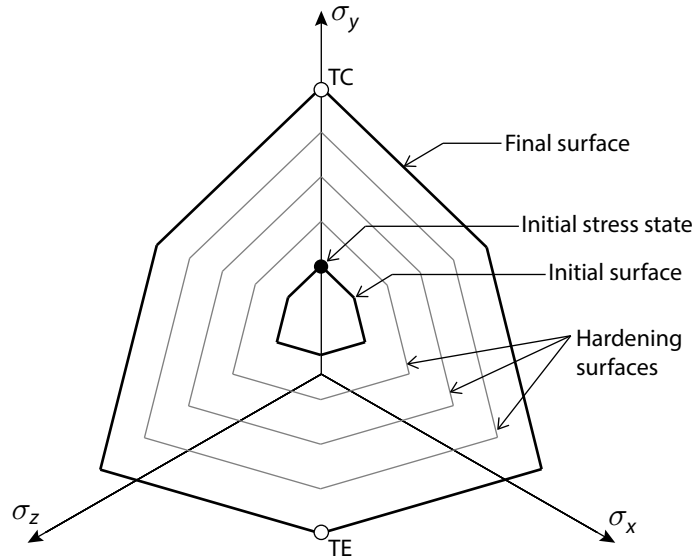


Figure 11.6: Hardening AUS yield surface (Anisotropic).

from an initial yield surface that contains the initial stress state, the yield surface expands in an affine manner as a result of plastic straining to reach its ultimate extent as given by the strength parameters. This is illustrated in Figure 11.6.

## 11.4 Plastic potential

The plastic potential of the AUS model is that of von Mises, i.e. a circle in the deviatoric plane. This type of plastic potential has long been used for clays (see e.g. Potts and Zdravkovic 2001; Roscoe and Burland 1968) and has a number of advantages over the immediate alternatives such as Tresca.

## 11.5 Parameter estimation

### 11.5.1 Strengths

Ideally speaking, the three different shear strengths should be determined in three independent experiments. If only data from one or two experiments are available, the remaining parameters can be estimated on the basis of previously published results. A data set involving all three strengths is that of Ladd (1991) shown in Figure 11.7. From this data set, the following approximate relations can be inferred:

$$\begin{aligned} s_{ue}/s_{uc} &\simeq 0.50 + 0.0034PI \\ s_{us}/s_{uc} &\simeq 0.69 + 0.0015PI \end{aligned} \quad (11.4)$$

and thereby:

$$s_{us}/s_{uc} \simeq 0.47 + 0.44s_{ue}/s_{uc} \quad (11.5)$$

for  $0.5 \leq s_{ue}/s_{uc} \leq 0.84$ .

In another study concerned with Norwegian clays, Karlsrud and Hernandez-Martinez (2013) linked

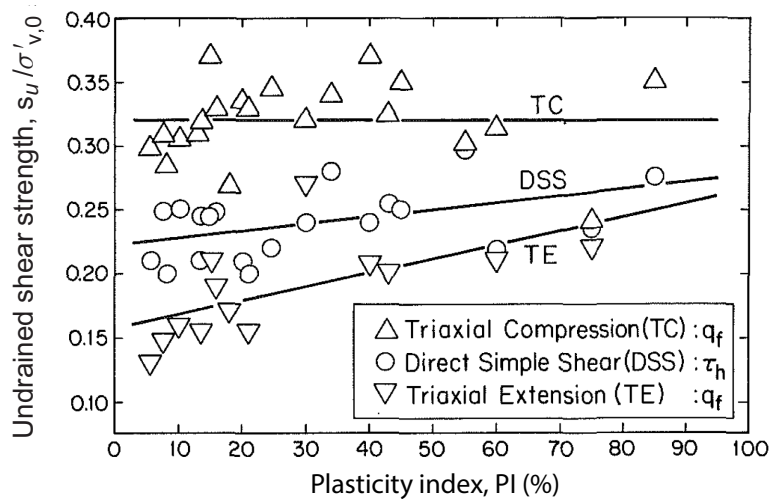


Figure 11.7: Variation of undrained shear strength with plasticity index for triaxial compression (TC), direct simple shear (DSS) and triaxial extension (TE). From Ladd (1991).

the strength ratio to the water content  $w$ :

$$\begin{aligned}
 s_{ue}/s_{uc} &= 0.277 + 0.0029w \\
 s_{us}/s_{uc} &= 0.454 + 0.00447w
 \end{aligned}
 \tag{11.6}$$

and thereby:

$$s_{us}/s_{uc} = 0.03 + 1.54s_{ue}/s_{uc}
 \tag{11.7}$$

for  $0.35 \leq s_{ue}/s_{uc} \leq 0.5$  (corresponding to the range of water contents considered,  $w \simeq 25\%$  to  $75\%$ ).

This above relations are shown in Figure 11.8 together with the minimum and maximum  $s_{us}/s_{uc}$  that are attainable with the AUS model. Also shown are various data collected by Muir Wood (1990). We see that the AUS model is capable of accommodating most of these experimentally determined shear strength ratios.

### 11.5.2 Strains halfway to failure

The axial strain halfway to failure in triaxial compression is usually of order  $\epsilon_{c,50} \simeq 0.5$  to  $2\%$  over a wide range of conditions. The strain at halfway to failure in extension is usually some 2 to 5 times  $\epsilon_{c,50}$ .

### 11.5.3 Example

Figure 11.9 shows the results of a triaxial compression test on Todi clay reported by Burland et al. (1996). The test was conducted under a confining pressure of  $p_0 = 3,200$  kPa.

From the test data shown in Figure 11.9, the undrained shear strength is immediately read off as:

$$s_{uc} = 2,035 \text{ kPa} \quad (p_0 = 3,200 \text{ kPa})
 \tag{11.8}$$

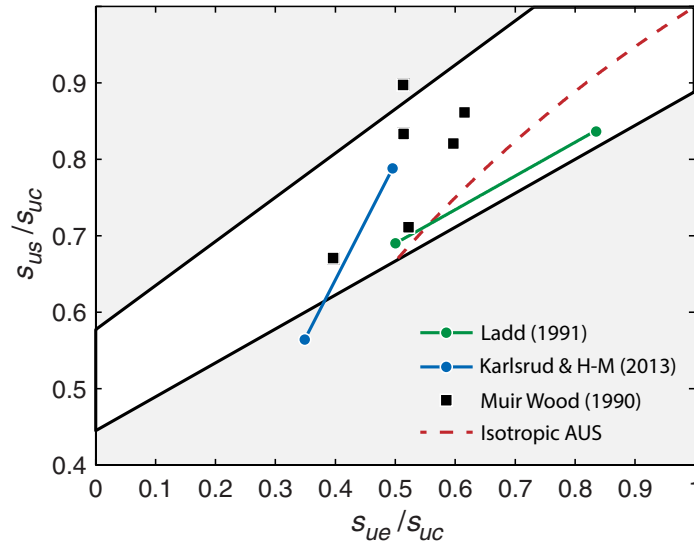


Figure 11.8: Admissible parameter space together with data from Ladd (1991), Karlsrud and Hernandez-Martinez (2013) and Muir Wood (1990) and  $s_{us}/s_{uc}$  as function of  $s_{ue}/s_{uc}$  for the Isotropic version of the AUS model.

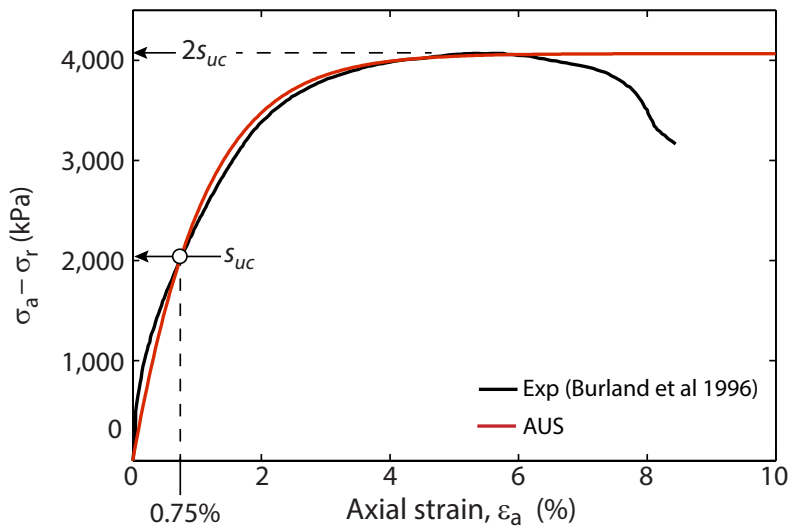


Figure 11.9: AUS fit to Burland et al. (1996) data.

The axial strain at this level of  $\sigma_a - \sigma_r$  is approximately  $\varepsilon_{c,50} = 0.75\%$ . A secant modulus can thus be defined by

$$E_{C,50} = \frac{2,035 \times 10^{-3} \text{ MPa}}{0.0075} = 271 \text{ MPa} \quad (p_0 = 3,200 \text{ kPa}) \quad (11.9)$$

Using an elastic modulus 10 times this,  $E_u = 2,710 \text{ MPa}$ , results in the fit shown in Figure 11.9. The remaining parameters (which have no influence on the behaviour in compression) must either be estimated or derived from an additional extension test.

## 11.6 Governing equations

The governing equations of the AUS model are summarized below.

The yield function is given by

$$F = \hat{q} - \left[ \frac{6w}{\sqrt{3}(1 + 1/\rho) \cos \hat{\theta} - 3(1 - 1/\rho) \sin \hat{\theta}} + 2(1 - w) \right] \kappa \quad (11.10)$$

where  $\kappa$  is a hardening variable and

$$\hat{q} = \sqrt{3\hat{J}_2} \quad (11.11)$$

$$\hat{J}_2 = J_2(\hat{\mathbf{s}}) = \frac{1}{2} \hat{\mathbf{s}}^T \mathbf{D} \hat{\mathbf{s}} \quad (11.12)$$

$$\hat{\mathbf{s}} = \boldsymbol{\sigma} - \mathbf{m}p - a\hat{s}_u \mathbf{r} \quad (11.13)$$

$$\mathbf{m} = (1, 1, 1, 0, 0, 0)^T \quad (11.14)$$

$$\mathbf{D} = \text{diag}(1, 1, 1, 2, 2, 2)^T \quad (11.15)$$

$$p = \frac{1}{3} \mathbf{m}^T \boldsymbol{\sigma} \quad (11.16)$$

$$\mathbf{r} = (\frac{1}{2}, -1, \frac{1}{2}, 0, 0, 0)^T \quad (11.17)$$

$$\hat{\theta} = \frac{1}{3} \arcsin \left( \frac{3\sqrt{3}}{2} \frac{\hat{J}_3}{\hat{J}_2^{3/2}} \right) \quad (11.18)$$

$$\hat{J}_3 = J_3(\hat{\mathbf{s}}) = \hat{s}_{11}\hat{s}_{22}\hat{s}_{33} + 2\hat{s}_{12}\hat{s}_{23}\hat{s}_{31} - \hat{s}_{12}^2\hat{s}_{33} - \hat{s}_{23}^2\hat{s}_{11} - \hat{s}_{31}^2\hat{s}_{22} \quad (11.19)$$

This produces the a rounded version of the Generalized Tresca surface with a shift in the  $y$ -direction of magnitude  $a\hat{s}_u$  and the rounding controlled by  $w$ . The parameters  $\hat{s}_u$  and  $a$  are related to the input parameters by:

$$\hat{s}_{uc} = \begin{cases} s_{uc} & \text{(Option = Isotropic)} \\ \frac{1 + s_{ue}/s_{uc}}{1 + \rho} s_{uc} & \text{(Option = Anisotropic)} \end{cases} \quad (11.20)$$

$$a = \begin{cases} 0 & \text{(Option = Isotropic)} \\ \frac{4\rho - s_{ue}/s_{uc}}{3(1 + s_{ue}/s_{uc})} & \text{(Option = Anisotropic)} \end{cases} \quad (11.21)$$

For the Isotropic option, the parameters  $\rho$  and  $w$  are given by:

$$\rho = \frac{s_{ue}}{s_{uc}}, \quad w = 1 \quad (11.22)$$

For the Anisotropic option,  $\rho$  is given by

$$\rho = \begin{cases} \frac{1 + r - s_{us}/s_{uc} - \sqrt{(1+r)(1+r-2s_{us}/s_{uc})}}{s_{us}/s_{uc}} & , \quad s_{us}/s_{uc} \leq M \\ 1 & , \quad s_{us}/s_{uc} > M \end{cases} \quad (11.23)$$

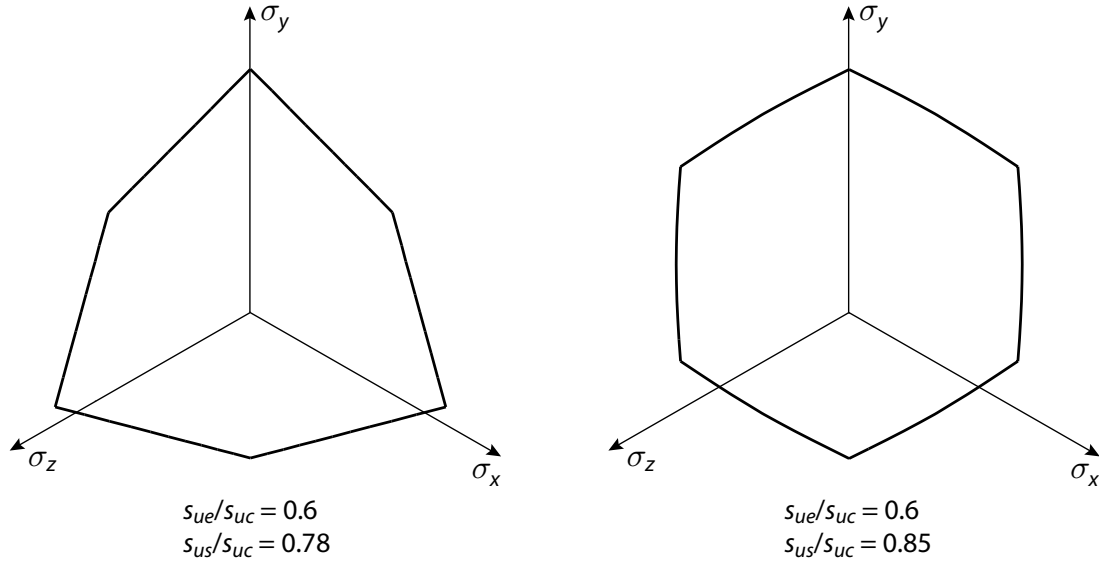


Figure 11.10: Examples of AUS yield surfaces (ultimate state).

and  $w$  is given by

$$w = \begin{cases} 1 & , s_{us}/s_{uc} \leq M \\ \frac{2\sqrt{3}(1+r-\sqrt{3}s_{us}/s_{uc})}{\sqrt{3}(2-\sqrt{3})(1+r)} & , s_{us}/s_{uc} > M \end{cases}$$

where

$$r = \frac{s_{ue}}{s_{uc}}, \quad M = \frac{1}{2}(1+r) \quad (11.24)$$

Therefore, below the line  $s_{us}/s_{uc} = \frac{1}{2}(1 + s_{ue}/s_{uc})$ , the yield surface is of the Generalized Tresca type ( $0.5 \leq \rho \leq 1$  and  $w = 1$ ), while above it, it comprises a rounded Tresca hexagon ( $\rho = 1$  and  $w < 1$ ). Some examples are shown in Figure 11.10.

The flow rule is given by

$$G = \hat{q} \quad (11.25)$$

The hardening rule is given by

$$\dot{\kappa} = \dot{\lambda} \frac{\ln 2}{\beta} (\hat{s}_u - \kappa) \quad (11.26)$$

where  $\dot{\lambda}$  is the plastic multiplier and

$$\beta = \left( \frac{1}{2} - \frac{\sqrt{3}}{2} \tan \hat{\theta} \right) \frac{\varepsilon_{c,50}}{100} + \left( \frac{1}{2} + \frac{\sqrt{3}}{2} \tan \hat{\theta} \right) \frac{\varepsilon_{e,50}}{100} \quad (11.27)$$

with  $\varepsilon_{C,50}$  and  $\varepsilon_{E,50}$  being the axial strains (in percent) halfway to failure in triaxial compression and extension respectively.

## 11.7 Notes

### 11.7.1 Limit analysis

Limit analysis is available for the AUS model as for all other models. Since iterations are required the results are somewhat influenced by the convergence tolerance which can be set under Convergence Parameters in Project. Moreover, since the AUS model is nonassociated (Generalized Tresca for the yield potential and von Mises for the flow potential) a situation may arise where where limit loads calculated with the Lower element are slightly larger than those calculated with the Upper element. However, in far most cases the difference between the two will be very small and the situation is in fact an indication that the solution is unlikely to change significantly upon further mesh refinement.

### 11.7.2 Strains halfway to failure

Strictly speaking, the input material parameters  $\varepsilon_{c,50}$  and  $\varepsilon_{e,50}$  refer to the the *plastic* strains halfway to failure in compression and extension. Usually, the distinction between total and plastic strains is immaterial as the elastic strains will be an order of magnitude smaller than the plastic strains. In some cases, however, the yield surface and initial stress state are such that a significant part of the initial stress-strain response will be purely elastic. In such cases,  $\varepsilon_{c,50}$  and  $\varepsilon_{e,50}$  can be estimated as shown in Figure 11.11. That is, the initial elastic part of the stress-strain curve (up to a level of  $\sigma_a - \sigma_r = \sigma_0$ ) is ignored and  $\varepsilon_{c,50}$  is taken as the axial strain at the halfway point to failure with respect to the remaining elastoplastic part of the stress-strain curve.

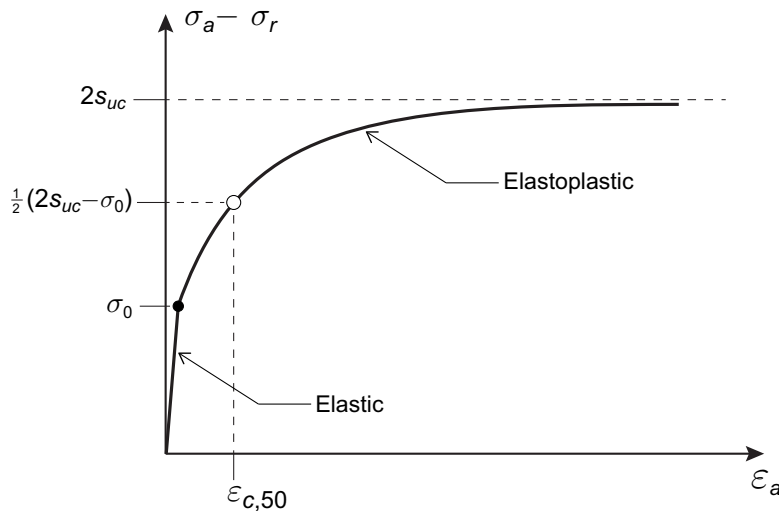


Figure 11.11: Definition of  $\varepsilon_{c,50}$  in the case where the initial response is pure elastic.



## 12 HOEK-BROWN

The Hoek-Brown criterion is commonly used to describe the strength of fractured rock. The Hoek-Brown model implemented in OptumG2 uses the 2007 version of the Hoek-Brown criterion (Hoek 2007) as the failure criterion while the Mohr-Coulomb surface is used as the plastic potential. In addition, it is possible to incorporate a compression cap as in the Mohr-Coulomb model. Similarly, regarding elasticity, the simple linear elastic model is used.

### Material, Drainage, Stiffness

See Section 8.

### Strength

The Hoek-Brown yield function is given by:

$$F = -(\sigma_1 - \sigma_3) - \sigma_{ci} \left( -m_b \frac{\sigma_3}{\sigma_{ci}} + s \right)^a \quad (12.1)$$

with

$$\begin{aligned} m_b &= m_i \exp \left( \frac{\text{GSI} - 100}{28 - 14D} \right) \\ s &= \exp \left( \frac{\text{GSI} - 100}{9 - 3D} \right) \\ a &= \frac{1}{2} + \frac{1}{6} \left( e^{\frac{-\text{GSI}}{15}} - e^{\frac{-20}{3}} \right) \end{aligned} \quad (12.2)$$

where GSI is the Geological Strength Index,  $\sigma_{ci}$  is the uniaxial compressive strength of the intact rock,  $m_i$  is a material constant, and  $D$  is the disturbance factor. In OptumG2, the following parameters are used as input:

- Geological Strength Index, GSI.
- Uniaxial compressive strength of the intact rock,  $\sigma_{ci}$  [kPa].
- Intact rock parameter,  $m_i$ .
- Disturbance factor,  $D$ .

### Flow Rule

The Hoek-Brown model makes use of a Mohr-Coulomb flow potential (see Section 8) with a variable dilation angle. For pure tension, the dilation angle is  $\psi = 90^\circ$  corresponding to separation. The dilation angle then decreases with  $\sigma_3$  to a user specified value of  $\psi_0$  for  $\sigma_3 = 0$ . A further linear decrease then takes place until  $\sigma_3 = -\sigma_\psi$ , where  $\sigma_\psi$  is a user defined parameter, after which the dilation angle remains at zero. In summary, the dilation angle varies with  $\sigma_3$  according to (see also Figure 12.1):

$$\psi = \begin{cases} \psi_0 + \frac{90^\circ - \psi_0}{\sigma_t} \sigma_3, & 0 \leq \sigma_3 \leq \sigma_t \\ \psi_0 + \frac{\psi_0}{\sigma_\psi} \sigma_3, & -\sigma_\psi \leq \sigma_3 \leq 0 \\ 0, & \sigma_3 \leq -\sigma_\psi \end{cases} \quad (12.3)$$

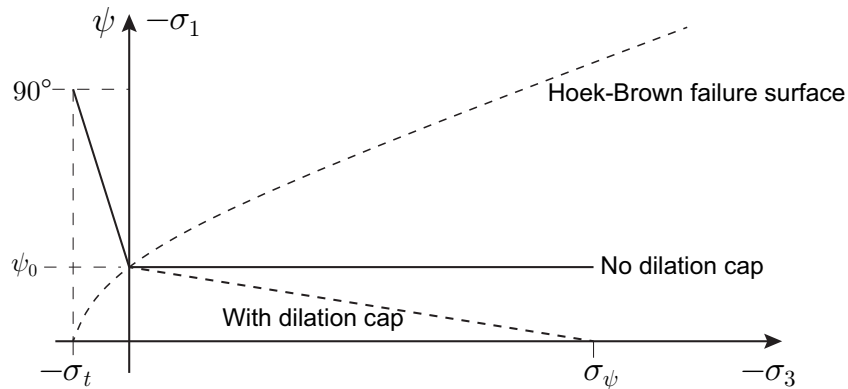


Figure 12.1: Variation of dilation angle.

As with the Mohr-Coulomb and Drucker-Prager models, it is also possible to use an associated flow rule in which case the plastic potential is the Hoek-Brown yield function. The parameters and settings of the Flow Rule category are:

- Flow Rule (Associated/Nonassociated)
  - Flow Rule = Nonassociated: Dilation angle  $\psi_0$  [°]
  - Flow Rule = Nonassociated: Dilation Cap (Yes/No)
    - Dilation Cap = Yes:  $\sigma_\psi$  [kPa]

### Compression cap, Unit Weights, Initial Stresses, Permeability

See Section 8.

## 12.1 Strength

Guidelines for estimating the four Hoek-Brown parameters GSI,  $\sigma_{ci}$ ,  $m_i$  and  $D$  are provided in Figures 12.4-12.8. Some typical Hoek-Brown yield envelopes are shown in the Figures below.

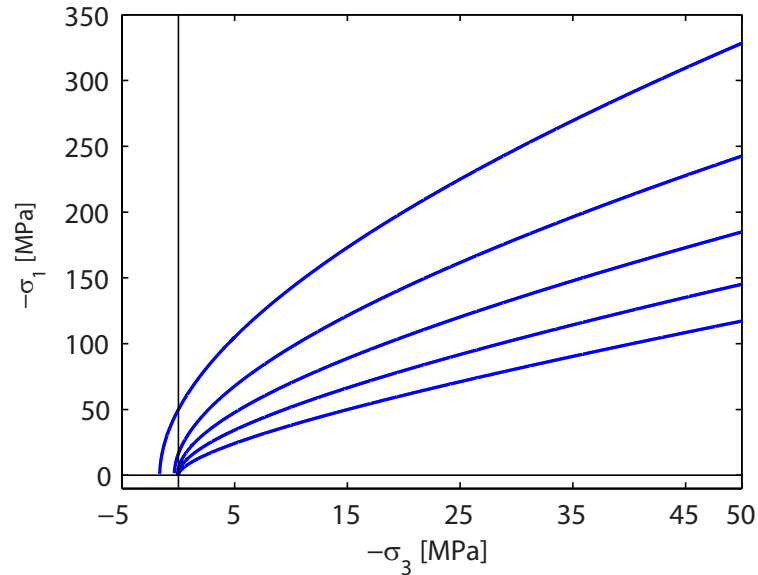


Figure 12.2: Yield envelopes for  $\sigma_{ci} = 50$  MPa,  $D = 0$ ,  $m_i = 30$  and different GSI (bottom to top): 20, 40, 60, 80, 100.

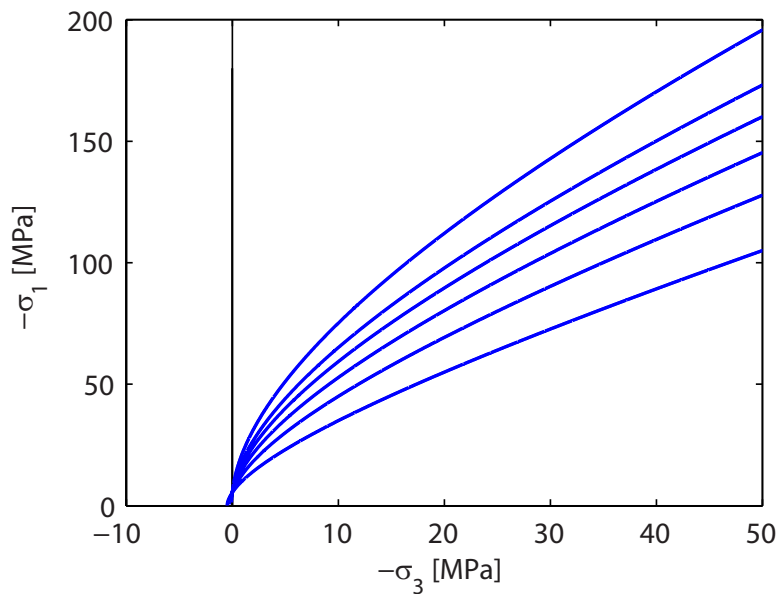


Figure 12.3: Yield envelopes for  $\sigma_{ci} = 50$  MPa,  $D = 0$ , GSI = 60, and different  $m_i$  (bottom to top): 5, 10, 15, 20, 25, 30.

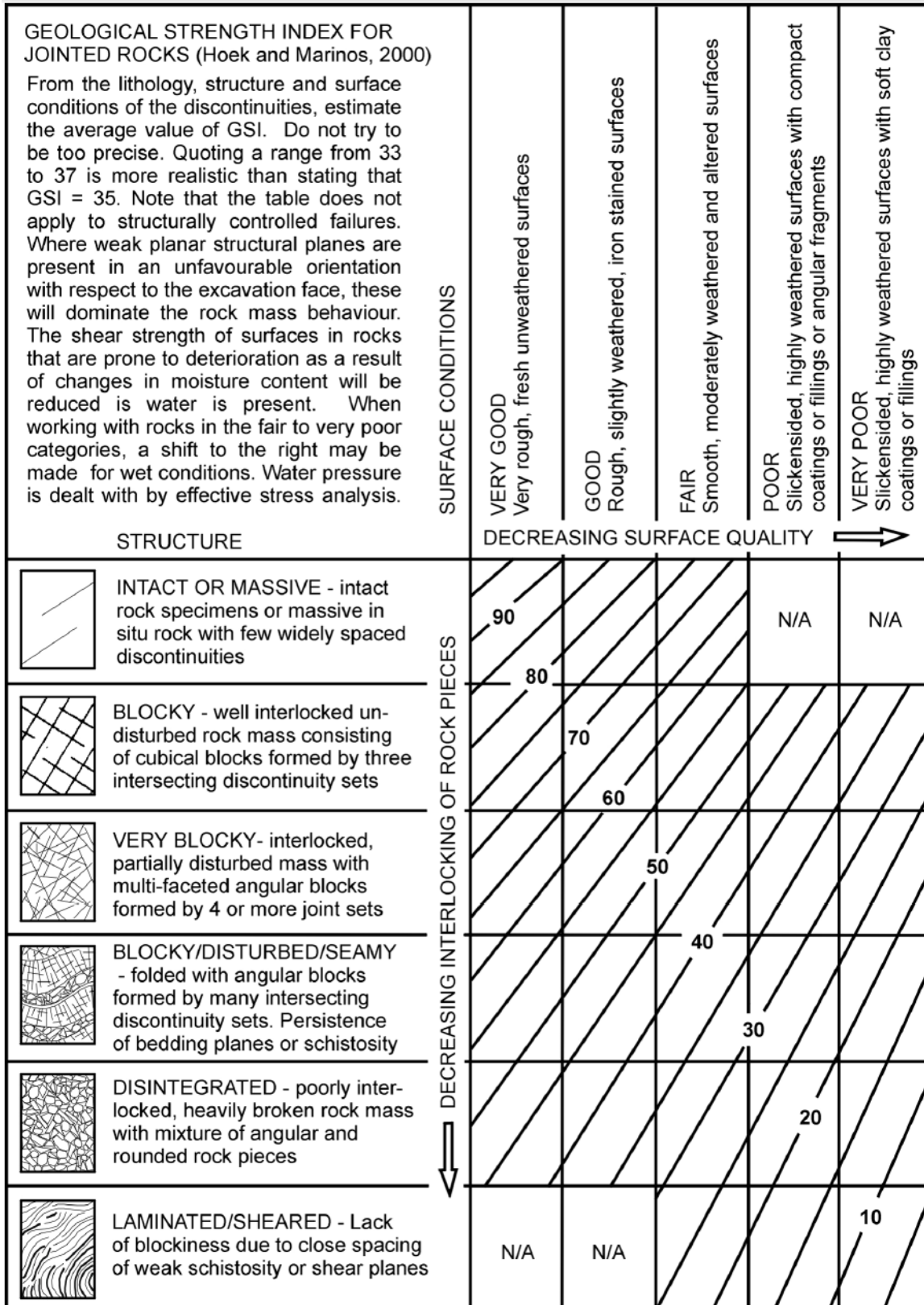


Figure 12.4: Geological Strength Index, GSI, for blocky rock masses on the basis of interlocking and joint conditions (after Hoek 2007).

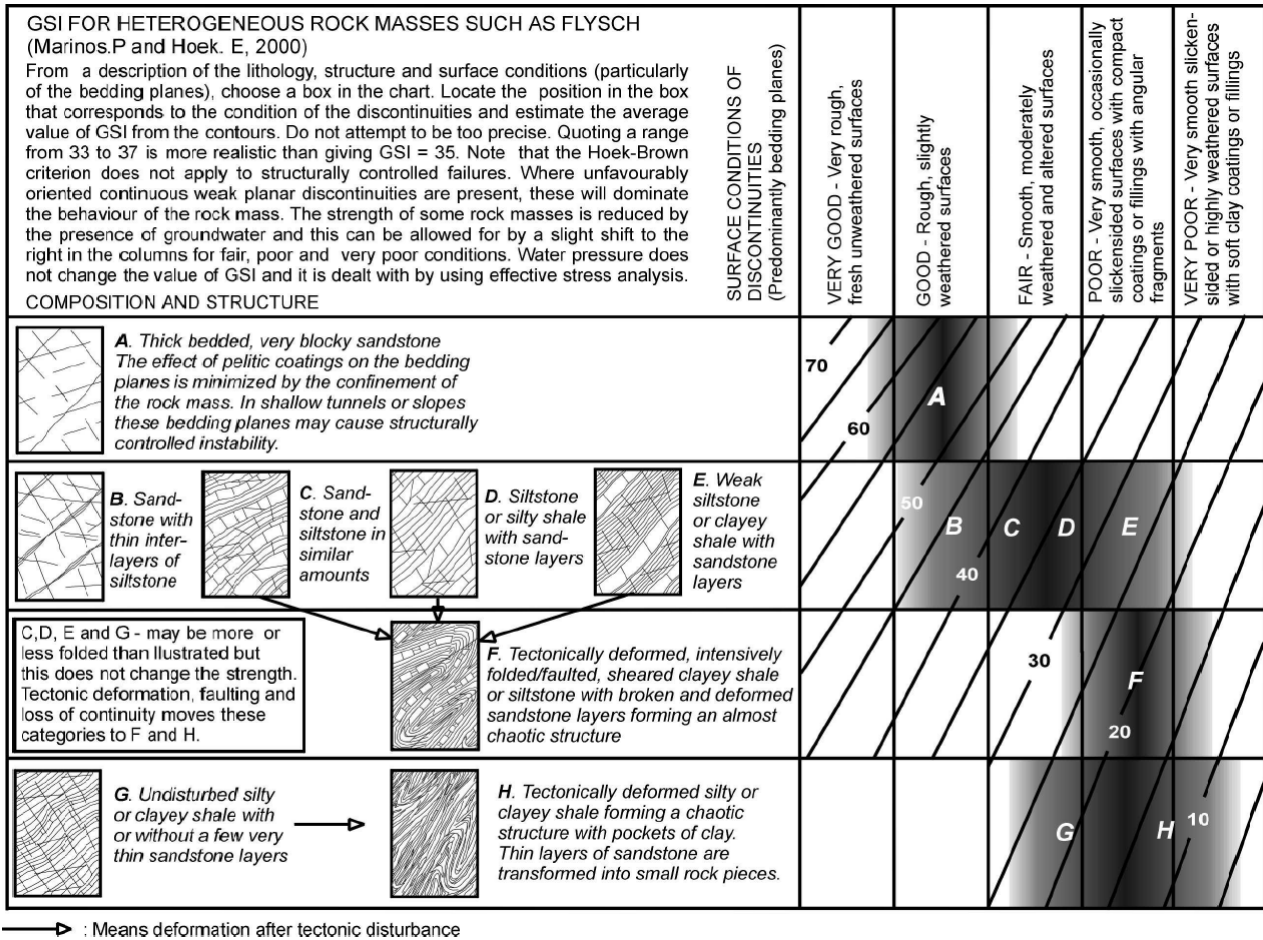


Figure 12.5: Geological Strength Index, GSI, for heterogeneous rock masses such as flysch (after Hoek 2007).

Grade	Term	Uniaxial Compressive Strength (MPa)	Field estimate of strength	Examples
R6	Extremely strong	> 250	Specimen can be chipped with a geological hammer	Fresh basalt, chert, diabase, gneiss, granite quartzite
R5	Very strong	100 – 250	Specimen requires many blows of a geological hammer to fracture it	Amphibolite, sandstone, basalt, gabbro, gneiss, granodiorite, limestone, marble, rhyolite, tuff
R4	Strong	50 – 100	Specimen requires more than one blow of a geological hammer to fracture it	Limitstone, marble phyllite, sandstone schist, shale
R3	Medium strong	25 – 50	Cannot be scraped or peeled with a pocket knife, specimen can be fractured with a single blow from a geological hammer	Claystone, coal, concrete schist, shale, siltstone
R2	Weak	5 – 25	Can be peeled with a pocket knife with difficulty, shallow indentation made by firm blow with point of a geological hammer	Chalk, rocksalt, potash
R1	Very weak	1 – 5	Crumbles under firm blows with point of a geological hammer, can be peeled by a pocket knife.	Highly weathered or altered rock
R0	Extremely weak	0.25 – 1	Indented by thumbnail	Stiff fault gouge

Figure 12.6: Field estimates of uniaxial compressive strength  $\sigma_{ci}$  (after Hoek 2007).

Rock type	Class	Group	Texture			
			Coarse	Medium	Fine	Very Fine
SEDIMENTARY	Clastic		Conglomerate (20)	Sandstone 19	Siltstone 9	Claystone 4
				Greywacke (18)		
	Non-Clastic	Organic			Chalk 7	
					Coal (8-21)	
		Carbonate	Breccia (22)	Sparitic Limestone (10)	Micritic Limestone 8	
	Chemical		Gypstone 16	Anhydrite 13		
METAMORPHIC	Non-Foliated		Marble 9	Hornfels (19)	Quartzite 24	
	Slightly Foliated		Migmatite (30)	Amphibolite (25-31)	Mylonites (6)	
	Foliated		Gneiss 33	Schists (4-8)	Phyllites (10)	Slate 9
IGNEOUS	Light		Granite 33		Rhyolite (16)	
			Granodiorite (30)		Dacite (17)	
	Dark		Diorite (28)		Andesite 19	
			Gabbro 27 Norite 22	Dolerite (19)	Basalt (17)	
Extrusive Pyroclastic Type		Agglomerate (20)	Breccia (18)	Tuff (15)		

Figure 12.7: Values of the constant  $m_i$  by rock group (after Hoek 2007).




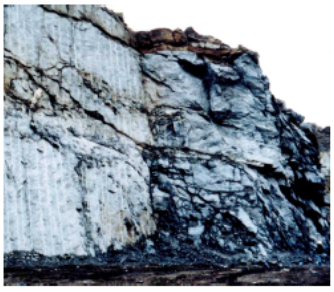

Appearance of rock mass	Description of rock mass	Suggested value of $D$
	Excellent quality controlled blasting or excavation by Tunnel Boring Machine results in minimal disturbance to the confined rock mass surrounding a tunnel.	$D = 0$
	Mechanical or hand excavation in poor quality rock masses (no blasting) results in minimal disturbance to the surrounding rock mass.  Where squeezing problems result in significant floor heave, disturbance can be severe unless a temporary invert, as shown in the photograph, is placed.	$D = 0$  $D = 0.5$ No invert
	Very poor quality blasting in a hard rock tunnel results in severe local damage, extending 2 or 3 m, in the surrounding rock mass.	$D = 0.8$
	Small scale blasting in civil engineering slopes results in modest rock mass damage, particularly if controlled blasting is used as shown on the left hand side of the photograph. However, stress relief results in some disturbance.	$D = 0.7$ Good blasting  $D = 1.0$ Poor blasting
	Very large open pit mine slopes suffer significant disturbance due to heavy production blasting and also due to stress relief from overburden removal.  In some softer rocks excavation can be carried out by ripping and dozing and the degree of damage to the slopes is less.	$D = 1.0$ Production blasting  $D = 0.7$ Mechanical excavation

Figure 12.8: Guidelines for estimating the disturbance factor  $D$  (after Hoek 2007).

### 12.2 Elastic parameters

There are several empirical equations relating the elastic parameters to measures of rock type and quality. For Young’s modulus, Hoek (2007) quotes the following correlation:

$$E = 10^5 \left( \frac{1 - \frac{1}{2}D}{1 + \exp\left(\frac{75+25D-GSI}{11}\right)} \right) \text{ [MPa]} \tag{12.4}$$

The variation of  $E$  with GSI for different values of  $D$  is shown in Figure 12.9.

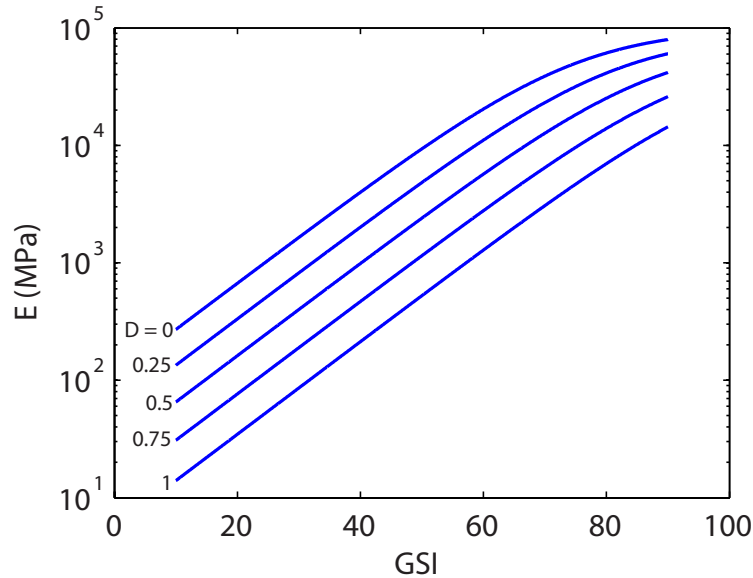


Figure 12.9: Variation of Young’s modulus with GSI for different values of  $D$ .

For most rock types Poisson’s ratio falls in the range of  $\nu = 0.1$  to  $\nu = 0.4$ , with a significant variation within the same rock type (see Figure 12.10).



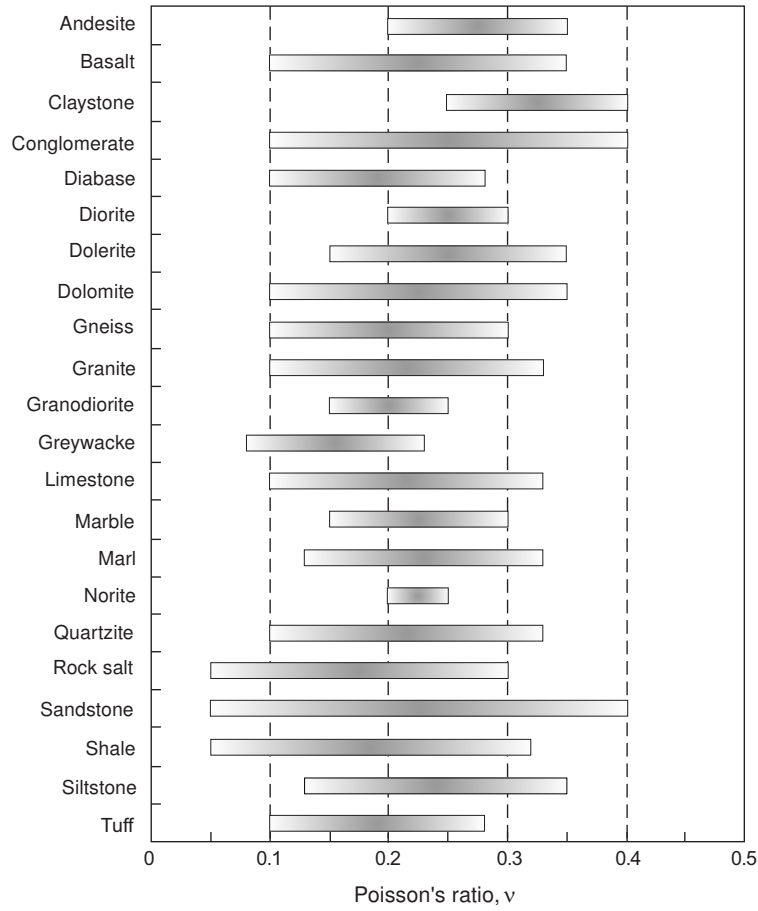


Figure 12.10: Poisson's ratio for some rock types (after Gercek 2007).

### 12.3 Relation to Mohr-Coulomb parameters

Following the approach described by Hoek (2007), the curved Hoek-Brown yield envelope may be approximated by the Mohr-Coulomb model using the standard Mohr-Coulomb cone augmented with a tension-cutoff.

Firstly, with reference to the Mohr-Coulomb model implemented in OptumG2, the tension cut-off parameters are given by

- $k_t = \frac{5\sigma_{ci}}{m_b}$  [kPa]
- $\phi_t = 90^\circ$

Secondly, a best-fit Mohr-Coulomb line in the interval between  $-\sigma_t \leq -\sigma_3 \leq \sigma_{3,\max}$ , leads to the following Mohr-Coulomb parameters:

- $\phi = \arcsin \left[ \frac{6am_b(s + m_b\sigma_{3n})^{a-1}}{2(1+a)(2+a) + 6am_b(s + m_b\sigma_{3n})^{a-1}} \right] [^\circ]$
- $c = \frac{\sigma_{ci}[(1+2a)s + (1-a)m_b\sigma_{3n}](s + m_b\sigma_{3n})^{a-1}}{(1+a)(2+a)\sqrt{1 + \frac{6am_b(s + m_b\sigma_{3n})^{a-1}}{(1+a)(2+a)}}}$  [kPa]

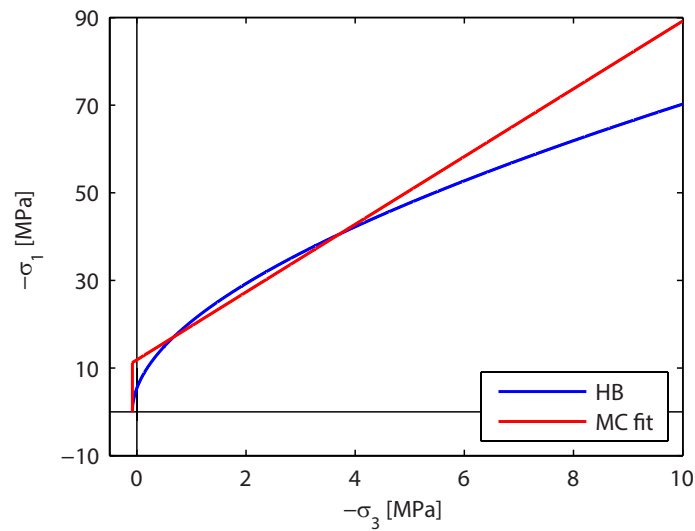


Figure 12.11: Mohr-Coulomb fit to Hoek-Brown envelope for  $GSI = 60$ ,  $\sigma_{ci} = 50$  MPa,  $m_i = 30$ ,  $D = 0$ , and  $\sigma_{3,max} = 5$  MPa.

where  $\sigma_{3n} = \sigma_{3,max}/\sigma_{ci}$  with  $\sigma_{3,max}$  being positive in compression. An example of a fit is shown in Figure 12.11.

As a rule of thumb, Hoek (2007) suggests that a first estimate of  $\sigma_{3,max}$  may be taken as  $\sigma_{3,max} = 0.25\sigma_{ci}$ .

### 12.4 Strength reduction

In Strength Reduction analysis (see the Analysis Manual), the Hoek-Brown criterion is treated by reducing the parameters  $\sigma_{ci}$  and  $m_b$  equally to induce a state of collapse. The resulting factor is the strength based factor of safety:

$$FS_s = \frac{\sigma_{ci}}{(\sigma_{ci})_{red}} = \frac{m_i}{(m_i)_{red}} \tag{12.5}$$

An example of the difference between the original yield envelope and that resulting from a factor of 1.25 is shown in Figure 12.12. While the decision as to which parameters are reduced is quite subjective, the approach used for the Hoek-Brown criterion is consistent with the one used for the Mohr-Coulomb criterion. As such, the tensile strength  $s\sigma_{ci}/m_b$  is unaffected by the reduction.

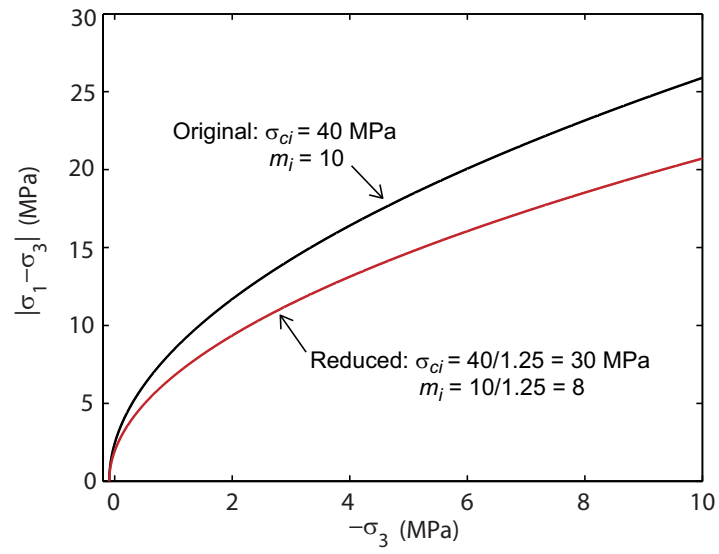


Figure 12.12: Original and reduced Hoek-Brown envelopes.

### 13 GSK

The GSK model is similar to the Hoek-Brown model in that a curved yield surface is used in place of the Mohr-Coulomb yield surface. The GSK yield function is a generalization of the one proposed by Krabbenhoft et al. (2012b) to account for the pressure dependence of the peak strength of granular materials such as sands, particularly at low stress levels. The generalized model allows for including a finite tensile strength. An attractive feature of the GSK criterion is that all parameters involved (four in total) may be interpreted in terms of a standard Mohr-Coulomb criterion.

#### Material, Drainage, Stiffness

See Section 8.

#### Strength

The yield function is given by:

$$F = -[\sigma_1 - a_2(\sigma_3 - \sigma_t)] - (k - a_2\sigma_t) \left\{ 1 - \exp \left[ \frac{a_1 - a_2}{k - a_2\sigma_t} (\sigma_3 - \sigma_t) \right] \right\} \quad (13.1)$$

where

$$a_1 = \frac{1 + \sin \phi_1}{1 - \sin \phi_1}, \quad a_2 = \frac{1 + \sin \phi_2}{1 - \sin \phi_2}, \quad k = \frac{2c \cos \phi_2}{1 - \sin \phi_2} \quad (13.2)$$

with the input parameters being:

- Friction angle at low stress levels,  $\phi_1$  [°]
- Friction angle at high stress levels,  $\phi_2$  [°]
- Apparent cohesion at high stress levels,  $c$  [kPa]
- Tensile strength,  $\sigma_t$  [kPa]

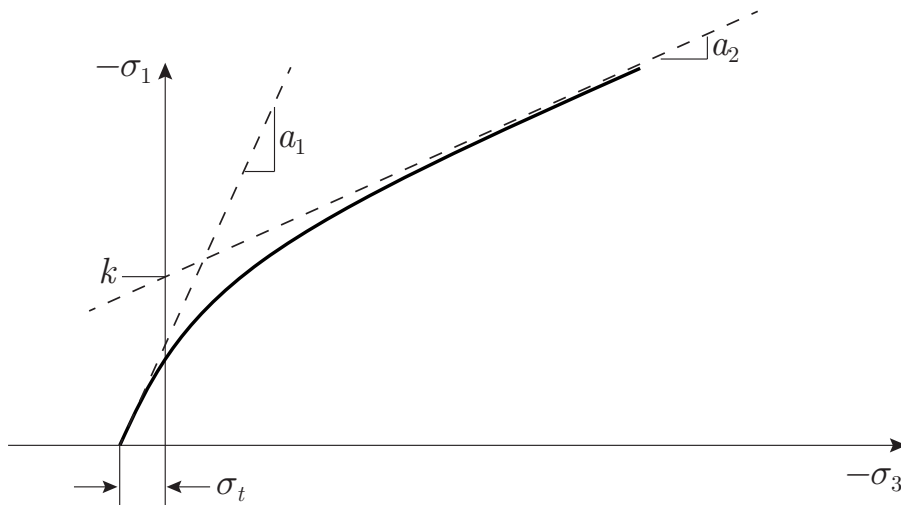


Figure 13.1: GSK yield envelope in  $\sigma_1$ - $\sigma_3$  space [compare to the standard Mohr-Coulomb envelope, Figure 8.1(b)].

The GSK yield envelope is shown in Figure 13.1. It may be interpreted as a nonlinear Mohr-Coulomb envelope with friction angle  $\phi_{MC}$  and cohesion  $c_{MC}$  given by (see Figure 13.2):

$$\phi_{MC} = \arcsin \left( \frac{B-1}{B+1} \right) \quad (13.3)$$

$$c_{MC} = \frac{1 - \sin \phi_{MC}}{2 \cos \phi_{MC}} (A + B\sigma_3)$$

where

$$A = a_2(\sigma_t - \sigma_3) + (k - a_2\sigma_t) \left\{ 1 - \exp \left[ \frac{(a_2 - a_1)(\sigma_t - \sigma_3)}{k - a_2\sigma_t} \right] \right\} \quad (13.4)$$

$$B = a_2 - (a_2 - a_1) \exp \left[ \frac{(a_2 - a_1)(\sigma_t - \sigma_3)}{k - a_2\sigma_t} \right]$$

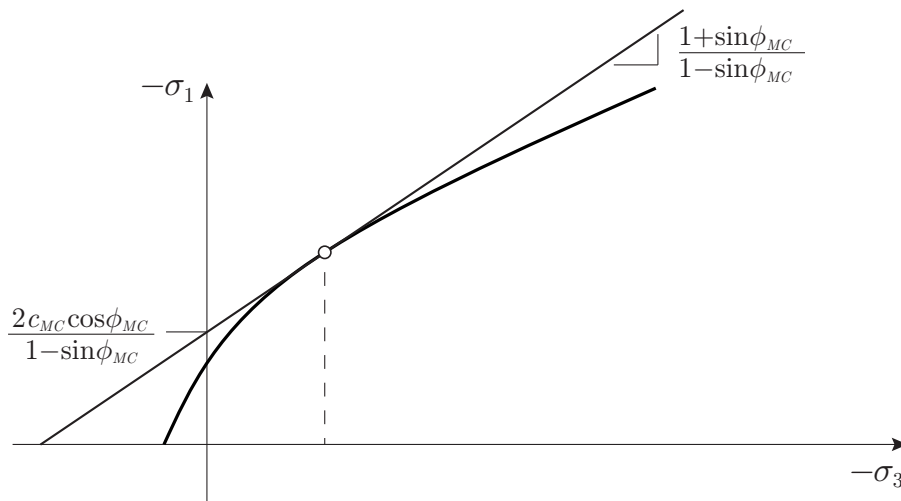


Figure 13.2: GSK envelope and Mohr-Coulomb tangent plane defined by  $c_{MC}$  and  $\phi_{MC}$  [compare to the standard Mohr-Coulomb envelope, Figure 8.1(b)].

For cohesionless materials such as sands, the strength is often specified in terms of the secant friction angle,  $\phi_{sec}$ , defined by

$$\left( \frac{\sigma_1}{\sigma_3} \right)_f = \frac{1 + \sin \phi_{sec}}{1 - \sin \phi_{sec}} \quad (13.5)$$

where  $(\sigma_1/\sigma_3)_f$  is the stress ratio at failure (see Figure 13.3). For the GSK model, the secant friction angle is given by

$$\phi_{sec} = \arcsin \left( \frac{A_f + \sigma_{3f}}{A_f - \sigma_{3f}} \right) \quad (\text{for } \sigma_t = 0) \quad (13.6)$$

where  $A_f = A(\sigma_{3f})$  is given by (13.4). With the secant friction angle at three different stress states, the three GSK parameters,  $a_1$ ,  $a_2$  and  $k$  (or, equivalently,  $\phi_1$ ,  $\phi_2$  and  $c$ ) can be determined.

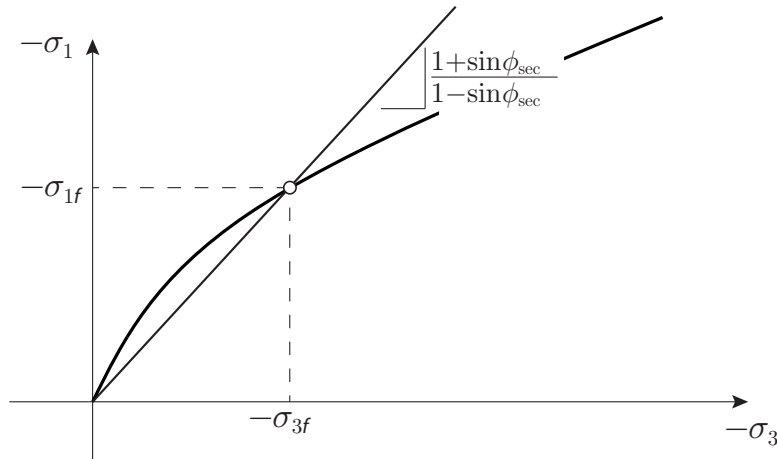


Figure 13.3: GSK yield envelope with definition of secant friction angle.

**Flow Rule**

The GSK model offers three different possibilities for specifying the flow rule:

- Associated. Standard associated flow rule the flow potential equal to the GSK yield function.
- GSK. Nonassociated flow rule with a dilation angle  $\psi = \beta(\phi - \phi_2)$  where  $\phi$  is the current equivalent Mohr-Coulomb friction angle and  $\beta$  is a parameter. This is similar to the flow rule of the Bolton model (see Section 14).
- Constant Dilation. Nonassociated flow rule with a constant dilation angle equal to  $\psi_0$  except for  $0 \leq \sigma_3 \leq \sigma_t$  where it varies linearly between  $\psi_0$  and  $\phi_1$  as shown in Figure 13.4.

The GSK and Constant Dilation flow rules may be further augmented by a strain based dilation cap as in the Mohr-Coulomb model.

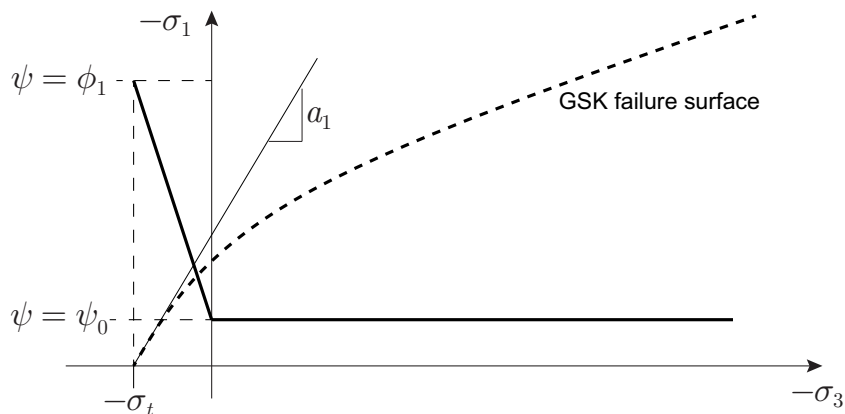


Figure 13.4: Variation of dilation angle.

**Compression Cap, Unit Weights, Initial Stresses, Permeability**

See Section 8.

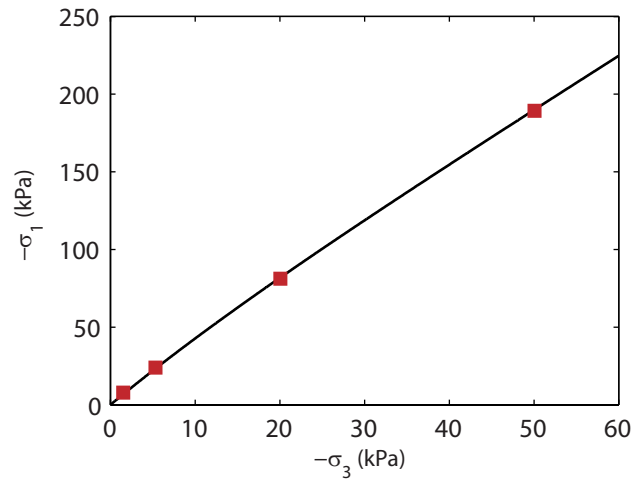


Figure 13.5: Triaxial test results matched to the GSK criterion with the parameters of Table 13.1.

### 13.1 Examples of application

Krabbenhoft et al. (2012b) conducted a series of triaxial tests on sands of variable density. The peak strengths were found to be fitted very well using the parameters shown in Table 13.1. It is noted that  $c \approx 5$  kPa is relatively insensitive of the relative density and that  $\phi_1 - \phi_2 \approx 7^\circ$  independent of  $D_r$ .

$D_r$	$\phi_1$ ( $^\circ$ )	$\phi_2$ ( $^\circ$ )	$c$ (kPa)
0.20	34.2	27.0	3.7
0.59	39.7	33.3	5.1
0.84	43.3	36.5	5.0

Table 13.1: GSK parameters as function of relative density for triaxial tests on sand (Krabbenhoft et al. 2012b). In all cases  $\sigma_t = 0$ .

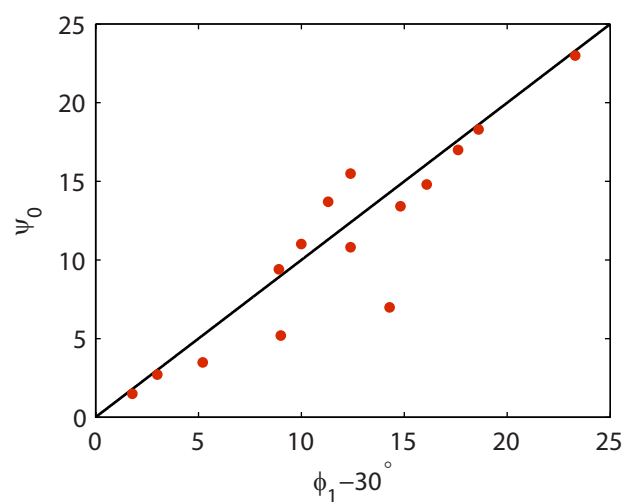


Figure 13.6: Relation between measured  $\phi_1$  and  $\psi_0$  (data from Krabbenhoft et al. 2012b).

Regarding the flow rule, the experiments mentioned above suggest a value of the dilation angle of (see Figure 13.6)

$$\psi_0 \simeq \phi_1 - 30^\circ \quad (13.7)$$

The value of the maximum volumetric strain,  $\varepsilon_{v,cr}$ , ranged from about 1% for the loose sand to about 10% for the dense sand and with a trend to decrease with increasing confining pressures.

In another study, Ahmed (1972) found a variation of the friction angle with the confining stress as shown in Figure 13.7. The tests were here conducted under plane strain conditions for sands with a relative density of approximately 0.7–0.75. Again the GSK model provides a reasonable fit to the data.

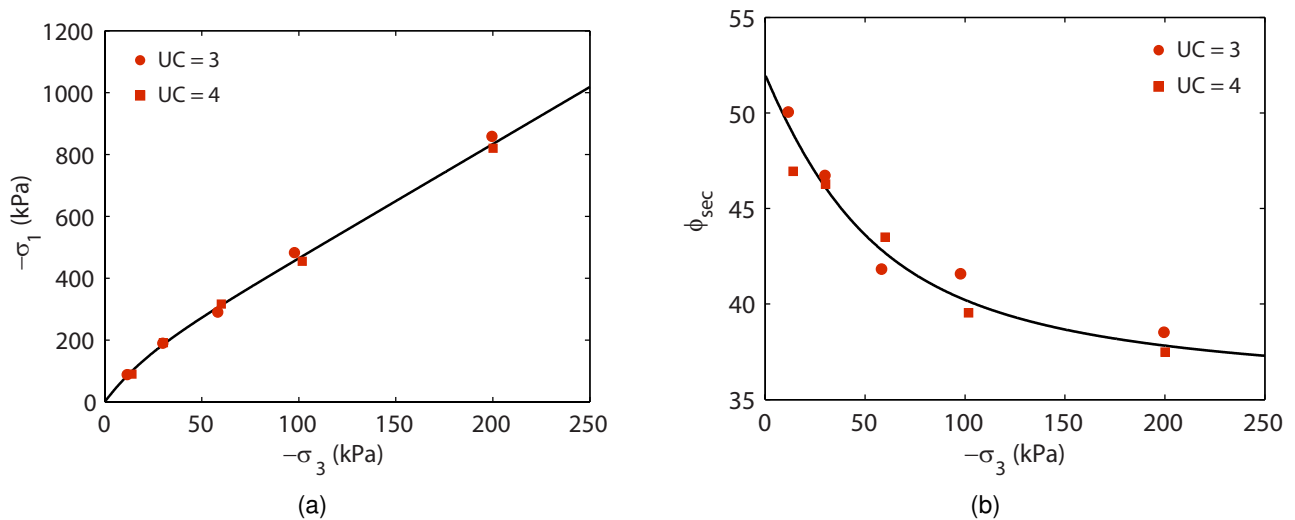
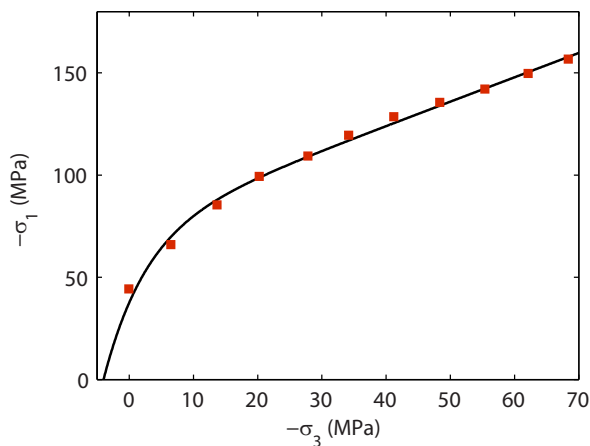


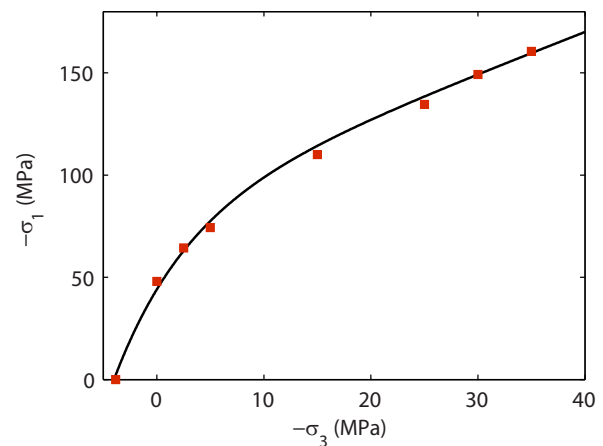
Figure 13.7: Plane strain test results for sands with two different uniformity coefficients (UC) matched to the GSK criterion with parameters  $\phi_1 = 52^\circ$ ,  $\phi_2 = 35^\circ$ ,  $c = 25$  kPa,  $\sigma_t = 0$  (test data from Ahmed 1972).

Finally, while the Hoek-Brown model is available for the modeling of rock, the GSK model is in many cases capable of reproducing typical experimental data rather well. Two examples are shown in Figure 13.8 where triaxial test data for a limestone and a sandstone have been fitted by the GSK criterion.





(a) Limestone:  $\phi_1 = 58^\circ$ ,  $\phi_2 = 5^\circ$ ,  $c = 35$  MPa,  $\sigma_t = 4$  MPa. Experimental data from Hoek (1983).



(b) Sandstone:  $\phi_1 = 60^\circ$ ,  $\phi_2 = 20^\circ$ ,  $c = 31$  MPa,  $\sigma_t = 4$  MPa. Experimental data from Sheorey (1997)

Figure 13.8: GSK fits to triaxial test data for limestone (left) and sandstone (right).

## 13.2 Strength reduction

In Strength Reduction analysis (see the Analysis Manual), the GSK criterion is treated by reducing the parameters  $c$ ,  $\tan \phi_1$  and  $\tan \phi_2$  equally (see Figure 13.9) to induce a state of collapse. The resulting factor is the strength based factor of safety:

$$FS_s = \frac{c}{c_{red}} = \frac{\tan \phi_1}{(\tan \phi_1)_{red}} = \frac{\tan \phi_2}{(\tan \phi_2)_{red}} \quad (13.8)$$

While the decision as to which parameters are reduced is quite subjective, the approach used for the GSK criterion is consistent with the one used for the Mohr-Coulomb criterion. As such, the tensile strength  $\sigma_t$  is unaffected by the reduction.

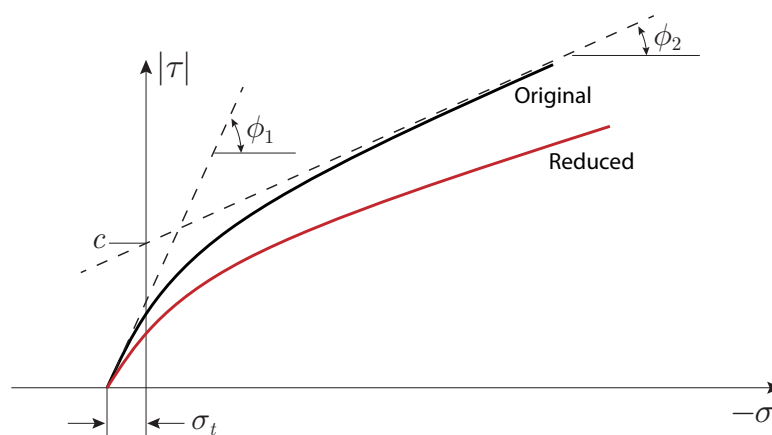


Figure 13.9: Original and reduced GSK envelopes.

**13.3 Notes**

The GSK criterion is convex only for

$$\sigma_t \leq \frac{2c \cos \phi_2}{1 + \sin \phi_2} \quad (13.9)$$

Analyses with parameter sets not satisfying this inequality will not be processed.

## 14 BOLTON

The Bolton model incorporates the stress-dilatancy correlations for sands proposed by Bolton (1986). These correlations provide peak friction and dilation angles as function of stress level and relative density. For a fixed density, the resulting failure envelope is nonlinear and similar to those of Hoek-Brown and GSK, i.e. the apparent friction angle increases with decreasing mean stress.

### Material, Drainage, Stiffness

See Section 8.

### Strength

The yield function of the Bolton model is of the Mohr-Coulomb type with a pressure and density dependent friction angle:

$$F_B = |\sigma_1 - \sigma_3| + (\sigma_1 + \sigma_3) \sin \phi_B \quad (14.1)$$

The friction angle is given by

$$\phi_B = \phi_{cv} + bI_R \quad (14.2)$$

where  $\phi_{cv}$  is the constant-volume (critical-state) friction angle,  $b$  is a model parameter and  $I_R$  is the relative dilatancy. The latter quantity is defined by Bolton (1986) as:

$$I_R = I_D(Q - \ln p) - R \quad (14.3)$$

where  $I_D$  is the relative density,  $p$  is the mean stress, and  $Q$  and  $R$  are model parameters. Bolton (1986) suggests that  $I_R$  is limited by:

$$0 \leq I_R \leq 4 \quad (14.4)$$

While some evidence for very large friction angles at very low stresses levels is available (e.g Alshibli et al. 2003) OptumG2 implements the above limits.

In summary, the Bolton model requires specification of five parameters:

1. The constant-volume (critical-state) friction angle  $\phi_{cv}$ . Typical values are in the range of  $30^\circ \leq \phi_{cv} \leq 36^\circ$  with  $\phi_{cv} = 33^\circ$  often being reported (Bolton 1986).
2. The relative density  $I_D$  varying between 0 and 1.
3. The model parameter  $Q$ . Bolton (1986) links this to the particle crushing strength,  $\sigma_c$ , by  $Q = \ln \sigma_c$  and suggests values of  $Q = 10$  for quartz and feldspar grains down to  $Q = 8$  for limestone,  $Q = 7$  for anthracite, and  $Q = 5.5$  for chalk.
4. The model parameter  $R$ . Bolton (1986) suggests a value of  $R = 1$  for a wide range of sands.
5. The model parameter  $b$ . Bolton (1986) suggests values of  $b = 3$  for triaxial compression and  $b = 5$  for plane strain. However, significantly lower values have also been reported, e.g.  $m = 1.6$  by White et al. (2008).

The variation of the friction angle  $\phi_B$  with mean stress is shown in Figure 14.1 for some typical parameter sets.

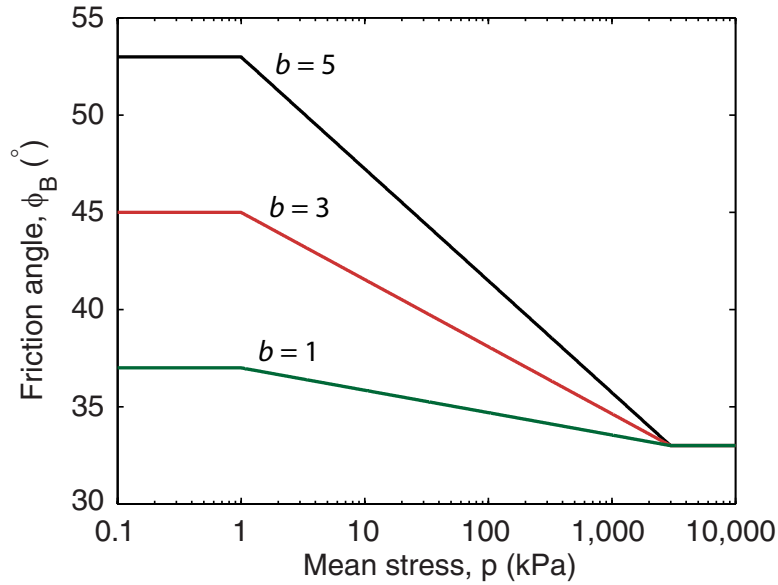


Figure 14.1: Variation of friction angle with mean stress for  $\phi_{cv} = 33^\circ$ ,  $I_D = 0.5$ ,  $Q = 10$ ,  $R = 1$ .

### Flow Rule

The flow potential of the Bolton model is given by

$$G_B = |\sigma_1 - \sigma_3| + (\sigma_1 + \sigma_3) \sin \psi_B \tag{14.5}$$

The Bolton model provides a choice of two flow rules:

- Associated. Standard associated flow rule with  $\psi_B = \phi_B$ .
- Bolton. Nonassociated flow rule with  $\psi_B = \beta(\phi_B - \phi_{cv})$  where  $\beta$  is a parameter. The original relations published by Bolton recommended  $\beta = 1.25$ .

In both cases, the dilation can be limited by a Dilation Cap of the Mohr-Coulomb type (see Section 8).

### Compression Cap, Unit Weights, Initial Conditions, Hydraulic Model

See Section 8.

#### 14.1 Strength reduction

In Strength Reduction analysis (see the Analysis Manual), the Bolton criterion is treated by reducing the friction angle  $\phi_B$  to induce a state of collapse. The resulting factor is the strength based factor of safety:

$$FS_s = \frac{\tan \phi_B}{(\tan \phi_B)_{red}} \tag{14.6}$$

While the decision as to which parameters are reduced is quite subjective, the approach used for the Bolton criterion is consistent with the one used for the Mohr-Coulomb criterion.

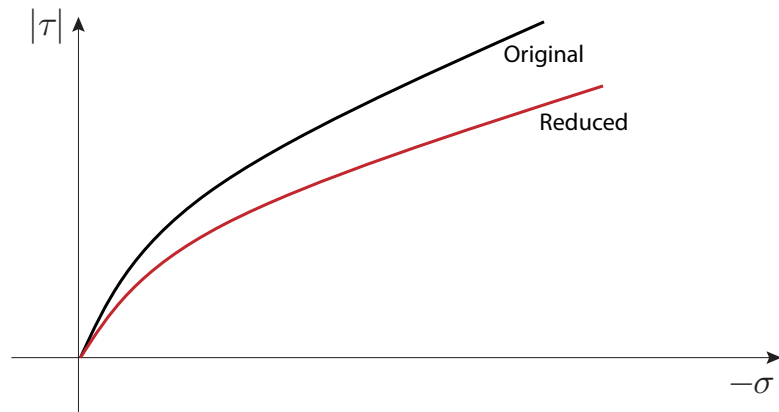


Figure 14.2: Original and reduced Bolton envelopes.

## 15 MODIFIED CAM CLAY

The critical state models developed by Roscoe and his coworkers (Roscoe and Burland 1968; Schofield and Wroth 1968) in the 1960s have been widely applied in geomechanics and form the basis of a large number of later models. The Modified Cam Clay model of Roscoe and Burland (1968) has been particularly popular. A slightly extended version of this model (including a finite cohesion) is implemented in OptumG2 following the scheme proposed by Krabbenhoft and Lyamin (2012).

The material parameters of Modified Cam Clay are to some extent interrelated and it is not possible to distinguish as sharply between strength and stiffness parameters as for other materials. In the following, the parameters are described in the sequence that they appear in OptumG2.

### Stiffness

One of the basic premises of Modified Cam Clay is that the specific volume versus effective mean stress in isotropic compression may be described by a relation of the type shown in Figure 15.1. In terms of elastoplasticity theory, the normal compression line may be interpreted as an elastoplastic branch while the response on an unloading/reloading line is elastic.

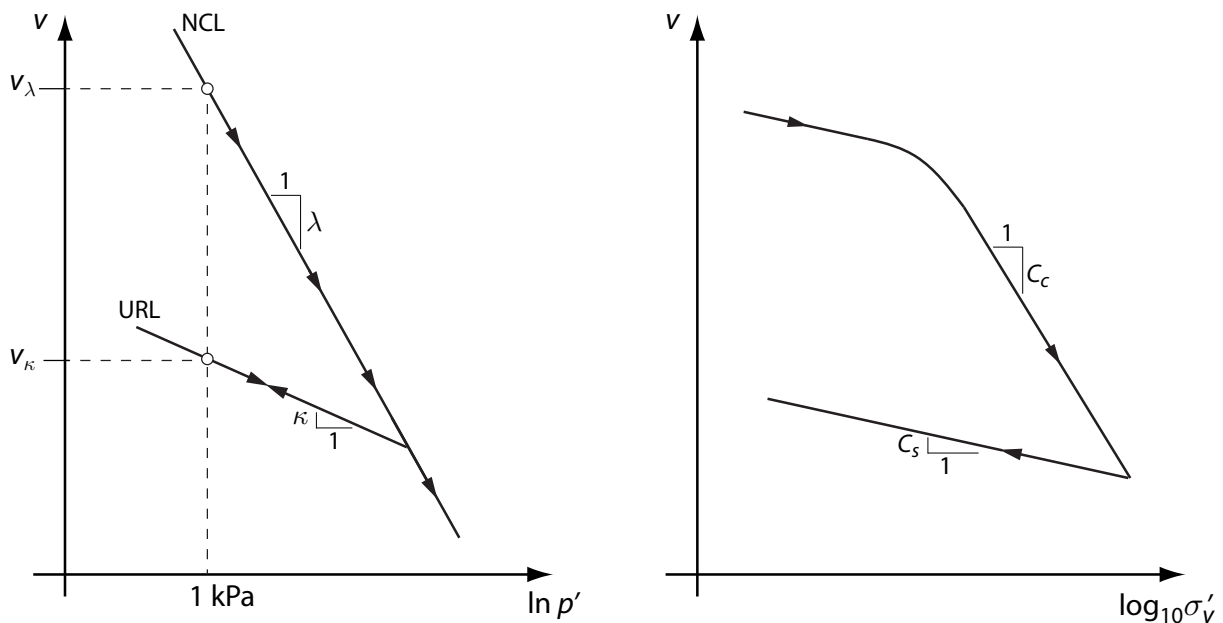


Figure 15.1: Normal compression line (NCL) and unloading-reloading line (URL) in  $\ln p', v$  space (left) and typical response in oedometer test in terms of  $\log_{10} \sigma'_v$  vs  $v$ .

With reference to Figure 15.1, the response in elastoplastic loading is given by

$$v = v_\lambda - \lambda \ln p' \tag{15.1}$$

while, the governing equation for unloading/reloading is

$$v = v_\kappa - \kappa \ln p' \tag{15.2}$$

In conventional oedometer tests where the void ratio is plotted as function of the base 10 logarithm of the vertical stress (see Figure 15.1). It may be shown that the Modified Cam Clay parameters  $\kappa$  and  $\lambda$  are related to the conventional oedometric parameters,  $C_s$  and  $C_c$ , by

$$\begin{aligned} C_c &= \ln(10)\lambda = 2.3\lambda \\ C_s &\simeq \ln(10)\kappa = 2.3\kappa \end{aligned} \quad (15.3)$$

While the relation between  $C_s$  and  $\kappa$  is not exact it is usually a good approximation (see Muir Wood 1990, for details).

For Modified Cam Clay, the incremental stress-strain relation may be written as

$$\dot{\varepsilon}_v = \begin{cases} \frac{\kappa}{1+e} \frac{\dot{p}'}{p'} & \text{in elastic unloading/reloading} \\ \frac{\lambda}{1+e} \frac{\dot{p}'}{p'} & \text{in elastoplastic loading} \end{cases} \quad (15.4)$$

where  $\kappa$  is the recompression index,  $\lambda$  is the compression index, and  $e$  is the void ratio which is related to the volumetric strain by

$$v = 1 + e = (1 + e_0)(1 - \varepsilon_v) \quad (15.5)$$

where  $e_0$  is the initial void ratio and  $\varepsilon_v = -(\varepsilon_x + \varepsilon_y + \varepsilon_z)$  is the volumetric strain (positive in compaction).

From the elastic part of (15.4), a tangent bulk modulus can be identified as

$$K_t = \frac{1+e}{\kappa} p' \quad (15.6)$$

By introducing a Poisson's ratio,  $\nu$  a tangent shear modulus is introduced as:

$$G_t = \frac{3}{2} \frac{1-2\nu}{1+\nu} K_t \quad (15.7)$$

Together,  $K_t$  and  $G_t$  define a tangent elastic modulus,  $\mathbb{C}_t$  such that the general three-dimensional elastic stress-strain relation is given by

$$\dot{\varepsilon}^e = \mathbb{C}_t \dot{\sigma}' \quad (15.8)$$

In summary, the three stiffness parameters are:

- Recompression index,  $\kappa$
- Compression index,  $\lambda$
- Poisson's ratio,  $\nu$

The initial void ratio,  $e_0$ , is considered part of the initial conditions (see below).

## Strength

The conventional Modified Cam Clay model makes use of a hardening yield surface given by

$$F(p', q, \kappa) = q^2 - M^2 p' (p_c - p') \quad (15.9)$$

where

$$\begin{aligned} p' &= -\frac{1}{3}(\sigma'_x + \sigma'_y + \sigma'_z) \\ q &= \left[ \frac{1}{2}(\sigma_x - \sigma_y)^2 + \frac{1}{2}(\sigma_y - \sigma_z)^2 + \frac{1}{2}(\sigma_z - \sigma_x)^2 + 3\tau_{xy}^2 + 3\tau_{yz}^2 + 3\tau_{zx}^2 \right]^{\frac{1}{2}} \end{aligned} \quad (15.10)$$

with  $p_c$  being the preconsolidation pressure which acts as a hardening variable. The friction parameter  $M$  is related to the frictional angle by

$$M = \frac{3 \sin \phi}{\sqrt{3} \cos \theta + \sin \theta \sin \phi} \quad (15.11)$$

where

$$\theta = \tan^{-1} \left[ \frac{1}{\sqrt{3}} \left( 2 \frac{\sigma_2 - \sigma_3}{\sigma_1 - \sigma_3} - 1 \right) \right] \quad (15.12)$$

is the Lode angle.

In OptumG2, cohesion is introduced by defining a new pressure variable:

$$\tilde{p} = p + c / \tan \phi \quad (15.13)$$

where  $c$  is the cohesion. The yield surface is then given by:

$$F(\tilde{p}', q, \kappa) = q^2 - M^2 \tilde{p}' (p_c - \tilde{p}') \quad (15.14)$$

For fixed  $p_c = p_{c,j} > 0$ , the yield functions  $F(\tilde{p}', q, p_{c,j}) = 0$  define ellipses in  $p'$ - $q$  space with the critical state line,  $q = M(p' + c / \tan \phi)$ , passing through the top point (see Figure 15.2).

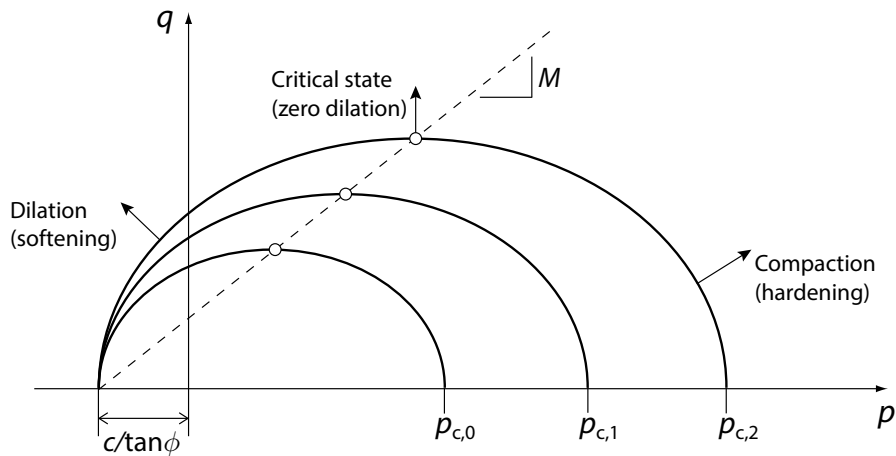


Figure 15.2: Modified Cam clay yield surfaces  $F(p, q, p_{c,j}) = 0$  for fixed  $p_{c,j} > 0$ .



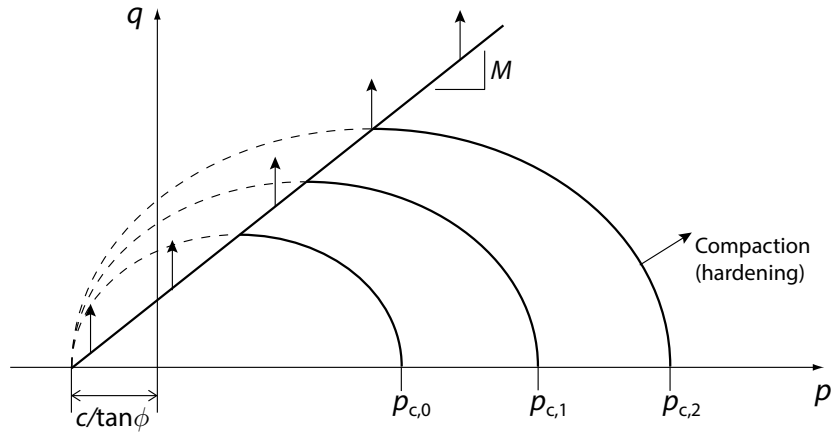


Figure 15.3: Yield surfaces with CSL Constraint = Yes. Only the domain below failure line  $q = M(p' + c/\tan \phi)$  is admissible.

The yield surface hardens or softens according to the following relation between  $\kappa$  and the volumetric plastic strain:

$$\frac{\dot{p}_c}{p_c} = \frac{1+e}{\lambda - \kappa} \dot{\epsilon}_v^p \quad (15.15)$$

where  $\lambda$  is the compression index and the plastic strains follow from the associated flow rule:

$$\dot{\epsilon}^p = \dot{\chi} \frac{\partial F}{\partial \sigma'} \quad (15.16)$$

Thus, for plastic compaction ( $\dot{\epsilon}_v^p > 0$ ) the yield surface expands (hardens) while plastic dilation ( $\dot{\epsilon}_v^p < 0$ ) leads to a shrinking (softening) of the yield surface. At the critical state,  $q = M(p' + c/\tan \phi)$ , the plastic volumetric strain rate is zero and the yield surface undergoes no further changes (see Figure 15.2).

Finally, while the critical state line in the basic Modified Cam Clay model is approached asymptotically by virtue of the hardening rule, the model implemented in OptumG2 gives the possibility to include  $q - M(p' + c/\tan \phi) \leq 0$  as an explicit constraint. In this way, the critical state line cannot be crossed and the softening that would otherwise take place is prevented. This additional constraint may be included via the CSL Constraint field.

In summary, the strength parameters of Cam clay are:

- Cohesion,  $c$  [kPa]
- Friction angle,  $\phi$
- CSL Constraint (Yes/No)

Setting CSL Constraint = Yes invokes the additional constraint  $q - M(p' + c/\tan \phi) \leq 0$  (see Figure 15.3). The CSL constraint is useful both numerically, as it eliminates potential softening, and physically, as it limits the possibly excessive strength implied by high overconsolidation ratios. The plastic volumetric strains associated with the CSL constraint are always zero, i.e. the flow rule of CSL the constraint is nonassociated with a dilation angle of zero.

## Initial Conditions

As for all other materials, the initial stresses can be generated by an Initial Stress analysis (manually or as part of other analyses). This requires specification of the earth pressure coefficient  $K_0$  and is done such that the resulting stress state is limited by the critical state line, i.e. the CSL constraint is effectively imposed.

With a set of initial stresses at hand, the initial value of  $p_c$  needs to be specified. This is done in terms of the overconsolidation ratio:

$$\text{OCR}^* = \frac{p_{c,0}}{\tilde{p}'_0} \quad (15.17)$$

where  $p_{c,0}$  and  $\tilde{p}'_0$  are the initial preconsolidation pressure and effective mean stress respectively. The above overconsolidation ratio differs from the usual overconsolidation ratio defined by

$$\text{OCR} = \frac{\sigma_{v,c}}{\tilde{\sigma}'_{v,0}} \quad (15.18)$$

where  $\sigma_{v,c}$  is the vertical preconsolidation stress and  $\tilde{\sigma}'_{v,0} = \sigma'_{v,0} + c/\tan \phi$  is the initial vertical effective stress (corrected for a possible cohesion). The two different overconsolidation ratios are related by

$$\text{OCR}^* = \frac{1 + 2K_0^{\text{nc}}}{1 + 2K_0^{\text{oc}}} \text{OCR} \quad (15.19)$$

where  $K_0^{\text{nc}}$  is earth the pressure coefficient for the soil in its initial normally consolidated state and  $K_0^{\text{oc}}$  is the earth pressure coefficient for the soil in its current, possibly overconsolidated, state. It is common practice to relate these coefficients to the friction angle and the overconsolidation ratio by

$$K_0^{\text{nc}} = 1 - \sin \phi, \quad K_0^{\text{oc}} = K_0^{\text{nc}} \text{OCR}^{\sin \phi} \quad (15.20)$$

In OptumG2, the earth pressure coefficient taken as input is the current earth pressure coefficient, i.e.  $K_0 = K_0^{\text{oc}}$ , while the earth pressure coefficient corresponding to normally consolidated conditions is calculated automatically from (15.20).

In summary, the parameters related to the initial state are:

- Initial void ratio,  $e_0$
- Overconsolidation ratio, OCR
- Earth pressure coefficient,  $K_0$

Regarding the calculation of  $p_{c,0}$  the following should be noted. As a general rule, we have  $p_{c,0} = \text{OCR}^* \tilde{p}'_0$  where  $\tilde{p}'_0$  is the initial effective pressure. However, depending on the initial value of the deviatoric stress  $q$ , the yield condition may not be satisfied for  $p_{c,0} = \text{OCR}^* \tilde{p}'_0$  (see Figure 15.4). To counter this situation and satisfy the yield condition  $F = 0$ ,  $p_{c,0}$  is adjusted to the smallest value,  $p_{c,\min}$ , that will ensure  $F(\tilde{p}'_0, q_0, p_{c,\min}) = 0$ . This means that the actual  $\text{OCR}^*$  (and thereby OCR) under which the calculations are initiated may be slightly higher than that specified.

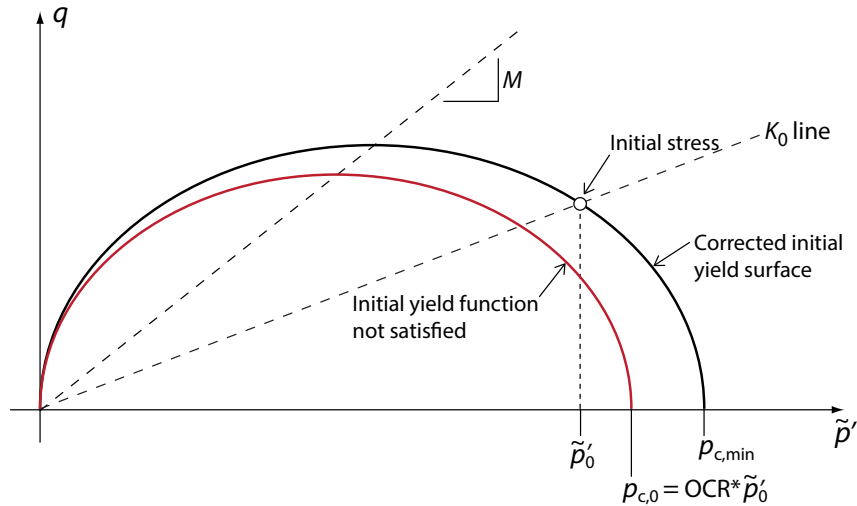


Figure 15.4: Initial value of  $p_c$  adjusted to satisfy  $F = 0$ .

## Unit Weights, Hydraulic Model

See Section 8.

### 15.1 Limit Analysis and Strength Reduction

For the Modified Cam Clay model, Limit Analysis and Strength Reduction are conducted by calculating equivalent Tresca (Standard or Genew parameters and then proceeding as for these materials.

#### 15.1.1 Drained conditions

Under drained conditions, the strength is governed by the material parameter  $\phi$ . Due to the effect of nonassociativity (the dilation is zero at the critical state) it may be shown that a limit analysis equivalent to a full elastoplastic analysis should be conducted at a slightly lower value of  $\phi$  (see Krabbenhoft et al. 2012a, for details). It should also be borne in mind that localization – accompanied by an apparent softening – is possible even for low to moderate overconsolidation ratios (Krabbenhoft and Lyamin 2012). The ultimate limit loads found by means of Limit Analysis will therefore usually only be in approximate agreement with those found from a full elastoplastic analysis to failure.

#### 15.1.2 Undrained conditions

Under undrained conditions, an equivalent undrained shear strength can be calculated and the Mohr-Coulomb or Tresca model then used to conduct the Limit Analysis. With the initial preconsolidation pressure and effective mean stress known, the equivalent undrained shear strength is given by

$$\begin{aligned}
 s_u &= M(\theta) \tilde{p}'_0 \left( \frac{p_{c,0}}{2p'_c} \right)^{1-\kappa/\lambda} \\
 &= M(\theta) \left[ \frac{1}{3}(1 + 2K_0)(\sigma'_{v,0} + c/\tan \phi) \right] \left[ \frac{(2K_0 + \text{OCR}^{\sin \phi})\text{OCR}}{2(1 + 2K_0)\text{OCR}^{\sin \phi}} \right]^{1-\kappa/\lambda}
 \end{aligned} \tag{15.21}$$

where  $K_0$  is the earth pressure coefficient and  $\sigma'_{v,0}$  is the initial vertical effective stress which is assumed to be related to the horizontal stress by  $\sigma'_{h,0} = K_0 \sigma'_{v,0}$ .

From the above expression it will be seen that the undrained shear strength at the ground surface ( $\sigma_{v,0} = 0$ ) is zero unless  $c$  is finite. In most cases, this is not reasonable and some finite amount of cohesion should therefore be used. Moreover, by varying  $c$  as well as OCR and  $K_0$  with depth, typical undrained shear strength profiles can in most cases be matched well. Some examples are shown in Figures 15.5 and 15.6. In these figures, OCR,  $K_0$  and  $c$  are varied with depth while the remaining parameters are kept fixed at:  $\kappa = 0.03$ ,  $\lambda = 0.15$ ,  $\phi = 25^\circ$ , and  $\sigma'_{v,0} = \gamma' d$  with  $d$  being the depth coordinate and  $\gamma' = 8 \text{ kN/m}^3$  the effective unit weight. The Lode angle as been set to  $\theta = 0^\circ$ .

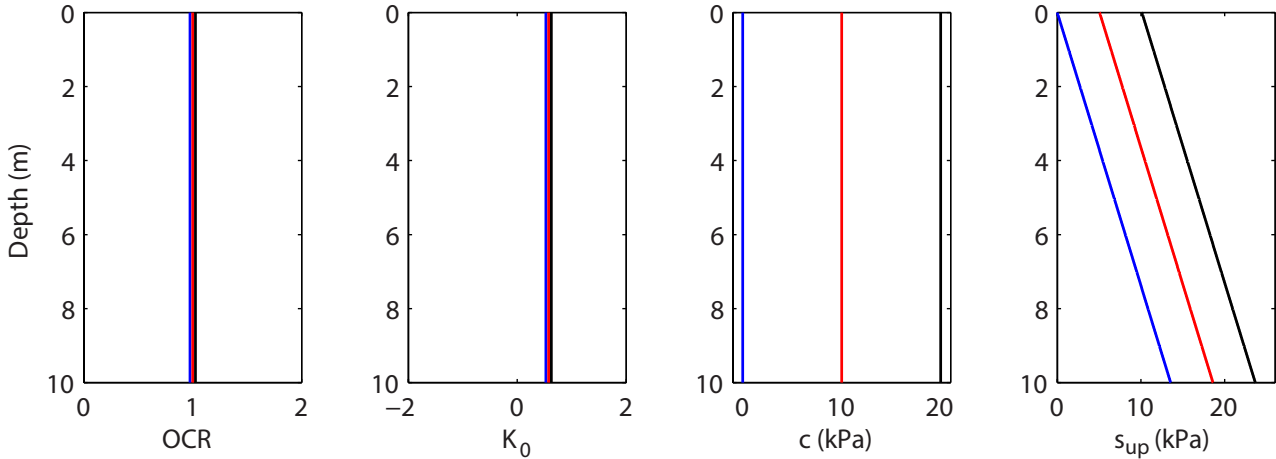


Figure 15.5: Variation of undrained shear strength with depth for constant OCR,  $K_0$ , and  $c$ .

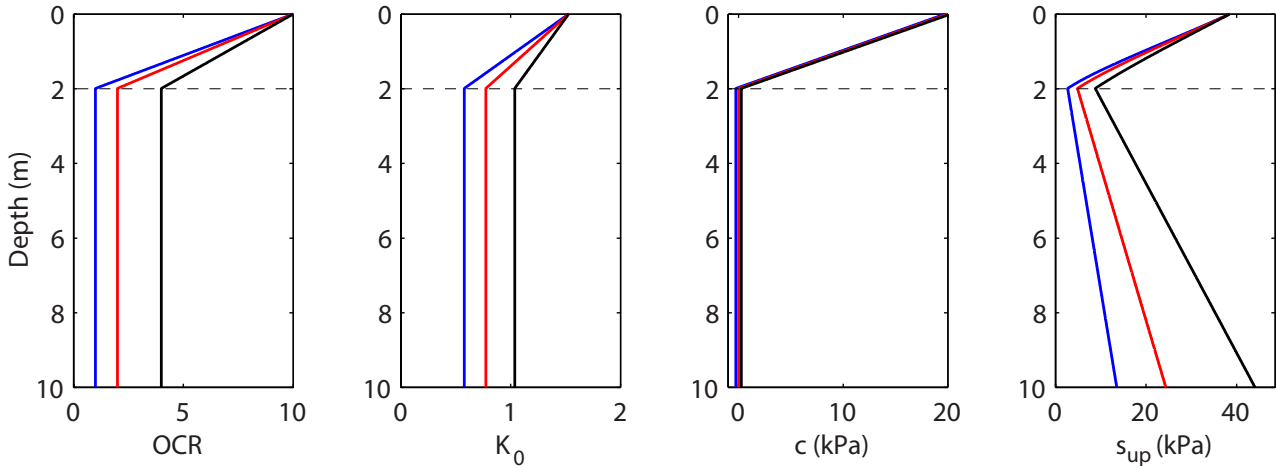


Figure 15.6: Variation of undrained shear strength with depth for linearly varying OCR,  $K_0$ , and  $c$ .

### 15.2 Creep

For certain clays, creep (or secondary compression) accounts for a significant part of the total deformation. An often used empirical law states that the volumetric creep strain following full primary consolidation is given by

$$\epsilon_v^c = \frac{C_\alpha}{1 + e} \log_{10}(t/t_{90}) \tag{15.22}$$

where  $\Delta\varepsilon_v^c$  is the volumetric creep strain,  $C_\alpha$  is the secondary compression coefficient,  $e$  is the void ratio,  $t_{90}$  is the time to 90% primary consolidation and  $t$  is the time at which the creep strain is evaluated. More generally, the increment in creep strain between two times  $t_n$  and  $t_{n+1}$  may be calculated as

$$\Delta\varepsilon_v^c = \frac{C_\alpha}{1+e} \log_{10}(t_{n+1}/t_n) \quad (15.23)$$

The creep strain may be integrated to give the total settlement. For a layer of depth  $H$  we have:

$$\Delta u^c = H \frac{C_\alpha}{1+e} \log_{10}(t_{n+1}/t_n) \quad (15.24)$$

where  $\Delta u^c$  is the increment of vertical settlement due to creep.

In OptumG2, creep is included using the approach of Borja and Kavazanjian (1985). The total strain is here given by

$$\varepsilon = \varepsilon^e + \varepsilon^p + \varepsilon^c \quad (15.25)$$

where  $\varepsilon^e$  and  $\varepsilon^p$  are the usual elastic and plastic strains respectively and  $\varepsilon^c$  is the creep strain. To describe the evolution of the creep strain with time, a creep potential,  $\Phi^c$ , is introduced by

$$\frac{d\Phi^c}{dt} = \frac{1}{\tau_0} \frac{\mu}{1+e} \exp\left(-\frac{1+e}{\mu} \Phi^e\right), \quad \Phi(0) = 0 \quad (15.26)$$

where  $\mu$  is a material parameter (equivalent to  $C_\alpha$  above),  $e$  is the void ratio and  $\tau_0$  is a constant which is set internally to 1 day. The evolution of the creep strain is then given by

$$\frac{d\varepsilon^c}{dt} = \mathbf{a} \frac{d\Phi^c}{dt} \quad (15.27)$$

where  $\mathbf{a}$  is a vector that gives the direction of the creep strain rate vector. Consistent with Modified Cam Clay, this quantity is taken as

$$\mathbf{a} = \frac{\partial F^c}{\partial \boldsymbol{\sigma}'} \quad (15.28)$$

where

$$F^c = \tilde{p} + \frac{q^2}{M^2 \tilde{p}} \quad (15.29)$$

In OptumG2, creep thus requires the specification of a single additional material parameter,  $\mu$ . This parameter is specified as a fraction of  $\lambda$ . The ratio  $\mu/\lambda$  typically falls in the range of 0.02 to 0.1 for a wide variety of natural materials prone to creep (Mesri and Castro 1986).

In the one-dimensional case, the above creep law leads to a volumetric creep strain given by

$$\varepsilon_v^c = \frac{\mu}{1+e} \ln\left(\frac{t + \tau_0}{\tau_0}\right) \quad (15.30)$$

The increment in creep strain over a time increment from  $t_{90}$  to  $t$  is thus given by

$$\Delta\varepsilon_v^c = \frac{\mu}{1+e} \ln\left(\frac{t + \tau_0}{t_{90} + \tau_0}\right) \quad (15.31)$$

which, with  $\mu = C_\alpha / \ln(10)$ , approaches the empirical relation (15.23) for times significantly greater than  $\tau_0 = 1$  day.

## 16 HARDENING MOHR-COULOMB (HMC)

The Hardening Mohr-Coulomb (HMC) model is designed to remedy some of the shortcomings of the standard Mohr-Coulomb model described in Section 8. The HMC model was first proposed by Muir Wood (2004) with reference to triaxial stress space and later extended to general stress space by Doherty and Muir Wood (2013). The version of the model implemented in OptumG2 follows these developments closely while incorporating a number of new features that allow for a better match of the model to experimental data.

### 16.1 Typical soil behavior

The typical behaviour of soil in drained triaxial compression experiments is as sketched in Figure 16.1. Compared to metals and other non-granular materials, a distinguishing feature of soils is that the apparent stiffness in initial loading is significantly less than that observed when the sample is later unloaded and reloaded. To characterize the initial stiffness, use is often made of the secant modulus,  $E_{50}$ , defined as:

$$E_{50} = \frac{\frac{1}{2}q_u}{\epsilon_{1,50}} \tag{16.1}$$

where  $q_u = (\sigma_1 - \sigma_3)_u$  is the ultimate shear stress and  $\epsilon_{1,50}$  is the axial strain at half the ultimate shear stress. Similarly, in unloading/reloading, the stiffness is characterized by the modulus  $E_{ur}$ . It should be noted that while  $E_{ur}$  is an elastic stiffness in the usual sense, the physics leading to  $E_{50}$  comprise both elastic and plastic characteristics. In general, both  $E_{ur}$  and  $E_{50}$  are pressure dependent and increase with increasing confining pressure. The ratio between the two moduli is usually in the range of  $E_{ur}/E_{50} \simeq 2$  to 5 or higher.

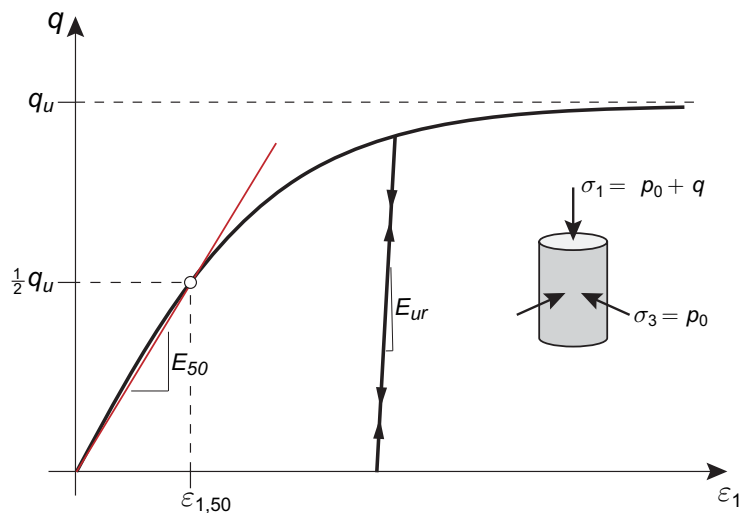


Figure 16.1: Typical behaviour of soil in drained triaxial compression.

The ultimate shear stress is proportional to the pressure,  $p$ , by  $q_u = Mp_u$  where  $M$  is a material parameter and  $p_u$  is the confining pressure at the ultimate limit state. In conventional triaxial compression where the stress path is such that  $dq/dp = 3$ , the ultimate shear stress for a purely frictional material is given by

$$q_u = \frac{3M}{3 - M}p_0 \tag{16.2}$$

where  $p_0$  is the confining pressure. Using the relation between  $M$  and the Mohr-Coulomb friction angle  $\phi$  in triaxial compression:

$$\sin \phi = \frac{3M}{6 + M} \quad \text{or} \quad M = \frac{6 \sin \phi}{3 - \sin \phi}, \quad (16.3)$$

the ultimate shear stress is given by

$$q_u = \frac{2 \sin \phi}{1 - \sin \phi} p_0 \quad (16.4)$$

In the general case, the relation between  $M$  and  $\phi$  is given by

$$M = \frac{3 \sin \phi}{\sqrt{3} \cos \theta + \sin \theta \sin \phi} \quad (16.5)$$

where

$$\theta = \tan^{-1} \left[ \frac{1}{\sqrt{3}} \left( 2 \frac{\sigma_2 - \sigma_3}{\sigma_1 - \sigma_3} - 1 \right) \right] \quad (16.6)$$

is the Lode angle (equal to  $-30^\circ$  in triaxial compression).

Regarding the strains, it is usually observed that the dilation which occurs at appreciable levels of shear strain is a function of the material density. Dense soils may undergo a significant amount of dilation under continued shearing while less dense soils will tend to dilate less or may even contract plastically, i.e. undergo negative dilation. These characteristics are sketched in 16.2.

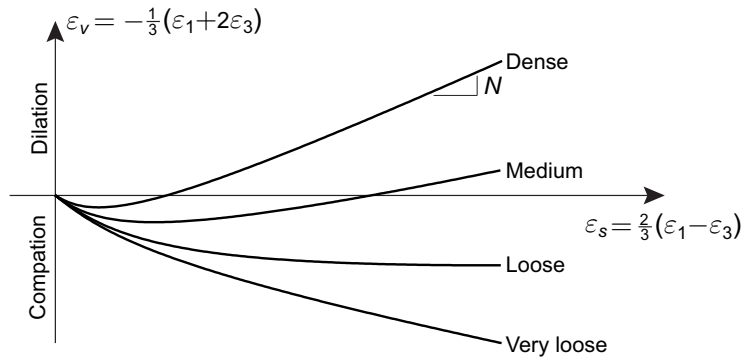


Figure 16.2: Typical shear-volumetric strain behavior in triaxial compression.

While many models operate with a constant dilation, the actual dilation observed in experiments is in fact quite variable. A common approach to describe this variability is to link the current dilation to the current stress ratio  $q/p$ . A common stress-dilatancy relations is that of Taylor:

$$\frac{\dot{\varepsilon}_v^p}{\dot{\varepsilon}_s^p} = M - N - q/p \quad (16.7)$$

where  $N$  is the dilation at the ultimate limit state, i.e. for  $q/p = M$ . With realistic pairs of  $M$  and  $N$ , the behavior will initially, for low  $q/p$ , be compactive with  $\dot{\varepsilon}_v^p/\dot{\varepsilon}_s^p = M - N$ . For larger ratios of  $q/p$  and depending on the values of  $M$  and  $N$ , the behavior may become dilative or remain compactive up to the ultimate limit state. Following (16.5),  $N$  can be interpreted in terms of a Mohr-Coulomb dilation angle,  $\psi$ , via the relation

$$N = \frac{3 \sin \psi}{\sqrt{3} \cos \theta + \sin \theta \sin \psi} \quad (16.8)$$

For triaxial compression ( $\theta = -30^\circ$ ) we have

$$\frac{\dot{\epsilon}_v^P}{\dot{\epsilon}_s^P} = \frac{6 \sin \phi}{3 - \sin \phi} - \frac{6 \sin \psi}{3 - \sin \psi} - q/p \quad (16.9)$$

It is often observed that  $\phi$  and  $\psi$  are quite closely correlated. For sands, the rule of thumb  $\phi - \psi = 30^\circ$  is often cited.

Alternatively, one may wish to use a constant dilation throughout. The HMC model implemented in OptumG2 offers this possibility as well. In that case, the ratio between the plastic volumetric and shear strain rates is simply:

$$\frac{\dot{\epsilon}_v^P}{\dot{\epsilon}_s^P} = -\frac{6 \sin \psi}{3 - \sin \psi} \quad (16.10)$$

independent of  $q/p$ .

On the basis of the preceding discussion, it can be concluded that any credible soil model should involve at least six parameters:

- Two elastic parameters, for example  $E_{ur}$  and  $\nu_{ur}$ .
- Two strength parameters and a dilation parameter, for example the Mohr-Coulomb  $c$ ,  $\phi$  and  $\psi$ .
- A 'fitting parameter' that reproduces a user specified secant modulus  $E_{50}$ .

In addition, it is desirable to include pressure dependence into  $E_{ur}$  and  $E_{50}$ . In OptumG2 this is done via two additional parameters: a reference pressure  $p_{ref}$  and an exponent  $m$ . The full set of parameters for the HMC model are given below.

## Stiffness

The HMC model makes use of three stiffness parameters which can be entered in two different ways, either (Set A):

- $E_{ur,ref}$  [MPa] : Young's modulus in unloading/reloading at reference pressure  $p_{ref}$ .
- $\nu_{ur}$  : Poisson's ratio in unloading/reloading at reference pressure  $p_{ref}$ .
- $E_{50,ref}$  [MPa] : Secant Young's modulus in triaxial compression under confining pressure  $\sigma_3 = p_{ref}$ .

or (Set B):

- $G_{ur,ref}$  [MPa] : Shear modulus corresponding to unloading/reloading at reference pressure  $p_{ref}$ .
- $K_{ur,ref}$  [MPa] : Bulk modulus corresponding to unloading/reloading at reference pressure  $p_{ref}$ .
- $G_{50,ref}$  [MPa] : Secant shear modulus in triaxial compression under confining pressure  $\sigma_3 = p_{ref}$ .

It should be noted that while  $E_{ur,ref}$ ,  $\nu_{ur}$ ,  $G_{ur,ref}$  and  $K_{ur,ref}$  are true elastic moduli and thus related via the usual elastic relations [ $E_{ur,ref} = 2(1 + \nu_{ur})G_{ur,ref}$ , etc], the elastoplastic secant moduli,  $E_{50,ref}$  and  $G_{50,ref}$ , are not related in an obvious linear fashion.



## Strength

The strength parameters are the same as for the standard Mohr-Coulomb model:

- $c$  [kPa] : Cohesion.
- $\phi$  [°] : Friction angle.

## Flow rule

- Flow Rule : Taylor/Constant Dilation
- $\psi$  [°] : Dilation angle.

For Flow Rule = Taylor, Taylor's stress-dilatancy relation (16.17) is used. This implies that the dilation increases as the ultimate limit state is approached. At the ultimate limit state, the dilation is characterized by the angle  $\psi$ . In contrast, for Flow Rule = Constant Dilation, the dilation is constant throughout, c.f. Eqn. (16.10).

It is possible to enforce a Dilation Cap following the Mohr-Coulomb material. Once the critical strain is reached (Volumetric or Shear), Flow Rule = Constant Dilation with  $\psi = 0$  is enforced.

## Pressure dependence

Pressure dependence of the stiffness moduli is included via the following relations:

$$\begin{aligned} E_{ur} &= E_{ur,ref} \Pi(\sigma_3) \\ G_{ur} &= G_{ur,ref} \Pi(\sigma_3) \\ K_{ur} &= K_{ur,ref} \Pi(\sigma_3) \end{aligned} \quad (16.11)$$

and

$$\begin{aligned} E_{50} &= E_{50,ref} \Pi(\sigma_3) \\ G_{50} &= G_{50,ref} \Pi(\sigma_3) \end{aligned} \quad (16.12)$$

where

$$\Pi(\sigma_3) = \left( \frac{\sigma_3 + c / \tan \phi}{p_{ref} + c / \tan \phi} \right)^m \quad (16.13)$$

with  $\sigma_3$  being the minor principal stress. The associated parameters are:

- $p_{ref}$  [kPa] : Reference pressure (confining pressure in triaxial compression test).
- $m$  : Fitting parameter.

The parameter  $m$  depends on the soil type. For soft clays,  $m$  should be chosen as  $m \approx 1$  (giving rise to relations similar to those used in the Modified Cam Clay model) while for sands and other coarse grained materials  $m \approx 0.5$  is appropriate.

## Unit Weights, Initial Conditions, Hydraulic Model

See Section 8.

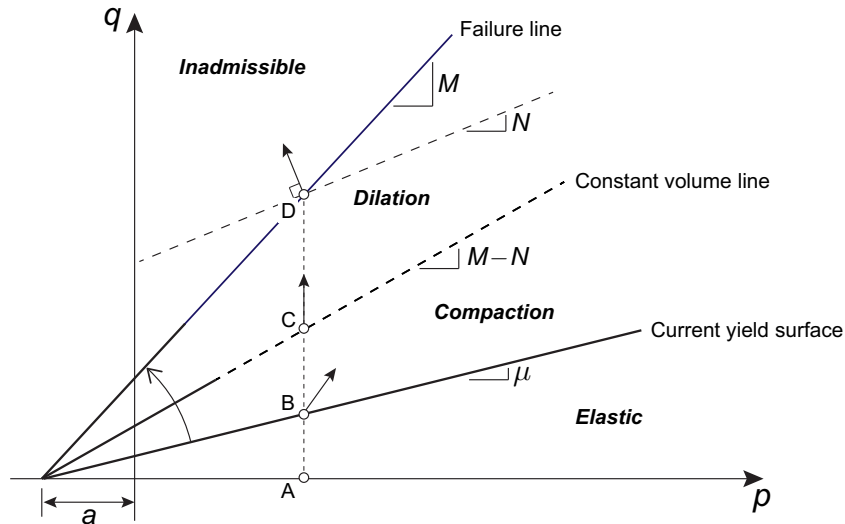


Figure 16.3: Hardening, compaction and dilation in the HMC model.

## 16.2 Model overview

The basic premise of the HMC model is sketched in Figure 16.3. In contrast to the standard Mohr-Coulomb model which consists of a single elastic region limited by the failure criterion, the HMC model operates with three regions in  $p$ - $q$  space:

1. An elastic region in which no plastic or otherwise irreversible straining takes place.
2. A compaction region where the soil undergoes compaction, i.e. negative dilation.
3. A dilation region where the soil undergoes plastic dilation.

Consider an initial stress point as indicated by A in Figure 16.3. Shear loading first implies an initially elastic response up to point B where the initial yield surface is reached. From point A to point B, the yield surface hardens, implying a decrease of stiffness, while the flow rule is such that a compaction takes place. As the loading continues, point C is reached. At this point, the behavior switches from being compactive to being dilative and remains so up to point D at which failure occurs, i.e. the yield surface ceases to harden and remains stationary.

### 16.2.1 Initial state and small-strain stiffness

In practice, the HMC model is initialized as follows:

1. The initial stress state is first calculated on the basis of the specified  $K_0$ . This is either done automatically (if no From stage is specified in Elastoplastic or Multiplier Elastoplastic analysis) or via a separate Initial Stress stage.
2. On the basis of the stress state at each point, a parameter  $\mu_{\min}$  is calculated such that the stress state will satisfy the initial yield criterion  $F_0 = q_0 - \mu_{\min}(p'_0 + a) = 0$  where subscript 0 refers to the initial state.
3. Finally, we set  $\mu_0 = \mu_{\min} + \delta\mu$  where  $\delta\mu$  is a user defined parameter and use  $F = q - \mu_0(p' + a)$  as the initial yield surface. This means that the initial point will be below yield, i.e.  $q_0 - \mu_0(p'_0 + a) < 0$  for  $\delta\mu > 0$ . This situation is sketched in Figure 16.4.

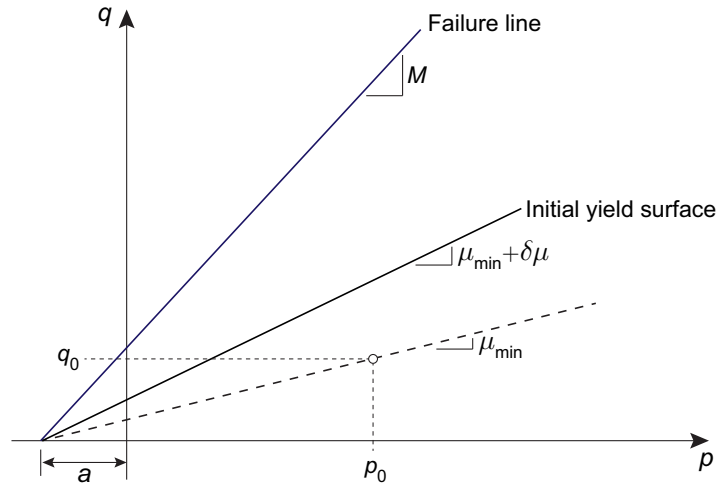


Figure 16.4: Initial state.

In OptumG2, rather than specifying  $\delta\mu$ , an equivalent friction angle  $\delta\phi$  is specified under Initial Conditions and the equivalent  $\delta\mu$  calculated by

$$\delta\mu = \frac{3 \sin \delta\phi}{\sqrt{3} \cos \theta + \sin \theta \sin \delta\phi} \tag{16.14}$$

where  $\theta$  is the Lode angle (16.6). The existence of a finite initial elastic range can be correlated to the concept of small-strain stiffness, i.e. the phenomenon that soils at very low levels of strain are much stiffer than at the strain levels usually experienced in standard laboratory tests and in typical boundary value problems. This is discussed in detail by Muir Wood (1990) and Doherty and Muir Wood (2013) with respect to the original Extended Mohr-Coulomb model from which the HMC model derives. While the values of  $\delta\phi$  leading to the desired stiffness degradation with strain is material dependent and must be calibrated in each individual case (from data that normally not is available),

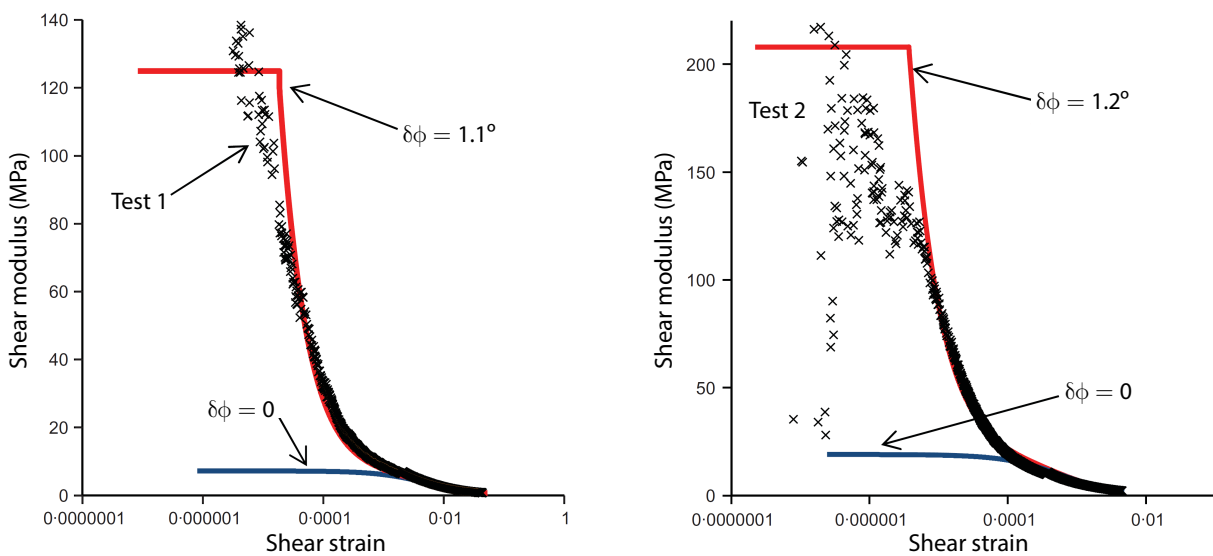


Figure 16.5: Experimental results and calibration for small-strain stiffness for two different tests on sand (after Doherty and Muir Wood 2013).

the results of Doherty and Muir Wood (2013) appear to indicate that a value of  $\delta\phi \simeq 1^\circ$  (together with reasonable values of  $E_{ur}$  and  $E_{50}$ ) may be quite typical.

Some of the experimental results and calibrations presented by Doherty and Muir Wood (2013) are shown in Figure 16.5. While these results reveal a rather dramatic degradation of stiffness with shear strain, the effect of small-strain stiffness is for typical boundary value problems (foundations, retaining wall, etc) usually fairly limited.

### 16.3 Calibration to Erksak sand

The HMC model has been calibrated to drained triaxial tests on Erksak sand at three different densities and at three different confining pressures. In all cases, the reference pressure was set to the default value of  $p_{ref} = 100$  kPa. The parameters used are given in Table 16.1 and the resulting fits are shown in Figure 16.6.

	Loose	Medium	Dense
$p_0$ (kPa)	200	60	130
$E_{ur,ref}$ (MPa)	39	75	150
$\nu_{ur}$	0.3	0.35	0.40
$E_{50,ref}$ (MPa)	13	25	50
$c$ (kPa)	0	0	0
$\phi$ ( $^\circ$ )	27	37	41
Flow Rule	Taylor	Taylor	Taylor
$\psi$ ( $^\circ$ )	-4	11	17
$p_{ref}$ (kPa)	100	100	100
$m$	0.5	0.5	0.5

Table 16.1: HMC model parameters for loose, medium and dense Erksak sand.

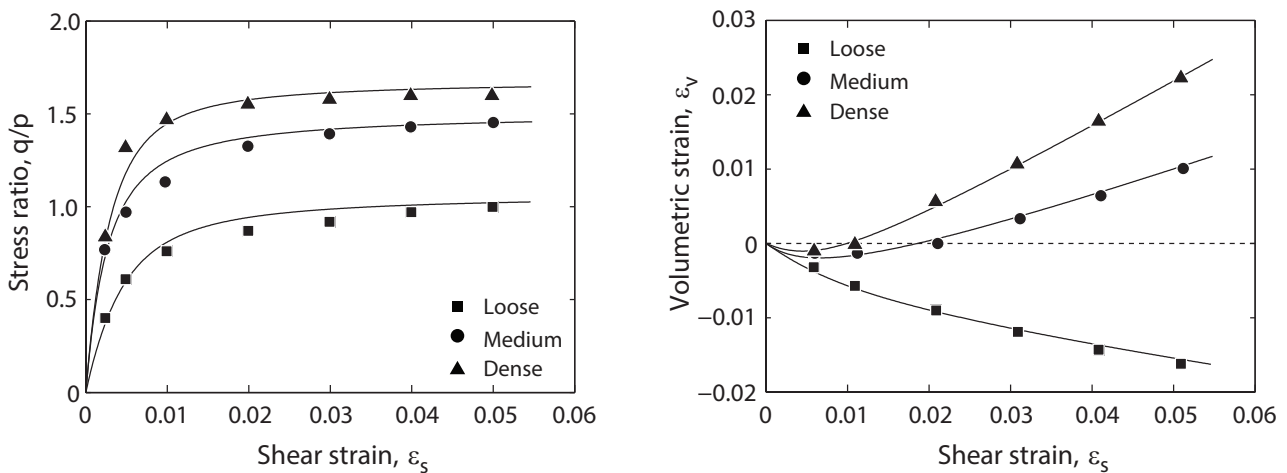


Figure 16.6: HMC fits to drained triaxial test data for loose, medium and dense Erksak sand (test data from Yu 2006).

## 16.4 Calibration to Lund sand

A key feature of the HMC model is that the stiffness moduli are pressure dependent. In this way, a set of parameters calibrated under one confining pressure should in principle be valid for all pressures. To verify this assertion, the model is first calibrated to a dense Lund sand under a confining pressure of  $p_0 = 160$  kPa using  $p_{ref} = 160$  kPa. Simulations are then run for confining pressures of  $p_0 = 40, 80, 320$  and  $640$  kPa using the same parameters, including  $p_{ref}$ .

The parameter set and the resulting fits are shown in Table 16.2 and Figure 16.7 respectively. As seen, the model generalizes rather well to both higher and lower pressures than originally calibrated for.

$p_0$ (kPa)	40, 80, 160, 320, 640
$E_{ur,ref}$ (MPa)	90
$\nu_{ur}$	0.4
$E_{50,ref}$ (MPa)	30
$c$ (kPa)	0
$\phi$ ( $^\circ$ )	44
Flow Rule	Taylor
$\psi$ ( $^\circ$ )	19
$p_{ref}$ (kPa)	160
$m$	0.55

Table 16.2: HMC model parameters for Lund sand.

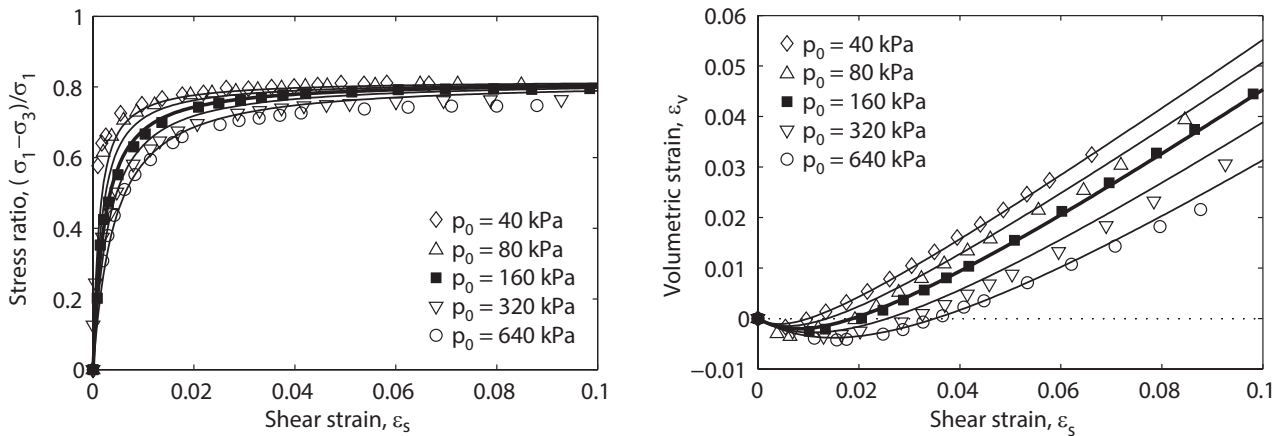


Figure 16.7: HMC fits to drained triaxial test data for dense Lund sand (test data from Ahadi and Krenk 2000). The model is fitted for a confining pressure of 160 kPa while the response at higher and lower pressures are predictions.

### 16.5 Calibrating $E_{ur}$ and $E_{50}$

The figures below illustrate the relative independence of  $E_{ur,ref}$  and  $E_{50,ref}$  for the Medium sand in Table 16.1. In the figures on the left, the reference unloading/reloading modulus is fixed at  $E_{ur,ref} = 75$  MPa while  $E_{50,ref}$  is varied between 1/5 to 1/2 of  $E_{ur,ref}$ . This has an immediate effect on the response in loading whereas the response in unloading/reloading is governed solely by  $E_{ur}$ . Conversely, in the figures on the right,  $E_{50,ref}$  is kept constant at 25 MPa while  $E_{ur,ref}$  is varied from 2 to 5 times  $E_{50,ref}$ . This has a much less dramatic effect on the results, except in unloading where the stiffness again is governed solely by  $E_{ur}$ .

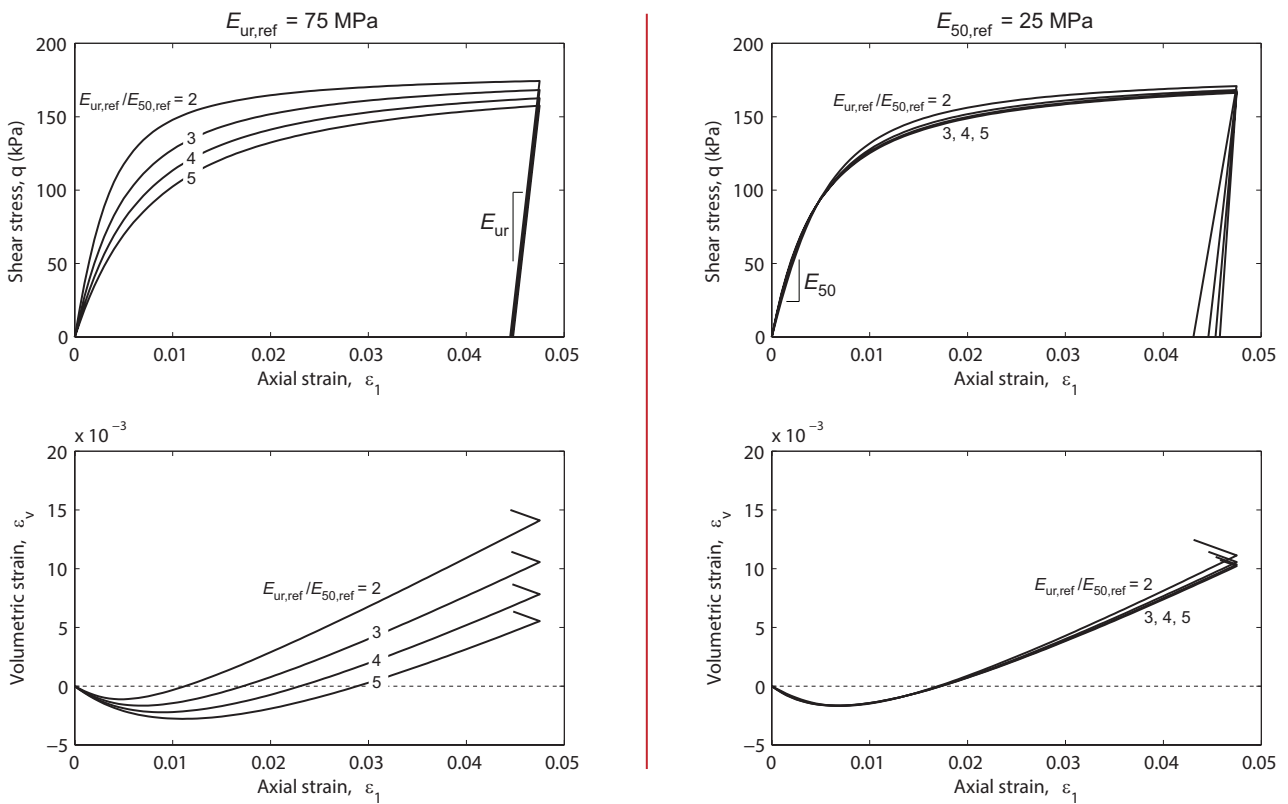


Figure 16.8: Model response (Medium sand in Table 16.1) as function of  $E_{ur,ref}$  and  $E_{50,ref}$ .

## 16.6 Undrained behavior

Under undrained conditions (Drainage Condition = Drained/Undrained in combination with Time Scope = Short Term), the overall behaviour depends on a combination of the strength and stiffness parameters. In particular, for a dilation angle of  $\psi > 0$ , the excess pore pressures will increase indefinitely resulting in an infinite strength (unless a cavitation cut-off is introduced in which case the strength will be finite). Conversely, for  $\psi < 0$ , the strength will eventually decrease to zero corresponding to static liquefaction. For the special case of  $\psi = 0$ , the strength is finite and depends on a combination of the strength and stiffness parameters. An example of the influence of the dilation angle on the overall response is shown in Figure 16.9.

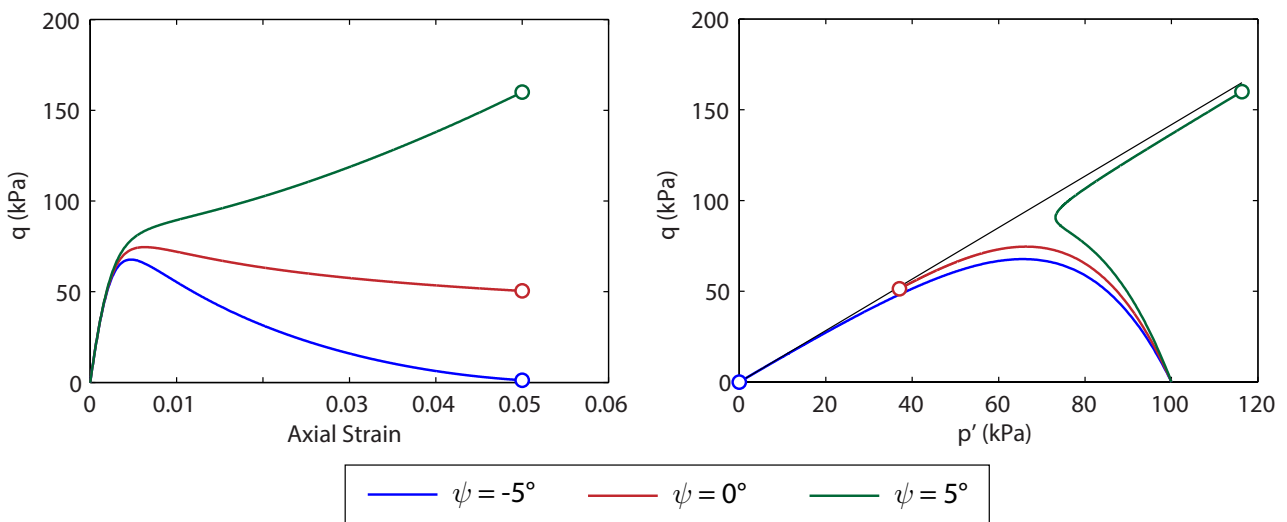


Figure 16.9: Response of HMC under undrained conditions for three materials with  $\psi = -5^\circ$ ,  $0^\circ$ , and  $5^\circ$ .

## 16.7 Governing equations

In the following, the governing equations of the HMC model are briefly summarized.

The basic premise of the HMC model is sketched in Figure 16.3. The current mobilized strength is characterized by the line  $q/(p + a) = \mu$  where  $\mu$  is the current mobilized friction coefficient and  $a$  is an attraction (tensile strength). As hardening proceeds, i.e. as  $\mu$  increases, the constant volume line  $q/(p + a) = M - N$  is reached. At this state, the dilation is zero. Hardening progresses further until  $q/(p + a) = M$  at which point the material behaves in a perfectly plastic manner with dilation coefficient  $N$ .

To capture this behaviour, and to account for elastic unloading, a hardening yield surface is introduced. This is given by

$$F = q - \mu(p + a) \quad (16.15)$$

What remains is to specify an appropriate flow rule that leads to the behaviour described above and to construct a hardening rule that prevents any further hardening of the yield surface at  $q/(p + a) = M$ .

Concerning the former, an appropriate plastic potential is (Doherty and Muir Wood 2013; Muir Wood 2004):

$$G = q - (M - N)(p + a) \ln \frac{p_r}{p + a} \quad (16.16)$$

where  $p_r$  should be chosen such that  $G$  passes through the current stress point, i.e.  $p_r = (p + a)e^{\frac{\mu}{M-N}}$ . This plastic potential implies the stress-dilatancy relation of Taylor:

$$\left. \begin{aligned} \dot{\varepsilon}_v^p &= \dot{\lambda}(M - N - \mu) \\ \dot{\varepsilon}_s^p &= \dot{\lambda} \end{aligned} \right\} \implies \frac{\dot{\varepsilon}_v^p}{\dot{\varepsilon}_s^p} = M - N - \mu \quad (16.17)$$

where  $\varepsilon_v^p$  and  $\varepsilon_s^p$  are the plastic volumetric and shear strains respectively.

Secondly, the stress ratio in elastoplastic loading is assumed to depend on the plastic shear strain as:

$$\frac{\mu}{M} = \frac{\varepsilon_s^p}{\beta M + \varepsilon_s^p} \quad (16.18)$$

where  $\beta$  is a model parameter. We note that  $\beta M$  in fact is the plastic shear strain at half the ultimate stress ratio. The incremental form of the above leads to the hardening rule:

$$\dot{\mu} = \frac{(1 - \mu/M)^2}{\beta} \dot{\varepsilon}_s^p \quad (16.19)$$

where it is evident that hardening terminates at  $\mu = M$ . The above hardening rule generally leads to stress-strain curves similar to those observed experimentally.

Finally, the behaviour within the elastic domain is based on linear elasticity:

$$\varepsilon_v^e = \frac{1}{K_{ur}} p, \quad \varepsilon_s^e = \frac{1}{3G_{ur}} q \quad (16.20)$$

### 16.7.1 Pressure dependence

The version of the HMC model implemented in OptumG2 differs from the original model in two ways.

Firstly, the elastic moduli are pressure dependent following (16.11).

Secondly, the hardening parameter  $\beta$  is adjusted to reproduce the user specified secant moduli,  $E_{50,ref}$  or  $G_{50,ref}$ . With  $E_{50,ref}$  specified, the expression for  $\beta$  is:

$$\beta = \begin{cases} \frac{3}{2}(p + c/\tan \phi) \frac{9 - M}{9 - (M - N)M \ln 2 - 3N} \frac{1 - E_{50}/E_{ur}}{E_{50}}, & \text{for Flow Rule = Taylor} \\ \frac{3}{2}(p + c/\tan \phi) \frac{9 - M}{9 - (3 - N)M \ln 2 - 3N} \frac{1 - E_{50}/E_{ur}}{E_{50}}, & \text{for Flow Rule = Constant Dilation} \end{cases}$$

while the expression consistent with a user specified  $G_{50,ref}$  is:

$$\beta = \frac{1}{6}(p + c/\tan \phi) \frac{3 - M}{3 - M \ln 2} \frac{1 - G_{50}/G_{ur}}{G_{50}}, \quad \text{independent of Flow Rule,} \quad (16.21)$$

where  $E_{50}$  and  $G_{50}$  are pressure dependent following (16.12). We note that for  $m = 1$ ,  $\beta$  becomes constant in the special case where the pressure remains constant and equal to the minor principal stress. In that case, the original HMC model of Muir Wood (2004) is recovered exactly.



## 16.8 Incremental stress-strain relations

Assuming that the initial stress is at the yield surface ( $\delta\phi = 0$ ), the incremental stress-strain relations for triaxial compression are given by

$$\dot{\boldsymbol{\varepsilon}} = (\mathbb{C}^e + \mathbb{C}^p)\dot{\boldsymbol{\sigma}} \quad (16.22)$$

where

$$\boldsymbol{\varepsilon} = (\varepsilon_v, \varepsilon_s)^\top, \quad \boldsymbol{\sigma} = (p, q)^\top, \quad (16.23)$$

$$\mathbb{C}^e = \begin{bmatrix} K_{ur}^{-1} & 0 \\ 0 & (3G_{ur})^{-1} \end{bmatrix}, \quad \mathbb{C}^p = \frac{1}{H} \begin{bmatrix} -\eta D & D \\ -\eta & 1 \end{bmatrix} \quad (16.24)$$

with

$$H = \frac{(p + c/\tan\phi)(1 - \eta/M)^2}{\beta}, \quad (16.25)$$

$$D = \begin{cases} M - N - \eta, & \text{for Flow Rule = Taylor} \\ -N, & \text{for Flow Rule = Constant Dilation,} \end{cases} \quad (16.26)$$

$$\eta = q/(p + c/\tan\phi),$$

and

$$M = \frac{6 \sin\phi}{3 - \sin\phi}, \quad N = \frac{6 \sin\psi}{3 - \sin\psi}. \quad (16.27)$$

## 16.9 Limit Analysis and Strength Reduction

Limit Analysis and Strength Reduction are carried out using equivalent Mohr-Coulomb parameters. The resulting limit loads may differ somewhat from those of a full elastoplastic analysis. Under drained conditions, the difference is due to the effects of nonassociativity. The same observations as for the standard Mohr-Coulomb model here apply. In particular, limit loads may be estimated using Davis parameters (see Section 8.2).

For undrained analysis, similar observations hold. The HMC plastic potential is essentially of the Drucker-Prager type and thus differs slightly from that used in the standard Mohr-Coulomb model. However, for the constant mean effective stress conditions that exist under undrained conditions, the effect on the bearing capacity is much less than under drained conditions.

## **17 LINEAR ELASTIC**

The Linear Elastic material type implements Hooke's law and does not involve any limitations on the strength in the form of yield conditions or similar. All other properties – Drainage, Stiffness, Unit Weights, Initial Conditions, and Hydraulic Model are as for the Mohr-Coulomb material (see Section 8).

## **18 RIGID**

The Rigid material type describes a perfectly rigid and infinitely strong material. Its only properties – Drainage, Unit Weights, and Hydraulic Model are as for the Mohr-Coulomb material (see Section 8). The Rigid material is convenient for the modeling of foundations, retaining walls and similar structures provided that one is confident that the failure as well as the majority of the deformations take place elsewhere.

## 19 FLUIDS

In OptumG2, Fluids are special cases of Solids. Internally, they are modeled as elastoplastic Solids capable of sustaining an indefinite amount of hydrostatic compression and no shear stress. The elastic parameter is the bulk modulus  $K$ . Internally, Poisson's ratio is chosen to balance the requirement that the material should be incompressible ( $\nu = 0.5$ ) together the requirement that the Young's modulus  $E = 3K(1 - 2\nu)$  should remain finite. The only other material parameter is the unit weight,  $\gamma$ . For the default material Water, the parameters are  $K = 2,200$  MPa and  $\gamma = 9.8$  kN/m<sup>3</sup> corresponding to water under standard atmospheric conditions. Furthermore, Fluids are assigned an artificial hydraulic conductivity of 1,000 times the largest hydraulic conductivity used in the stage for any Solid material.

## 20 PLATES

Plates are structural elements used to model elements whose thickness is sufficiently small to be negligible compared to the overall problems dimensions. Common examples are foundation plates and sheet pile walls. Plates may also be useful in a number of other situations to model objects whose overall properties are not well defined other than they are very stiff (or very flexible) compared to the surrounding solid materials. Two types of Plates are available: Plate and Rigid Plate.

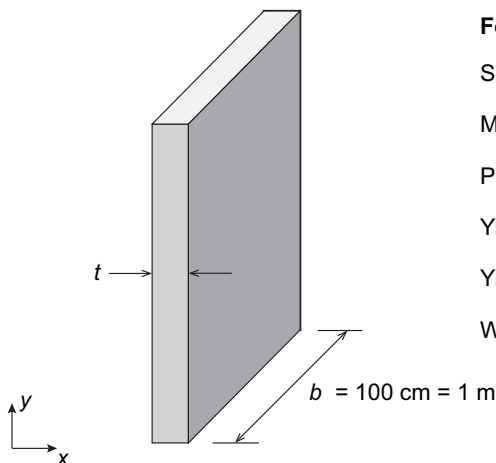
### 20.1 Plate

The material type Plate is an elastoplastic plate which in plane strain is equivalent to a standard Euler-Bernoulli beam.

The model parameters can be entered in two different formats referred to as Parameter Sets A and B respectively. These are shown in Figure 20.1 which also summarizes the relation between the parameters of the different sets.

Model Parameters	
Yield Envelope	Square
Parameter Set	A
Normal Stiffness, EA (kN/m)	6000
Bending Stiffness, EI (kNm <sup>2</sup> /m)	45
Yield Force, $n_p$ (kN/m)	9000
Yield Moment, $m_p$ (kNm/m)	675
Weight, $w$ (kg/m/m)	690
Permeable	<input checked="" type="checkbox"/>

Model Parameters	
Yield Envelope	Square
Parameter Set	B
Sectional Area, A (cm <sup>2</sup> /m)	3000
Plastic Section Modulus, S (cm <sup>3</sup> /m)	22500
Moment of Inertia, I (cm <sup>4</sup> /m)	225000
Young's Modulus, E (MPa)	20
Yield Strength, $\sigma_0$ (MPa)	30
Weight, $w$ (kg/m/m)	690
Permeable	<input checked="" type="checkbox"/>



**For thickness  $t$  in cm and density  $\rho$  in kg/m<sup>3</sup>:**

$$\text{Sectional Area, } A = b \times t = 100 \times t \text{ [cm}^2\text{/m]}$$

$$\text{Moment of Inertia, } I = \frac{1}{12} b \times t^3 = 100 \times \frac{1}{12} t^3 \text{ [cm}^4\text{/m]}$$

$$\text{Plastic Section Modulus, } S = \frac{1}{4} b \times t^2 = 100 \times \frac{1}{4} t^2 \text{ [cm}^3\text{/m]}$$

$$\text{Yield Force, } n_p = A \times \sigma_0 \text{ [kN/m]}$$

$$\text{Yield Moment, } m_p = S \times \sigma_0 \text{ [kNm/m]}$$

$$\text{Weight, } w = A \times \rho = 0.01 \times t \times \rho \text{ [kg/m/m]}$$

Figure 20.1: Parameter Sets A and B (top) and relation between the parameters of the two sets for a solid rectangular section with  $t = 30 \text{ cm}$ .

The two sets share two properties: Yield Envelope and Permeable (Yes/No). The latter setting concerns Seepage analysis and determines whether the plate will be considered as an impermeable barrier or a fully permeable boundary between two solids. Note that the Permeable setting is a material setting and relates to all plates assigned the material in all stages.

Regarding the yield envelope, two options are available. Square (the default setting) imposes the following yield criterion:

$$\left| \frac{m}{m_p} \right| \leq 1, \quad \left| \frac{n}{n_p} \right| \leq 1 \quad (20.1)$$

A more conservative estimate of the strength of the wall may be realized by use of the Diamond yield criterion:

$$\left| \frac{m}{m_p} \right| + \left| \frac{n}{n_p} \right| \leq 1 \quad (20.2)$$

The two yield criteria are shown in Figure 20.2. Usually, the difference in results between the two criteria is relatively minor as most problems relevant to geotechnics tend to be dominated by bending.

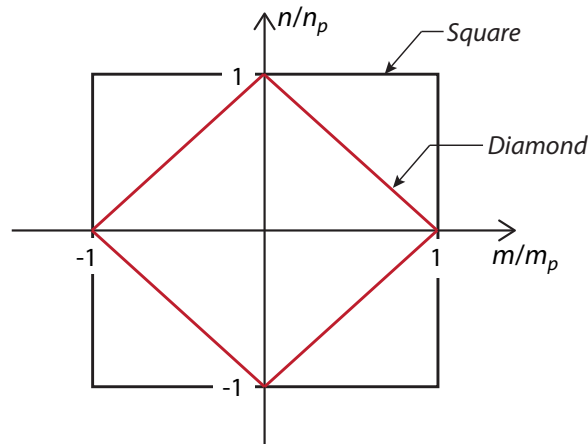


Figure 20.2: Square and Diamond yield criteria.

## 20.2 Rigid Plate

The Rigid Plate material type is a special case of the material described above. It involves only two parameters: weight and Permeable (Yes/No). This element is convenient in cases where the exact properties of the actual plate are not well defined, but where it can be assumed that it has a much higher strength and stiffness than the surrounding material.

### 20.3 Additional features

Plates may be assigned interface materials from the Solids category and hinges which in themselves require a set of material parameters (see Section 23). Both these additional features may be accessed and edited via the property window by selecting a given plate. An example is shown in Figure 20.3.

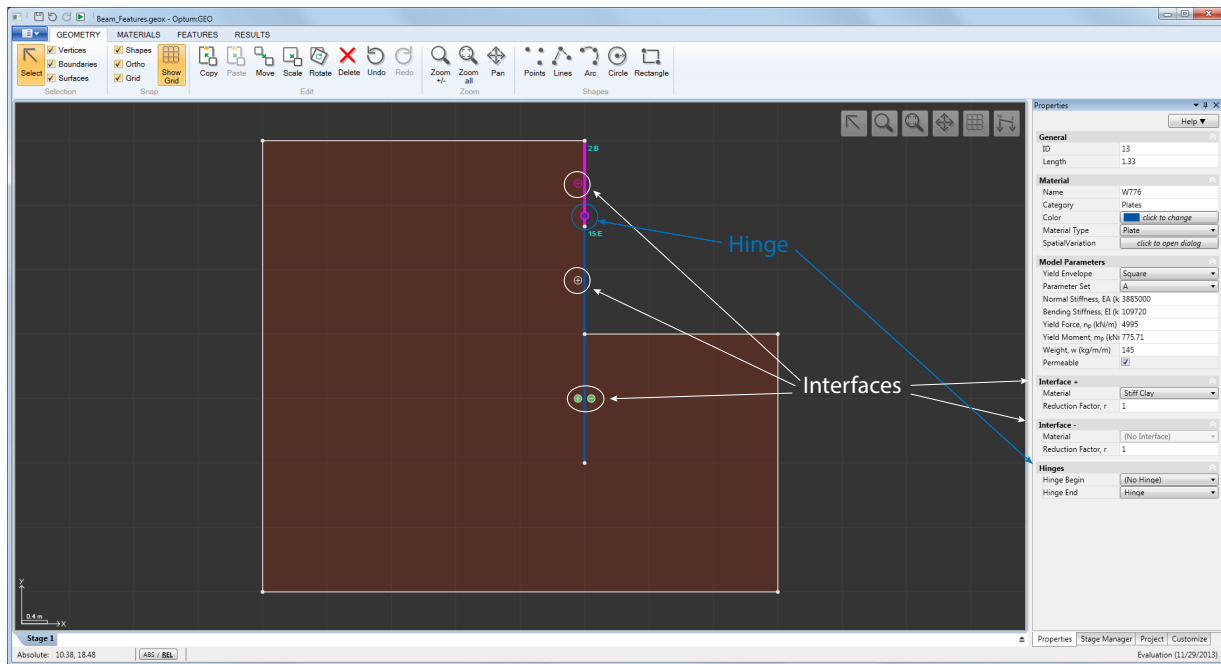


Figure 20.3: Beams with interfaces and a hinge.

OptumG2 offers two possibilities for defining the Reduction Factor,  $r$ , used to modify the interface strength parameters. These may be set under Physical Parameters in Project (see Figure 20.4). For the Mohr-Coulomb model, the default option “c, phi” reduces the cohesion and friction angle by the factor  $r$ . This follows many codes of practice including Eurocode 7. The second option “c, tan(phi)” reduces  $c$  and  $\tan \phi$  by the specified factor  $r$ . The rules for other models are given in the table below.

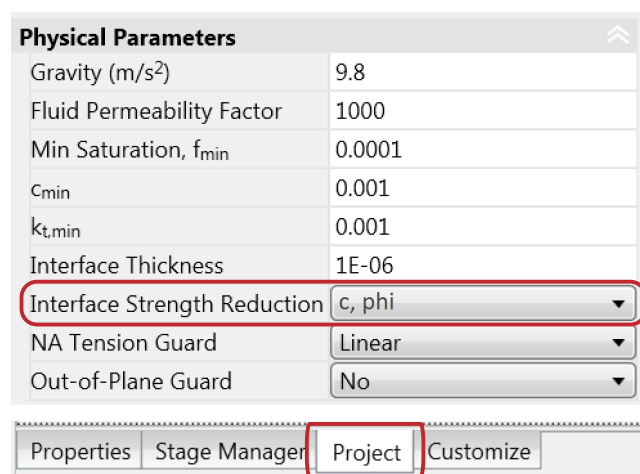


Figure 20.4: Interface Strength Reduction option.

	Original Parameters	Reduced Parameters Option = c, phi	Reduced Parameters Option = c, tan(phi)
Mohr-Coulomb	$c, \phi$	$rc, r\phi$	$rc, \arctan(r \tan \phi)$
Drucker-Prager	$k, M$	$rk, rM$	$rk, rM$
Tresca (Standard)	$s_u$	$rs_u$	$rs_u$
Tresca (Generalized)	$s_{uc}, s_{ue}$	$rs_{uc}, rs_{ue}$	$rs_{uc}, rs_{ue}$
AUS	$s_{uc}$	$rs_{uc}$	$rs_{uc}$
Hoek-Brown	$\sigma_{ci}, m_i$	$r\sigma_{ci}, rm_i$	$r\sigma_{ci}, rm_i$
GSK	$c, \phi_1, \phi_2$	$rc, r\phi_1, r\phi_2$	$rc, \arctan(r \tan \phi_1), \arctan(r \tan \phi_2)$
Bolton	$\phi_{cv}$	$r\phi_{cv}$	$\arctan(r \tan \phi_{cv})$
Modified Cam Clay	$\phi$	$r\phi$	$\arctan(r \tan \phi)$
HMC	$c, \phi$	$rc, r\phi$	$rc, \arctan(r \tan \phi)$

Table 20.1: Modified interface strength parameters.



## 21 GEOGRIDS

Geogrids are similar to Plates, but cannot sustain uniaxial compression and offer no resistance to bending. As such, the material parameters concern only the tensile stiffness and strength (see Figure 21.1). Geogrids are considered weightless and may be either fully permeable or impermeable.

Model Parameters	
Parameter Set	A
Stiffness, EA (kN/m)	450
Yield Force, $n_p$ (kN/m)	45
Permeable	<input checked="" type="checkbox"/>

Model Parameters	
Parameter Set	B
Sectional Area, A (cm <sup>2</sup> /m)	10
Young's Modulus, E (MPa)	450
Yield Strength, $\sigma_0$ (MPa)	45
Permeable	<input checked="" type="checkbox"/>

For thickness  $t$  in cm:

$$\text{Sectional Area, } A = b \times t = 100 \times t \text{ [cm}^2\text{/m]}$$

$$\text{Yield Force, } n_p = A \times \sigma_0 \text{ [kN/m]}$$

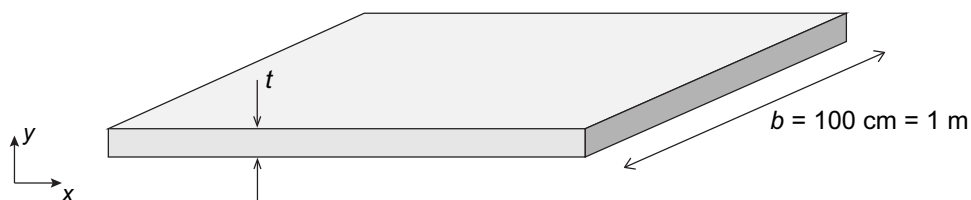


Figure 21.1: Parameter Sets A and B (top) and relation between the parameters of the two sets for a solid rectangular section with  $t = 0.1$  cm.

Besides geogrids, geotextiles, thin membranes, etc, Geogrid elements can also be used to account for grouting in connection with soil anchors (see the Examples Manual).

As for Plates (see the previous section), it is possible to assign arbitrary Solid materials to the interfaces of Geogrids and to apply a strength reduction factor  $r$ .

## 22 CONNECTORS

Materials in the Connectors category can be assigned to Connectors and Fixed End Anchors. Connectors are one-dimensional truss elements that do not interact with the solid domain. In other words, they may be viewed as existing in a layer outside the solid domain. These elements are commonly used to account for anchoring systems. As for Geogrids, Connectors can only sustain normal forces. The material parameters can be entered via two Parameter Sets as shown in Figure 22.1. All parameters refer to the individual rods. Similar, the results reported are for the individual Connectors.

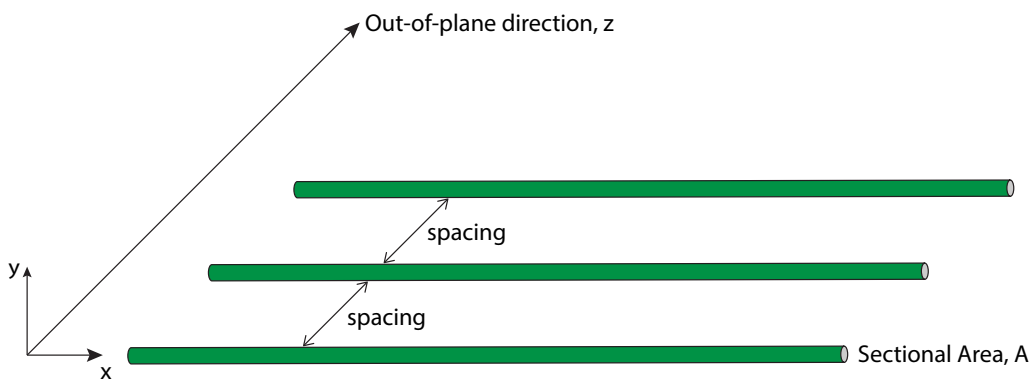
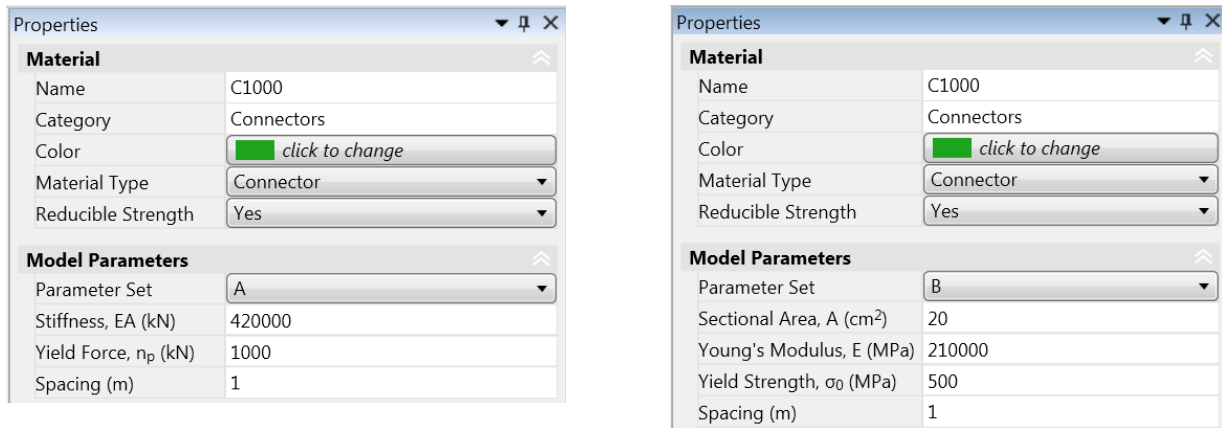


Figure 22.1: Connector with parameters defined via Set A or B.

## 23 HINGES

Hinges can be applied at the end of plates (see Section 20). These are elastoplastic elements defined by two material parameters:

- Rotational Stiffness,  $k$  (kNm/m/rad)
- Yield Moment,  $m_p$  (kNm/m)

The moment-rotation behavior of Hinge elements is shown in Figure 23.1. For moments  $|m| < m_p$ , the mutual rotation of the Plates on either side of the hinge is given by

$$\theta = \frac{m}{k} \quad (23.1)$$

For moments  $|m| = m_p$ , the hinge behaves in a perfectly plastic manner with zero rotational stiffness. The default settings,  $k = 0$  and  $m_p = 0$ , thus correspond to a standard hinge not offering any resistance to rotation. Similarly, for  $k = m_p = \infty$  a standard rigid connection is reproduced.

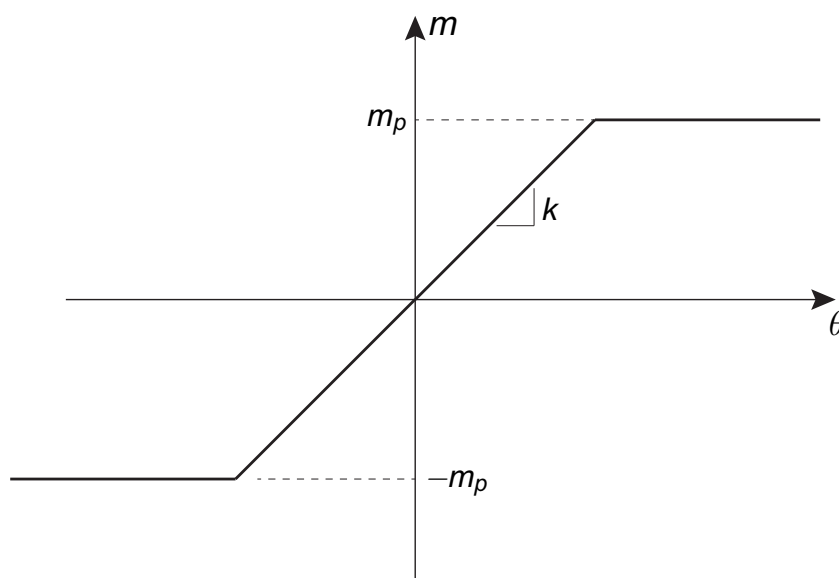


Figure 23.1: Moment-rotation behavior of Hinge element.

## 24 PILE ROWS

While the rigorous modeling of piles subjected to arbitrary loading (lateral, axial, moment) requires a full three-dimensional analysis, a number of special cases can be handled in two spatial dimensions. A single pile subjected to axial loading can be modeled as an axisymmetric structure. Furthermore, a pile row subjected to more general loading can be modeled using a Plate element in an plane strain analysis – provided the spacing between the piles is sufficiently small for the row to behave more or less as a monolithic structure.

The case of pile row with a spacing in the order of several pile diameters is more challenging to model. On one hand, the individual piles interact with the soil in much the same way as a Plate element. On the other hand, the soil may flow between the piles. Indeed, if the spacing is sufficiently large, part of the soil between the piles will be unaffected by the pile movement.

The Pile Row feature available in OptumG2 attempts to cater for this partial interaction between the piles and the soil. Following Sluis et al. (2014), the basic idea is to consider the soil and the piles as being located in two different ‘layers’ similar to what is the case with Connectors. However, while Connectors have no interaction with the soil at all, the piles in a Pile Row are connected to the soil by means of springs, the properties of which imply more or less of an interaction. The principle is sketched in Figure 24.1.

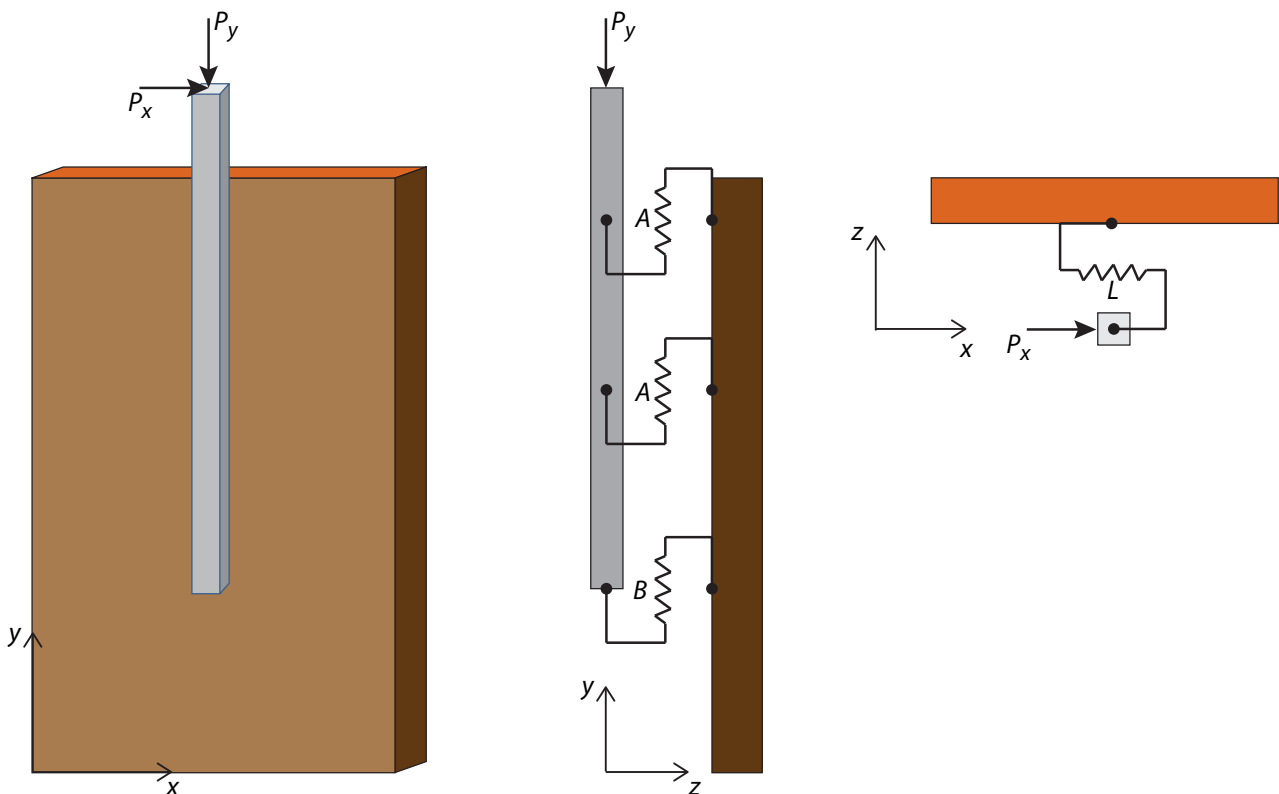


Figure 24.1: Partial interaction between pile and soil. The pile and the soil nodes are independent but have the same coordinates

Three different types of springs, accounting for three different types of interaction are considered: axial (A) for interaction in the direction of the pile, lateral (L) for interaction perpendicular to the pile,

and base (B) for interaction between the soil and the base of the piles in the row. The interaction springs all have a finite strength. In the following, the parameters associated with Pile Rows are discussed in detail.

### 24.1 Piles

The pile of the Pile Row are modeled using standard beam elements. The input parameters are those of the individual piles. Three different types of piles requiring input of the specific dimensions are available: Massive Circular, Circular Tube, and Massive Square. In addition, the cross section area and moment of inertia for a pile with an arbitrary cross section can be entered via the User option. The different parameter sets are shown in Figure 24.2.

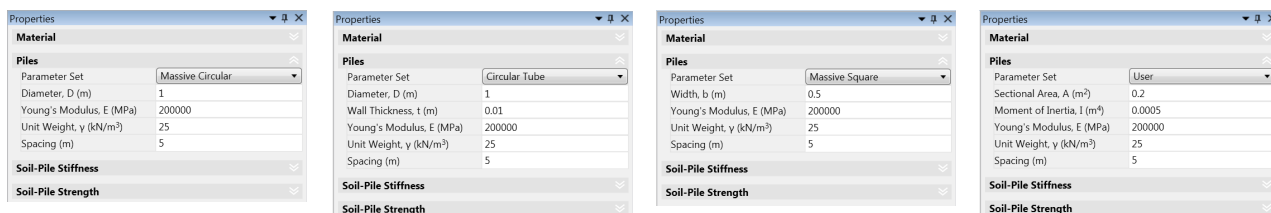


Figure 24.2: Parameters for Pile Rows (Piles).

Following Sluis et al. (2014), the Young's modulus and unit weight used internally for the beam elements are calculated as:

$$\hat{E} = \frac{EA}{D_{eq}s}, \quad \hat{\gamma} = \gamma \frac{A}{s} \tag{24.1}$$

where

$$D_{eq} = \sqrt{\frac{12I}{A}} \tag{24.2}$$

and  $s$  is the spacing.

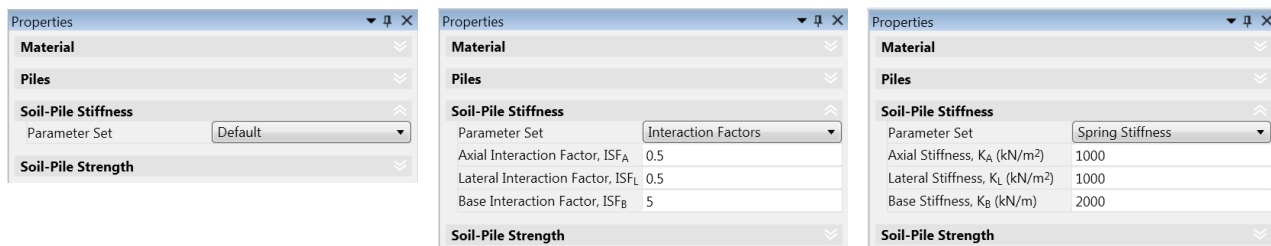


Figure 24.3: Parameters for Pile Rows (Soil-Pile Stiffness).

### 24.2 Soil-Pile Stiffness

Following, Sluis et al. (2014), the stiffness of the springs connecting the pile and the soil are calculated as:

$$\begin{aligned}
 K_A &= IFS_A \frac{G_{soil}}{s} \\
 K_L &= IFS_L \frac{G_{soil}}{s} \\
 K_B &= IFS_B \frac{G_{soil}}{s} \frac{D_{eq}}{2}
 \end{aligned}
 \tag{24.3}$$

where  $K_A$ ,  $K_L$  and  $K_B$  are the axial, lateral and base springs respectively,  $IFS$  are interaction factors and  $G_{soil}$  is the shear modulus of the soil. Sluis et al. (2014) suggests the following interaction factors:

$$\begin{aligned}
 IFS_A &= 2.5 \left( \frac{s}{D_{eq}} \right)^{-0.75} \\
 IFS_L &= 2.5 \left( \frac{s}{D_{eq}} \right)^{-0.75} \\
 IFS_B &= 25 \left( \frac{s}{D_{eq}} \right)^{-0.75}
 \end{aligned}
 \tag{24.4}$$

These are the interaction factors implemented with the Default option (see Figure 24.3). Alternatively, the interaction factors or the spring stiffnesses can be entered manually.

### 24.3 Soil-Pile Strength

All the interaction springs have a finite strength that can be specified as shown in Figure 24.4. The base spring cannot sustain tension.



Figure 24.4: Parameters for Pile Rows (Soil-Pile Strength).

### 24.4 Additional properties

#### 24.5 Base

For a given Pile Row segment, the base can either be specified as being located at the end (E) of the beginning (B) of the segment (see Figure 24.5). Alternatively, None specifies that no base stiffness and strength are available. A Pile Row base is denoted by a gray arrow as shown in Figure 24.5.

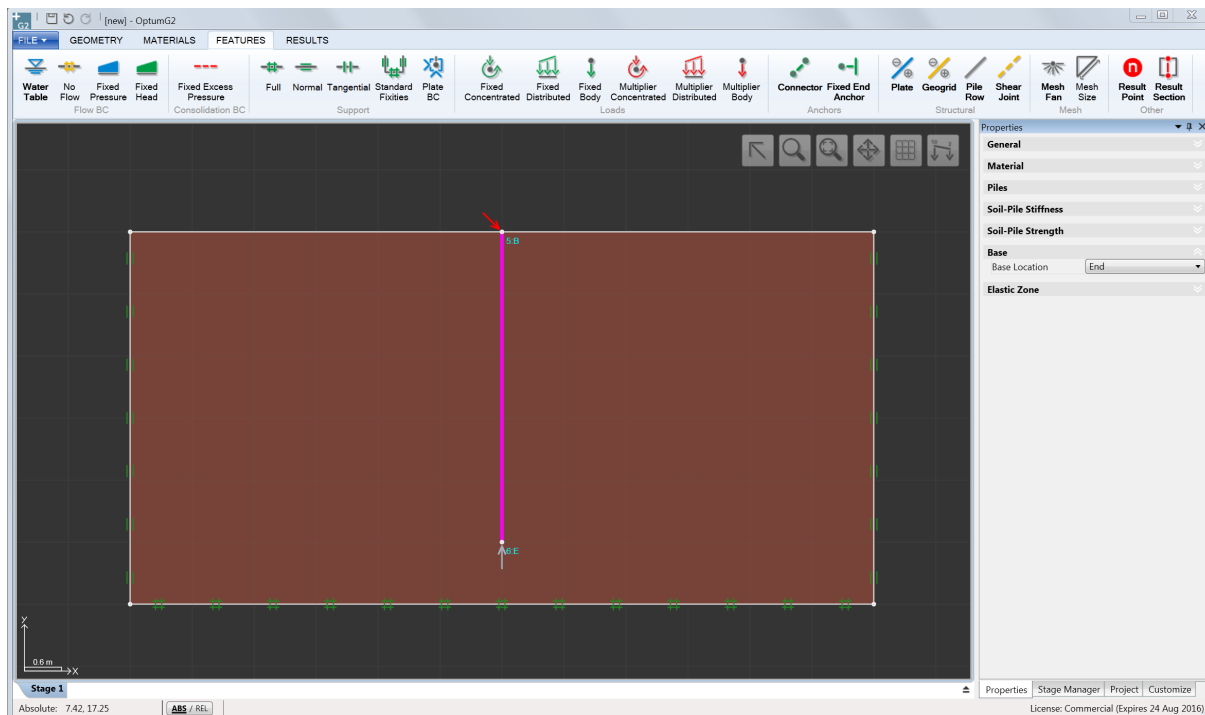


Figure 24.5: Pile Row Base.

## 24.6 Elastic Zone

Following Sluis et al. (2014), the elements in a finite zone around the pile are assumed to be elastic. By default, the width of this elastic zone is  $D_{eq}/2$  (see Figure 24.6). A user defined width of the elastic

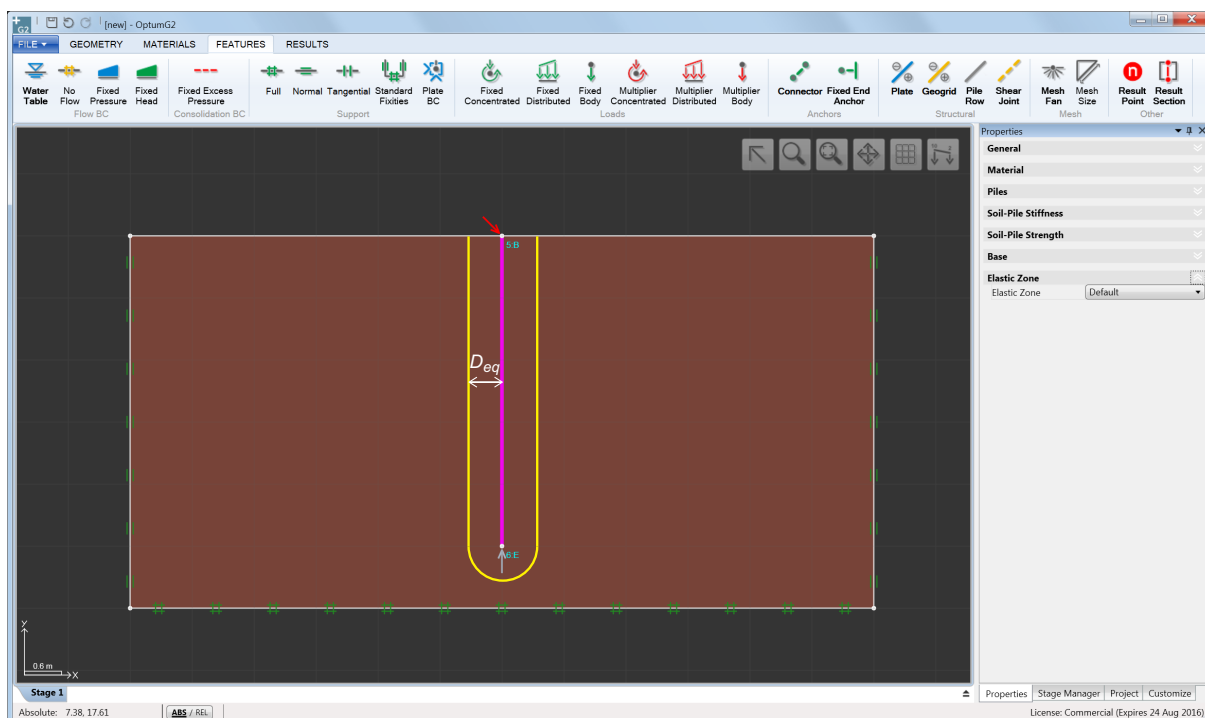


Figure 24.6: Elastic zone.

zone can be set by selecting User under Elastic Zone. Alternatively, no elastic zone is included by selecting None.



## 25 NAIL ROWS

Nail Rows are as special case of Pile Rows corresponding to the settings shown in Figure 25.1. The user input are: Nail Diameter (cm), Young's Modulus (MPa), Spacing (m) and Axial Strength along the Nail (kN/m). The base strength is zero while the lateral strength is unlimited, implying failure of the surrounding soil rather than in the springs connecting the Nail to the soil. Finally, in contrast to Piles, no elastic zone around the Nail is considered.

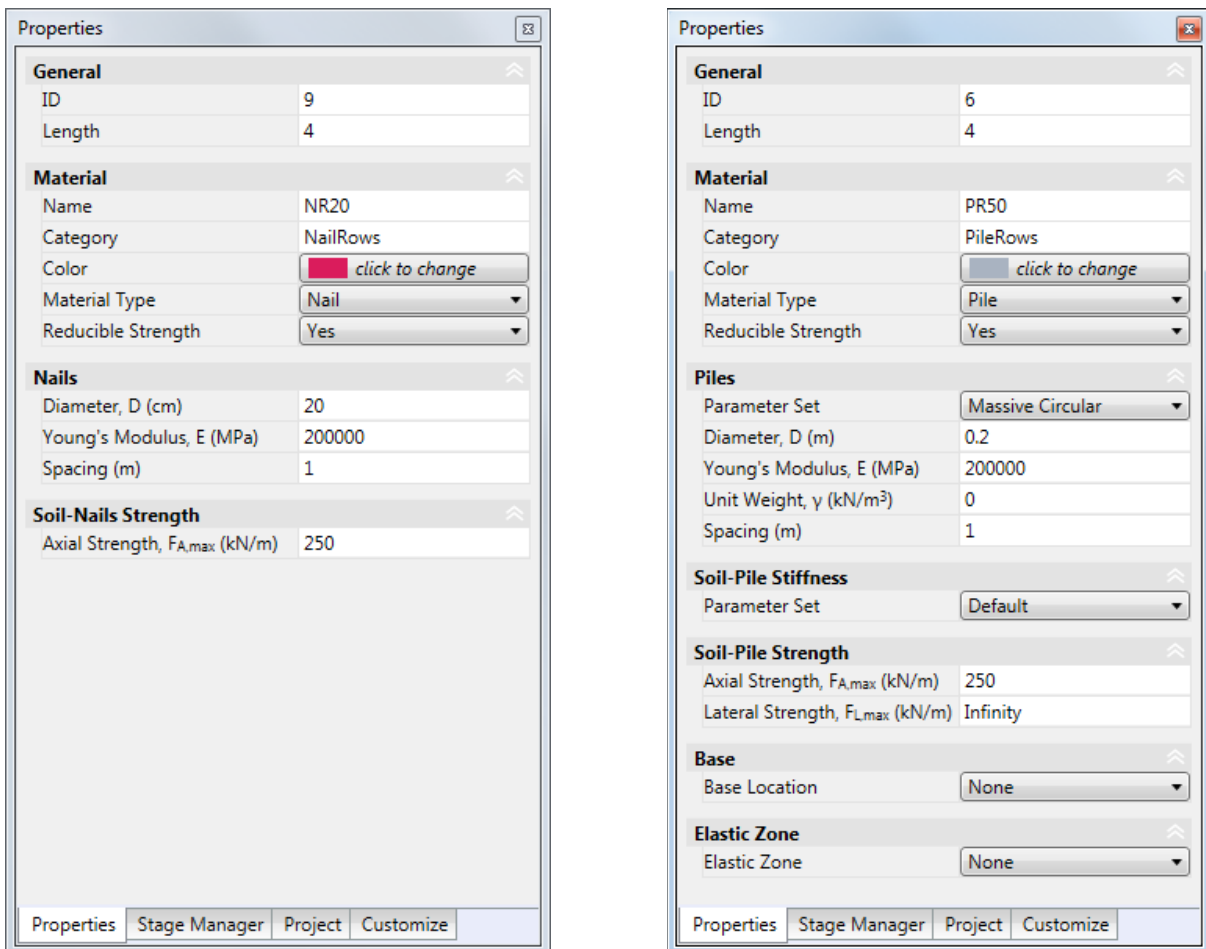


Figure 25.1: Nail Row (left) and equivalent Pile Row (right).

## References

- Ahadi, A. and Krenk, S. (2000). Characteristic state plasticity for granular materials. Part II: Model calibration and results. *International Journal of Solids and Structures*, 37:6361–6380.
- Ahmed, S. M. U. (1972). *A Study of the Influence of Confining Pressure on the Behaviour of Sands*. PhD thesis, McGill University, Montreal, Canada.
- Alshibli, K. A., Batiste, S. N., and Sture, S. (2003). Strain localization in sand: Plane strain versus triaxial compression. *Journal of Geotechnical and Geoenvironmental Engineering*, 129:483–494.
- Bolton, M. D. (1986). The strength and dilancy of sands. *Geotechnique*, 36:65–78.
- Borja, R. I. and Kavazanjian, E. (1985). A constitutive model for the stress-strain-time behaviour of 'wet clays'. *Geotechnique*, 35:283–298.
- Burland, J. B., Rampello, S., Georgiannou, V. N., and Calabresi, G. (1996). A laboratory study of the strength of four stiff clays. *Geotechnique*, 146:491–514.
- Davis, E. H. (1968). Theories of plasticity and the failure of soil masses. In Lee, I. K., editor, *Soil Mechanics: Selected Topics*, pages 341–380, Butterworth, London.
- Davis, E. H. (1980). Some plasticity solutions relevant to the bearing capacity of rock and fissured clay. In *Proc. 3rd ANZ Conf. on Geomechanics, vol. 3. Wellington, New Zealand*, pages 27–36.
- Doherty, J. P. and Muir Wood, D. (2013). An extended Mohr-Coulomb (EMC) model for predicting the settlement of shallow foundations on sand. *Geotechnique*, 63:661–673.
- Gercek, H. (2007). Poisson's ratio values for rocks. *International Journal of Rock Mechanics and Mining Sciences*, 44:1–13.
- Ghanbarian-Alavijeh, B., Liaghat, A., Huang, G. H., and van Genuchten, M. T. (2010). Estimation of the van genuchten soil water retention properties from soil textural data. *Pedosphere*, 20:456–465.
- Graham, J. and Houlsby, G. T. (1983). Anisotropic elasticity of a natural clay. *Geotechnique*, 33:165–180.
- Hara, A., Otha, T., Niwa, M., Tanaka, S., and Banno, T. (1974). Shear modulus and shear strength of cohesive soils. *Soils and Foundations*, 14:1–12.
- Hoek, E. (1983). Strength of jointed rock masses. *Geotechnique*, pages 187–223.
- Hoek, E. (2007). *Practical Rock Engineering*. Available at: <http://www.rocscience.com>.
- Karlsrud, K. and Hernandez-Martinez, F. G. (2013). Strength and deformation properties of norwegian clays from laboratory tests on high-quality block samples1. *Canadian Geotechnical Journal*, 50:1273–1293.
- Krabbenhoft, K., Karim, M. R., Lyamin, A. V., and Sloan, S. W. (2012a). Associated computational plasticity schemes for nonassociated frictional materials. *International Journal for Numerical Methods in Engineering*, 89:1089–1117.

- Krabbenhoft, K. and Lyamin, A. V. (2012). Computational Cam clay plasticity using second-order cone programming. *Computer Methods in Applied Mechanics and Engineering*, 209–212:239–249.
- Krabbenhoft, S., Clausen, J., and Damkilde, L. (2012b). The bearing capacity of circular footings in sand: Comparison between model tests and numerical simulations based on a nonlinear Mohr failure envelope. *Advances in Civil Engineering*, Article ID: 947276:1–10.
- Ladd, C. C. (1991). Stability evaluation during staged construction. *Journal of Geotechnical Engineering*, 117:540–615.
- Ladd, C. C. and DeGroot, D. J. (2003). Recommended practice for soft ground site characterization: Arthur Casagrande Lecture. In *Proceedings of the 12th Panamerican Conference on Soil Mechanics and Geotechnical Engineering, Cambridge, MA*, volume 1, pages 1–60.
- Larsson, R. (1980). Undrained shear strength in stability calculation of embankments and foundations on soft clays. *Canadian Geotechnical Journal*, 17:591–602.
- Mesri, G. (1975). Discussion of "New design procedure for stability of soft clays" by Ladd, C. C. and Foott, R. *Journal of the Geotechnical Engineering Division*, 101:409–412.
- Mesri, G. and Castro, A. (1986).  $C_\alpha/C_c$  concept and  $K_0$  during secondary compression. *Journal of Geotechnical Engineering*, 113:230–247.
- Muir Wood, D. (1990). *Soil Behaviour and Critical State Soil Mechanics*. Cambridge University Press.
- Muir Wood, D. (2004). *Geotechnical Modelling*. Cambridge University Press.
- Potts, D. M. and Zdravkovic, L. (2001). *Finite Elements Analysis in Geotechnical Engineering*. Thomas Telford.
- Roscoe, K. H. and Burland, J. B. (1968). On the generalized stress-strain behaviour of wet clay. In Heyman, J. and Leckie, F. A., editors, *Engineering Plasticity*, pages 535–609. Cambridge University Press.
- Schofield, A. and Wroth, P. (1968). *Critical State Soil Mechanics*. Cambridge University Press. Available online: <http://www.geotechnique.info/>.
- Sheorey, P. R. (1997). *Empirical Rock Failure Criteria*. Taylor & Francis.
- Skempton, A. W. (1957). Discussion: The planning and design of the new Hong Kong airport. *Proceedings of the Institution of Civil Engineers London*, 7:305–307.
- Sluis, J. M. M., Besseling, F., and Stuurwold, P. H. H. (2014). Modelling of a pile row in a 2D plane strain FE-analysis. In *Numerical Methods in Geotechnical Engineering*, pages 277–282. Taylor & Francis.
- Vardenega, P. J. and Bolton, M. D. (2013). Strength mobilization in clays and silts. *Canadian Geotechnical Journal*, 2048:1485–1503.
- White, D. J., Teh, K. L., Leung, C. F., and Chow, Y. K. (2008). A comparison of the bearing capacity of flat and conical circular foundations on sand. *Geotechnique*, 58:781–792.

## REFERENCES

---

Yu, H. S. (2006). *Plasticity and Geotechnics*. Springer-Verlag.

Zheng, Z., Booker, J. R., and Carter, J. P. (1997). Limit analysis of the bearing capacity of fissured materials. *International Journal of Solids and Structures*, 37:1211–1243.